

Mechanisms of force-mediated regulation of transcription,  
chromatin remodeling and cell fate decisions

Inaugural-Dissertation  
zur  
Erlangung des Doktorgrades  
der Mathematisch-Naturwissenschaftlichen Fakultät  
der Universität zu Köln

vorgelegt von  
Quang-Huy Le  
aus Ho Chi Minh Stadt, Viet Nam

Berichterstatter:

Dr. Sara A. Wickström

Prof. Dr. Matthias Hammerschmidt

Prüfungsvorsitzender:

Univ.-Prof. Dr. Angelika A. Noegel

Tag der mündlichen Prüfung:

04.11.2016

## **Table of contents**

<b>Abstract</b>	<b>7</b>
<b>Zusammenfassung</b>	<b>8</b>
<b>1. Introduction</b>	<b>9</b>
<b>1.1 Mammalian skin as a model system for adult stem cells</b>	<b>9</b>
1.1.1 Skin architecture	9
1.1.2 Epidermal homeostasis and stem cells	11
<b>1.2 Mechanotransduction</b>	<b>12</b>
1.2.1 Mechanosensors	14
1.2.2 Actomyosin contractility	15
1.2.2.1 Non-muscle myosin II	16
1.2.2.2 Actin dynamics	18
1.2.2.3 Force transmission through actomyosin networks	20
<b>1.3 The nucleus</b>	<b>21</b>
1.3.1 Nuclear envelope	22
1.3.2 The LINC complex	24
1.3.2.1 Nesprins and SUN domain proteins	24
1.3.2.2 Emerin	26
1.3.3 Chromatin architecture	27
1.3.4 Epigenetic regulation of chromatin dynamics	31
1.3.4.1 Polycomb repressive complexes	32
1.3.4.2 H3K9 methylation	35
1.3.5 RNA polymerase II	36
1.3.6 Function of actin during transcription process	39
<b>2. Aims of the thesis</b>	<b>40</b>
<b>3. Methods</b>	<b>41</b>
3.1 Cell culture of EPCs	41
3.2 Mechanical straining	42
3.3 RNA sequencing analysis and bioinformatics	42
3.3 Chemical treatments	43
3.4 Biochemical fractionations, immunoprecipitation and western blotting	44
3.4.1 Preparation of histones	44
3.4.2 Determining G- to F-actin ratio	44

3.4.3 Nuclear fractionation	45
3.4.5 Immunoprecipitation	46
3.4.6 Western blotting	46
3.5 FACS analysis of apoptosis and proliferation	49
3.6 qPCR	50
3.7 ChIP analyses	53
3.8 FAIRE	55
3.9 RNAi	58
3.10 Immunofluorescence and confocal microscopy	58
3.11 Chromosome FISH	61
3.12 Mouse strains	61
3.13 Histology	62
3.14 Statistics	62
<b>4. Results</b>	<b>63</b>
4.1 Mechanical strain represses global transcription	63
4.1.1 Mechanical strain has no major impact on cell growth	63
4.1.2 Mechanical strain represses global transcription	64
4.1.3 Mechanical strain mediates H3K27me3 and RNAPII-S2p occupancy	67
4.1.4 Mechanical strain induces chromatin remodeling	72
4.2 Mechanosensory complex of Emd-Actin-NMIIA	73
4.2.1 Strain induces enrichment of H3K27me3 in an actomyosin dependent manner	73
4.2.2 Strain induces enrichment of Emd at the outer nuclear membrane to control localized actin remodeling	76
4.2.3 Emd-actin-NMIIA complex functions as a nuclear force sensor	79
4.2.4 Strain regulates RNAPII-S2p and H3K27me3 occupancy through Emd-actin-NMIIA complex	80
4.3. Strain induces global chromatin reorganization	82
4.3.1 Strain reduces H3K9me2,3 levels	82
4.3.2 Strain leads to a compensation between H3K9me2,3 and H3K27me3	84
4.3.3 Strain induces global chromatin reorganization	86

<b>4.4 Nuclear actin regulates transcription activity upon strain</b>	<b>88</b>
4.4.1 Strain reduces nuclear actin levels in an Emd-dependent manner	90
4.4.2 Accumulation of nuclear actin reverses the effect of strain on transcription and H3K27me3	91
4.4.3 Strain-induced chromatin remodeling is independent on nuclear actin-mediated transcription	93
<b>4.5 Strain regulates EPC lineage commitment</b>	<b>94</b>
4.5.1 Strain attenuates differentiation gene expression in a myosin dependent manner	94
4.5.2 PRC2 activity is required for strain-repressed differentiation genes expression	97
4.5.3 Strain-induced repression of transcription in an Emd-dependent manner	97
4.5.4 Nuclear actin is required to mediate the adjustment of transcription	98
<b>4.6 NMIIA activity regulates terminal differentiation in vivo</b>	<b>99</b>
<b>5. Discussion</b>	<b>104</b>
5.1 Strain induces global transcriptional repression and subsequent H3K27me3-mediated gene silencing	105
5.2 Strain regulates transcription through Emd	107
5.3 Strain induces large-scale rearrangement of chromatin through Emd	109
5.4 Perspective	111
5.5 Strain-induced Emd-actin-NMIIA nuclear force sensor affects nuclear actin availability	112
5.6 Nuclear actin is required to mediate transcription activity	113
<b>References</b>	<b>115</b>
<b>Appendix</b>	<b>123</b>
<b>ABBREVIATIONS</b>	<b>124</b>
<b>ACKNOWLEDGEMENTS</b>	<b>126</b>
<b>Publication</b>	<b>127</b>
<b>Erklärung</b>	<b>128</b>
<b>Lebenslauf</b>	<b>129</b>



## Abstract

Tissue mechanics and cellular interactions influence every single cell in our bodies to drive the growth and shape of tissues and organs. However, little is known about mechanisms by which cells sense physical forces and transduce them from the cytoskeleton to the nucleus to control gene expression and stem cell fate. We have identified a novel nuclear-mechanosensor complex, consisting of the nuclear membrane protein emerin (Emd), actin and non-muscle myosin IIA (NMIIA), that regulates transcription, chromatin remodeling and lineage commitment. Force-induced enrichment of Emd at the outer nuclear membrane leads to a compensation between H3K9me<sub>2,3</sub> and H3K27me<sub>3</sub> on constitutive heterochromatin. This strain-induced epigenetic switch is accompanied by the global rearrangement of chromatin. In parallel, forces promote local F-actin polymerization at the outer nuclear membrane, which limits the availability of nuclear G-actin. Subsequently, the reduction of nuclear G-actin results in attenuated global transcription and therefore increased H3K27me<sub>3</sub> occupancy to reinforce gene silencing. Restoring nuclear actin levels in the presence of mechanical strain counteracts PRC2-mediated silencing of transcribed genes. This mechanosensory circuit is also observed *in vivo*. Depletion of NMIIA in mouse epidermis leads to decreased H3K27me<sub>3</sub> levels and precocious lineage commitment, thus abrogating organ growth and patterning. Our results reveal how mechanical signals regulate nuclear architecture, chromatin organization and transcription to control cell fate decisions.

## Zusammenfassung

Gewebe mechanisch und zelluläre Interaktionen beeinflussen jede einzelne Zelle in unserem Körper, um Wachstum und Form von Gewebe und Organen zu regulieren. Es ist jedoch wenig über die Mechanismen bekannt, durch die Zellen mechanische Signale erkennen und diese Informationen vom Zytoskelett an den Zellkern weitergeben, um Genexpression zu steuern. Wir zeigen, dass mechanische Kräfte eine wichtige Rolle bei der Regulation epidermaler Stammzellen / Vorläuferzellen spielen, indem sie H3K27me<sub>3</sub>-gesteuerte Repression der Transcription und die Verdichtung von Chromatin induzieren. Diese kraftabhängigen Änderungen sind auf einen mechanosensorischen Komplex von Nicht-Muskel-Myosin IIA (NMIIA), das Kernmembran-Protein Emerin (Emd) und Aktin zurückzuführen, die auf lokale Kräfte an der äußeren Kernmembran reagieren. Diese kraftabhängige Anreicherung von Emd an der äußeren Kernmembran führt zum Verlust von H3K9me<sub>2,3</sub> bei gleichzeitigen Gewinn von H3K27me<sub>3</sub> auf Heterochromatin und zu einer Umstrukturierung des Chromatins. Zugleich organisiert Emd lokale Aktin-Polymerisation am äußeren Kernmembran, um so die Verfügbarkeit von nuklearem Aktin zu begrenzen. Das führt zu einer Verringerung der gesamten Transkription und Akkumulation von H3K27me<sub>3</sub> an Promotoren dieser Gene und sichert den Zustand der Repression. Diese mechanosensorischen Abläufe finden auch *in vivo* statt. Die Deletion von NMIIA in der Epidermis der Maus führt zur H3K27me<sub>3</sub>-vermittelten Repression, frühzeitiger Differenzierung und schließlich zur Aufhebung des Organwachstum und Strukturierung. Unsere Ergebnisse zeigen, wie mechanische Signale die Kernarchitektur, Chromatinorganisation und Transkriptionsregulation beeinflussen und den Differenzierungsweg steuern.

## **1. Introduction**

Stem cells have a remarkable capacity to both self-renew and differentiate to specific lineages. They serve critical roles during development, regeneration, and tissue homeostasis (Tajbakhsh et al., 2009). Based on their properties and capabilities, stem cells are classified into totipotent, pluripotent, multipotent, oligopotent and unipotent (Wagers and Weissman, 2004). Recent studies have revealed that even complex structures such as our tissues can be generated from a pool of homogenous stem cells by a self-organization process, in which morphogenesis is driven by cellular interactions and local mechanical forces (Sasai, 2013). However, little is known about molecular mechanisms involved in this process. Therefore, it is critical to understand how mechanical forces regulate stem cell self-organization in order to control tissue growth and patterning.

### **1.1 Mammalian skin as a model system for adult stem cells**

#### **1.1.1 Skin architecture**

The skin is the largest organ that covers the entire body. It functions as a highly effective barrier to protect the inner organs from the environment while being constantly exposed to external stresses such as injuries, pathogens, radiation, and mechanical strain. The skin consists of two main compartments: the epidermis comprising mainly of keratinocytes at the outer surface of the skin, and the underlying dermis comprising mainly of connective tissue and mesenchymal cells. The two compartments are separated by a complex, dense, sheet-like extracellular matrix (ECM), called the basement membrane (BM) (Simpson et al., 2011).

Epidermal keratinocytes are organized into stratified layers, including one basal layer of proliferating keratinocytes, and several suprabasal layers of differentiated cells, including spinous layers, granular layers and the cornified layers (Fig. 1.1.1). The basal keratinocytes, also known as epidermal stem/progenitor cells (EPCs) are attached to the BM. They are characterized by their high proliferative potential and ability to give rise to differentiated daughter cells.(Simpson et al., 2011)

Keratins are the largest group of intermediate filaments in EPCs, providing mechanical support for epidermal architecture, cells viability and regulating certain signaling pathways. In epidermis, keratins display complex expression patterns. Keratin 5 (K5) and K14 are strongly expressed in the basal layer and have been suggested to maintain the proliferative potential of basal EPCs. During a stepwise process of stratification and terminal differentiation, EPCs switch off the expression of basal markers (K5 and K14) and ECM receptors (integrins). They become post-mitotic, detach from the basal layer. This is accompanied by the expression of specific markers for spinous layers, granular layers and cornified layers such as K10, Lorcrin (Lor) and Filagrin (Flg), respectively (Alam et al., 2011; Fuchs, 2008; Moll et al., 1982; Simpson et al., 2011).

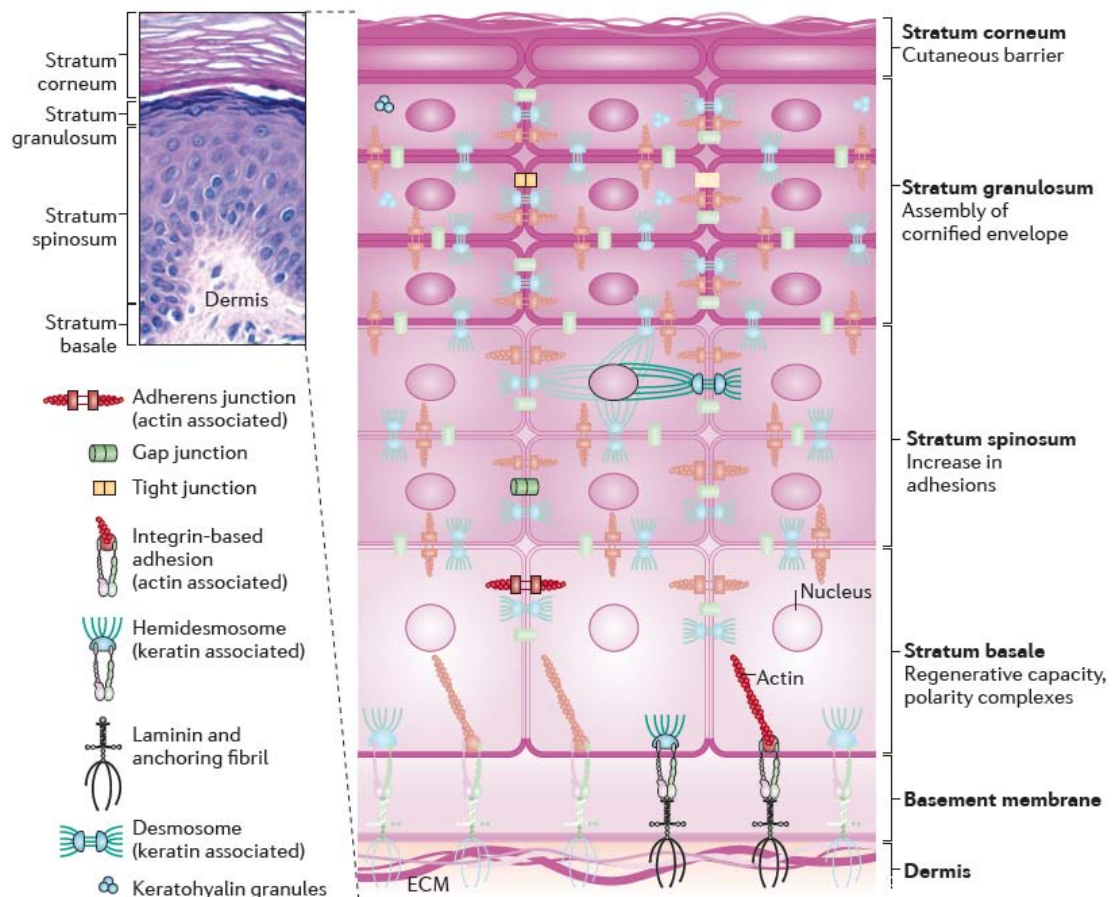


**Fig. 1.1.1. Schematic representation of epidermal architecture.** The skin can be divided into dermis and epidermis, which are separated by the BM. The epidermis consists of stratified layers. Proliferating cells reside at the basal layer, whereas

*differentiated cells are relocated into the spinous, granular and cornified layers (Simpson et al., 2011).*

The dermis is a supportive connective tissue between the epidermis and the subcutaneous fat layer. It is divided into two subcompartments: the upper papillary dermis adjacent to the BM, and the reticular dermis underneath. ECM is the main component of the dermis. In addition to ECM, the dermis also contains fibroblasts, immune cells and blood vessels. The main function of the dermis is to maintain architecture and mechanical properties of the skin (Quan et al., 2013).

The BM is a 50 – 100 nm layer of specialized ECM. Its composition varies both within and between tissues, results in different ECM properties. It serves as an anchoring platform for EPCs through several receptors, in which the main component is integrin. Although the BM was considered a supportive scaffold for a long time, it becomes evident that the BM also regulates cell behavior and fate decisions, thus functioning as an essential component of the epidermal stem cell niche (Watt and Fujiwara, 2011; Watt and Huck, 2013).

### **1.1.2 Epidermal homeostasis and stem cells**

A physiological process, in which cells are constantly produced to offset cell death, is called tissue homeostasis. Mammalian skin is known to renew itself approximately every two weeks continuously throughout life, making the skin one of the most active self-renewing organs. Hence, the epidermal homeostasis needs to be tightly regulated to maintain tissue function; however, mechanisms that regulate epidermal homeostasis are still controversial (Blanpain and Fuchs, 2009; Sotiropoulou and Blanpain, 2012).

Previous studies have proposed two potential models describing the epidermal homeostasis process: an asymmetric cell division model and a stochastic model. The asymmetric cell division model represents early embryonic skin development. EPCs can undergo symmetric and asymmetric cell divisions. The symmetric divisions allow EPCs to expand and increase at the basal layer, whereas the asymmetric model results

in uncommitted and committed daughter cells. By coupling the asymmetric cell divisions with perpendicular spindle orientation to the BM, the committed daughter cells can be translocated directly to the suprabasal layers (Blanpain and Fuchs, 2009; Poulson and Lechler, 2012). However, this model is found to occur rarely in adult skin. Therefore there must be other mechanisms (Clayton et al., 2007). Tracing the fate of EPCs *in vivo* revealed an alternative mechanism. The basal EPCs can undergo an unlimited number of cell divisions, and have equal chance to either stay at progenitor cells or delaminate to enter the terminal differentiation process. The fate decisions occur at rates that ensure epidermal homeostasis (Rompolas et al., 2016). In principle, regardless of which model is correct, a stable pool of EPCs needs to exist to replace those that are lost during tissue turnover.

Moreover, the ease of isolation and maintenance in culture together with the ability to manipulate differentiation *in vitro* by controlling calcium concentration have made EPCs an excellent model to dissect the cellular and molecular mechanisms of stem cell behavior and fate decisions (Watt, 2002).

## **1.2 Mechanotransduction**

Mechanotransduction describes a cellular process that converts mechanical stimuli into biochemical signals to generate responses that, enable cells to adapt to their physical surroundings (Jaalouk and Lammerding, 2009). Various studies have shown that every complex structure, from a non-living matter to a human being, requires physical forces to keep its parts together. Since 1917, when a book of D'Arcy W. Thompson – On Growth and Form – was first published, it has been clear that physical forces or mechanical interactions are one of the most essential driven forces in determining size and geometry in any biological systems (Paluch et al., 2015; Sasai, 2013; Thompson, 1917). All cells from the simplest form to the most complex organism are mechanosensitive (Ingber, 2006; Orr et al., 2006). They are subjected to different types of mechanical stimuli *in vivo*: cyclic stress (heart), shear stress (fluid flow over the cell surface), stretch or tensile strain (skin), distension (bladder), compression (bone, cartilage). Each of these stimuli plays a specific role in the regulation of proliferation, differentiation, migration or morphology of the respective cells (Fig. 1.2) (DuFort et al.,

2011; Reichelt, 2007). Any disruption or altering cellular response to mechanical stimuli can lead to severe human diseases such as deafness, muscular dystrophies, premature ageing, developmental disorders and cancer (Jaalouk and Lammerding, 2009). Therefore, it is important to understand the molecular principles of sensing mechanical stimuli and the subsequent cellular response. Although the transmission of extrinsic forces from the external environment to the cell, including mechanosensitive channels and cytoskeleton, as well as biochemical response is partially understood, the molecular principles of how forces control tissue homeostasis are still unclear.

The epidermis of skin is exposed to constant mechanical stimuli, mostly stretch or tensile strain, as the skin has to expand to cover the whole body, for example during growth and development, pregnancy, weight gain, or wound healing (Evans et al., 2013). In addition, EPCs also experience constant changes in their mechanical microenvironment, such as ECM stiffness, making them a relevant model system to study mechanical stress responses (Reichelt, 2007).

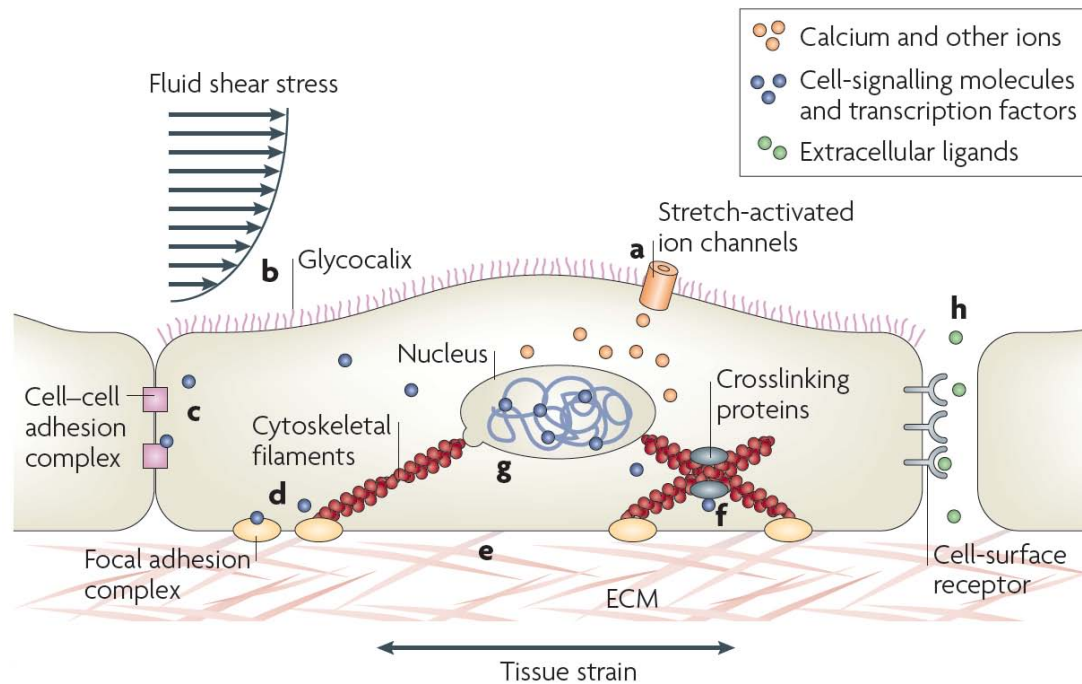


**Fig. 1.2. Cellular mechanotransduction.** Cells are exposed to many types of forces, including shear forces through fluid flow over the cell, and tensile forces through the ECM. Forces are sensed by membrane surface receptors, such as integrin, focal adhesion complex, or ion channels, and transmitted through the actin cytoskeleton to the nucleus, which in turn generates cellular responses (Jaalouk and Lammerding, 2009).

### 1.2.1 Mechanosensors

Cells can probe and detect extrinsic mechanical stimuli by numerous cell surface receptors including stretch-sensitive ion channels, cadherin complexes, G protein-coupled receptors, Tyr kinase receptors and integrins (Fig. 1.2) (DuFort et al., 2011; Zhu et al., 2000). Among them, integrins have received the most attention because of following reasons: 1) they are the main receptors that link the ECM to the cytoskeleton (Campbell and Humphries, 2011), 2) they play an essential role in cell proliferation, differentiation, migration and survival (Hood and Cheresch, 2002), 3) their ability to mediate bi-directional signaling into and from the cells (Radovanac et al., 2013), 4) it has been demonstrated that mechanical stimuli are transduced via integrins in various cell types and 5) integrins are well-characterized (DuFort et al., 2011; Reichelt, 2007).

Each integrin contains a large extracellular region to mediate the interactions between cells and the ECM, a short membrane-spanning domain, and a short cytoplasmic tail that tightly connected to the cytoskeleton (Campbell and Humphries, 2011). The transmission of forces at the cell-ECM interface requires integrins, the actomyosin cytoskeleton and many different focal adhesion proteins. In response to mechanical stimuli, integrins are activated and undergo conformational changes to promote the recruitment of other focal adhesion proteins on the cytoplasmic site of the plasma membrane. The assembly of multiprotein complexes upon integrin engagement triggers actomyosin contractility to transmit signals to the cells, this also provide a feedback loop to reinforce cells adhesion. These bidirectional interactions direct cellular response and adhesion strength (Clark et al., 2007; DuFort et al., 2011; Parsons et al., 2010).

In addition, forces can also be transmitted across cells in tissues to coordinate and generate certain responses within a tissue; for example, during development, tissue remodeling, cell migration and wound healing. The adherens junctions and tight junctions provide important cell-cell adhesive contacts. Despite different components, they both connect to the actin cytoskeleton (Hartsock and Nelson, 2008; Niessen et al., 2011). It was reported that cell-cell adhesions through cadherins can transmit mechanical forces (Ganz et al., 2006). Classical type I cadherins including E-cadherin and P-cadherin are widely expressed in epithelial, VE-cadherin in endothelial, and N-cadherin in other non-epithelial cells (Ladoux et al., 2015). These cadherins bind to  $\beta$ - and  $\alpha$ -catenin in the cytoplasm, which then links to vinculin and filaments (F)-actin network, providing a mechanosensor complex at cell-cell adhesion (Huveneers and de Rooij, 2013; Ladoux et al., 2015).

### **1.2.2 Actomyosin contractility**

The process in which myosins interact with two parallel actin filaments (F-actin) to generate mechanical energy from chemical energy (ATP), is actomyosin contractility (Zaidel-Bar et al., 2015). The actomyosin cytoskeleton is critical for generation of contractile forces that are required for fundamental processes such as cell shape regulation, migration and cell division (Murrell et al., 2015). In addition, the actomyosin cytoskeleton acts as a linker between cell adhesion sites and the nucleus,

allowing direct force transmission from the extracellular environment to the nucleus and eventually to chromatin. The precise molecular mechanisms and functional relevance of this direct mechanical link are unclear (Simon and Wilson, 2011).

### **1.2.2.1 Non-muscle myosin II**

There are at least 24 different classes, but most myosins belong to class II. They are ubiquitously expressed not only in muscle cells but also in non-muscle cells, in which they are called non-muscle myosins (NMs). NMs are a family of actin-binding, ATP-dependent motor proteins that generate forces by moving antiparallel actin filaments (Betapudi, 2014; Hartman and Spudich, 2012; Vicente-Manzanares et al., 2009). NMII is composed of two heavy chains of 230 kDa (NMHC), two regulatory light chains of 20 kDa (MLC) which mediate NMII activity, and two essential light chains of 17 kDa (ELC) which stabilize the heavy chain structure (Vicente-Manzanares et al., 2009). NMHC is organized into three major domains: the globular head, neck and tail. The two globular head domains (N-terminal) bind F-actin and use energy released from ATP hydrolysis to pull against F-actin, thus generating contractile force. The neck domain, which has MLC and ELC binding sites, acts as a lever arm to generate movement (Korn, 2000; Uyeda et al., 1996). The C-terminal tail domain has binding sites to other structures and determines specific role of myosin. This domain dimerizes and form coiled-coil helical structure (Fig. 1.2.2.1A) (Korn, 2000).

In mammals, there are three different NMII isoforms: IIA, IIB and IIC, encoded by three separate heavy chain genes, myosin heavy chain 9 (*Myh9*), *Myh10* and *Myh14*, respectively. Importantly, although these three isoforms share approximately 60 – 80% identity in amino acid sequence, their *in vivo* functions do not fully overlap (Clark et al., 2007; Vicente-Manzanares et al., 2009). NMIIA and IIB are widely expressed in various tissues and cell lines, whereas NMIIIC is more restricted (Golomb et al., 2004). Constitutive deletion of NMIIA expression leads to early embryonic lethality at E6.5 because of defects in cell-cell adhesions and visceral endoderm formation (Conti et al., 2004). Furthermore, previous studies reported that NMIIA is highly expressed in EPCs and is required for contact conformation, reinforcement and cadherin clustering (Sarkar et al., 2009; Vicente-Manzanares et al., 2009). NMIIIB is highly expressed in brain and heart, and ablation of NMIIIB expression results in severe defects in these tissues (Uren

et al., 2000). The function of NMIIC has not yet been fully characterized; however, it is suggested that this isoform is expressed during postnatal development (Golomb et al., 2004). In addition to their different expression patterns, the NMII isoforms also have different kinetic properties. NMIIA has the highest actin-activated ATPase activity and it moves more rapidly among actin filaments, whereas NMIIB is more stably associated with actin (Vicente-Manzanares et al., 2009).

The ELCs are responsible for stabilization of the NMHC structure do not regulate activity. The MLCs bind tightly but non-covalently to the NMHCs (Conti and Adelstein, 2008). NMII activity is regulated by the reversible phosphorylation on serine 19 and in some extent threonine 18 of the regulatory light chains (MLC) (Vicente-Manzanares et al., 2009). MLC is phosphorylated by number of kinases, such as  $\text{Ca}^{2+}$ -calmodulin-dependent MLC kinase (MLCK), Rho-kinase, or activated protein kinase. Inactive NMII folds into a compact incompetent structure, in which the tail bends and interacts with the head of the same myosin. This structure prevents the association with other NMIIIs. In the presence of P-MLC, NMII is activated and transforms into an elongated filament. These elongated NMII filaments further self-assemble into bipolar NMII filaments through interaction between their tails, which initiates the interaction with actin filaments (Fig. 1.2.2.1B). The phosphorylated MLC can be dephosphorylated by myosin phosphatase, which is also regulated by Rho-kinase. Inhibition of myosin phosphatase increases NMIIA activity (Conti and Adelstein, 2008; Vicente-Manzanares et al., 2009).

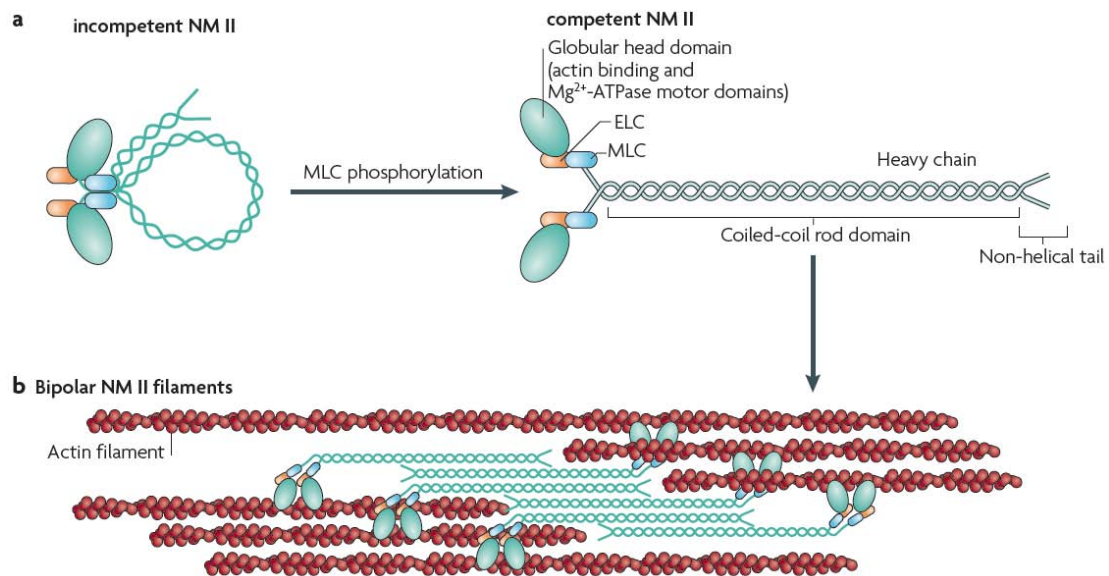


**Fig. 1.2.2.1. Structure of NMII.** *a.* Domain structure of NMII, including two actin-binding globular head domains, two ELCs and two MLCs. In the absence of MLC phosphorylation, NMII forms a compact incompetent structure. Phosphorylation of MLC activates NMII into an elongated molecule. *b.* Activated NMII molecules self-assemble into bipolar filaments, initiating the interaction with F-actin (Vicente-Manzanares et al., 2009).

### 1.2.2.2 Actin dynamics

The most abundant cytoskeletal protein in various cell types is actin. The basic unit of actin is a 43 kDa monomeric globular protein of 375 amino acids (G-actin). Each G-actin has an enzymatic catalytic binding site for ATP or ADP in the center of the molecule, called cleft. The cleft is orientated toward minus end (between subunit 2 and 4). Actin can hydrolyze ATP to ADP and releases Pi during filament assembly. Although F-actin polymerization does not depend on ATP, ATP-bound G-actin assembles more rapidly than ADP-bound. As G-actin molecules within a filament all orient in the same direction, actin filaments also have polarity (plus and minus ends) (Fig. 1.2.2.2). The polarity of F-actin is important both for assembly and direction of myosin movement. The plus end has high concentration of ATP-bound actin, whereas ADP-bound actin is at minus end. This polarity of actin filaments reflects different rates of monomeric assembly, the plus end elongates 5 to 10 times faster than the minus end.

The F-actin comprises of two parallel protofilaments that gently twist around each other into a right-handed double helix. It is a thin and flexible fiber, which is up to several micrometers in length and around 5 – 9 nm in diameter. Actin filaments are organized in higher order structure *in vivo* such as stress fibers or contractile bundles (Alberts et al., 2007; Cooper and Hausman, 2013).

Actin polymerization is reversible, monomeric actin can assemble and disassemble at both ends of the filament, allowing actin filaments to be broken down as needed. The polymerization of F-actin occurs in three phases: a lag phase, an elongation phase and a steady state. During the lag phase, monomeric actin aggregates into dimeric and trimeric forms in a head-to-tail fashion, a process called nucleation. After this, actin is able to polymerize spontaneously by adding G-actin at both ends. During the growth of F-actin, the concentration of G-actin continuously drops until it reaches equilibrium, known as the critical concentration. At this concentration, the polymerization of F-actin is at the steady state, meaning the rate of assembling G-actin into F-actin equals to the rate of disassembly (Alberts et al., 2007; Cooper and Hausman, 2013).

The polymerization of actin also requires other additional factors to stabilize this process. The most common and well-studied factors are Arp2/3 and formins. The Arp2/3 complex mediates the nucleation of new side branches on existing actin filaments, resulting in a Y-shaped structure. Formins are found at the plus end of unbranched filaments, such as stress fibers, to promote the growing of filament. Networks of branched actin are stiff enough to resist compression, whereas networks of unbranched actin are relatively soft, even at high density. These networks can resist or rupture in response to forces, which determined the dynamics of cell and tissue (Alberts et al., 2007; Lecuit et al., 2011; Murrell et al., 2015).

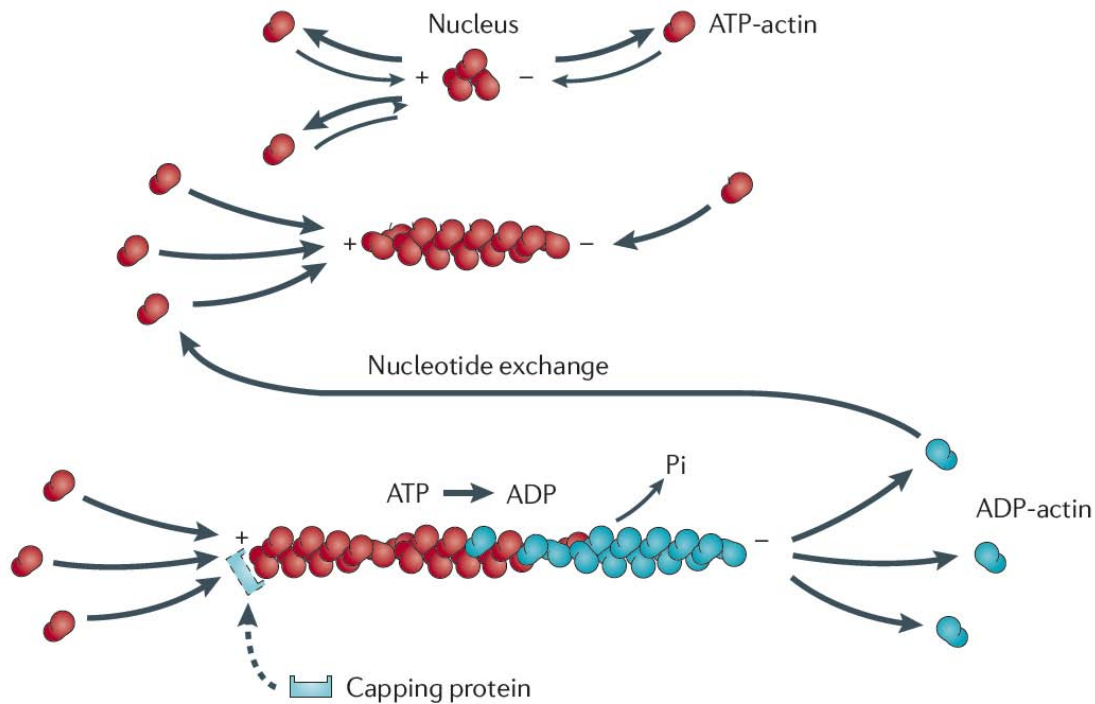


**Fig. 1.2.2.2. Actin dynamics.** Monomeric ATP-bound actin spontaneously aggregates in a process called nucleation. Once an actin nucleus is formed, the polymerization of actin proceeds quickly, with the plus end growing much faster than the minus end. During the growing process, actin can hydrolyse ATP to ADP and release phosphate. Dissociation of ADP-actin occurs at the minus end. ADP-actin undergoes nucleotide exchange to ATP-actin. Capping proteins can associate with the growing plus end and regulate filament elongation (Nurnberg et al., 2011).

### 1.2.2.3 Force transmission through actomyosin networks

Force generation and transmission are controlled by actomyosin networks, in particular their architecture and mechanics. Any small change in internal or external mechanical forces can alter, for example, the stiffness of the actomyosin networks, resulting in changing cell shape, behavior or gene expression (Lecuit et al., 2011; Murrell et al., 2015). The immediate responses of cells to extrinsic mechanical forces involve changes in their adhesive and cytoskeletal organization; for example, increasing actomyosin activity and stiffness, to serve as a scaffold structure so that the cells can resist and adapt to mechanical stress. Thus, forces must be sufficient to drive long-term effects on

cell fate specification and differentiation, in which their scale depends on the physical properties of the cells. The combination of these responses subsequently drives changes in tissue architecture and size (Dmitrieff and Nedelec, 2016; Houben et al., 2007; Wozniak and Chen, 2009).

### **1.3 The nucleus**

In mammalian cells, the nucleus is the largest and stiffest membrane-enclosed organelle. It is physically linked to the cell membrane through the cytoskeleton and the linker of nucleoskeleton and cytoskeleton (LINC) complex (Wang et al., 2009). This physical interaction has been demonstrated to play many essential cellular functions, including cell migration, cytoskeletal organization, nuclear movement and positioning (Isermann and Lammerding, 2013). It is demonstrated that the nucleus also experiences mechanical forces, and has an important role in generating the cellular responses. For example, force-induced altered nuclear shape causes changes in chromatin architecture and affects gene expression (Dahl et al., 2008; Guilluy and Burrige, 2015), as well as feeds back onto the mechanical properties of cells and tissues (Swift and Discher, 2014). Although some studies suggested that force-induced cellular responses occur through some mechanotransduction cascades that alter transcription factors activities (e.g. MAL/SRF and/or YAP/TAZ pathways) (Connelly et al., 2010; Dupont et al., 2011), it is tempting to consider a direct impact of forces across the nuclear envelope (NE) on genomic processes and chromatin dynamics (Chang et al., 2015; Fedorchak et al., 2014; Schreiner et al., 2015). This type of effects have, however, not been experimentally demonstrated.

The LINC complex is speculated to serve as a conduit to transmit mechanical cues into the nucleus (Pederson et al., 2015). Failure of cells to respond to mechanical forces due to impaired NE structure or function can result in a broad range of diseases, including dystrophy, cardiomyopathy, and premature ageing (Isermann and Lammerding, 2013). Importantly, many questions regarding the mechanisms and physiological significance of force transduction across the NE remain, and further studies are therefore required to unravel these (Fedorchak et al., 2014; Pederson et al., 2015).

### 1.3.1 Nuclear envelope

The nucleus can be divided into at least two compartments, the NE and the nucleoplasm. The nuclear envelope functions as a selective permeable boundary between the cytoplasm and the nucleoplasm. It consists of two phospholipid-bilayers, the inner (INM) and the outer nuclear membrane (ONM), nuclear pore complexes (NPCs) and an underlying nuclear lamina (Fig. 1.3.1). This barrier regulates the availability of factors required for chromosomal events, such as DNA replication, transcription and processing, and prevents free diffusion of macromolecules in and out of the nucleus (Alberts et al., 2007; Cooper and Hausman, 2013).

The ONM is continuously linked with the rough endoplasmic reticulum (RER). The ONM shares similar functions as the RER, and also has ribosomes attached to its surface. Both membranes are separated by a 30 nm luminal space, which is fused into the RER's lumen (Hetzer, 2010; Mekhail and Moazed, 2010). The INM is enriched in a wide range of proteins that are specific to the nucleus. These proteins are required for nuclear structure, chromosome organization, DNA repair machinery and transcriptional regulation (Katta et al., 2014). At least 60 proteins have been identified to associate with the INM. However, their functions are mostly unknown (Hetzer, 2010). Among them, LEM (lamina-associated polypeptides (*LAP*) – *emerin* – *Man1*) domain proteins are well characterized. They can both anchor the nuclear lamina to the INM and interact with chromatin (Berk et al., 2013; Katta et al., 2014).

The ONM and INM are fused together at nuclear pores, which are aqueous channels, providing gateways for bidirectional trafficking between the nucleus and the cytoplasm. Ions and small molecules (< 40 kDa) can freely cross the NE, whereas larger molecules, such as proteins and RNA can only be actively transported through the pores. The active transportation of macromolecules requires the interaction between the cargo, its specific transporter (e.g. exportin, importin, transportin, or karyopherin) and the GTPase Ran (Cooper and Hausman, 2013; Kabachinski and Schwartz, 2015; Strambio-De-Castillia et al., 2010). Although this process is a critical regulator of cellular responses for internal and external cues, the mechanisms and regulations of nuclear transport machinery remain undefined (Chaumet et al., 2015).

The nuclear lamina is a scaffold protein structure comprised of type V intermediate filaments called nuclear lamins, which are closely associated with the INM and attached to the periphery of NPCs and to chromatin (Dechat et al., 2008). This structure provides a mechanical support for the nucleus as well as a scaffold for multiple nuclear processes (Isermann and Lammerding, 2013). In mammals, lamins are divided into two classes: A and B. Lamin A and C are the most common type of A-type lamins. They are derived from *LMNA* gene by alternative splicing. Two major B-type lamins, B1 and B2, are encoded by *LMB1* and *LMB2*, respectively. The expression of lamins depends on cell type and developmental stage. All mammalian cells express at least one B-type lamin, whereas A-type lamins become expressed later in development (Burke and Stewart, 2013; Goldman et al., 2002). For many years, the nuclear lamina has been viewed as primarily a structural compartment, contributing to the nuclear integrity, particularly in mechanically stress tissues. Recent studies, however, highlight the importance of the nuclear lamina in chromatin function and gene expression. Importantly, mutations or mislocalization of any components of NE result in numerous severe human diseases, emphasizing the crucial role of the NE and its components for cell function (Burke and Stewart, 2013; Cohen et al., 2008; Hetzer, 2010).

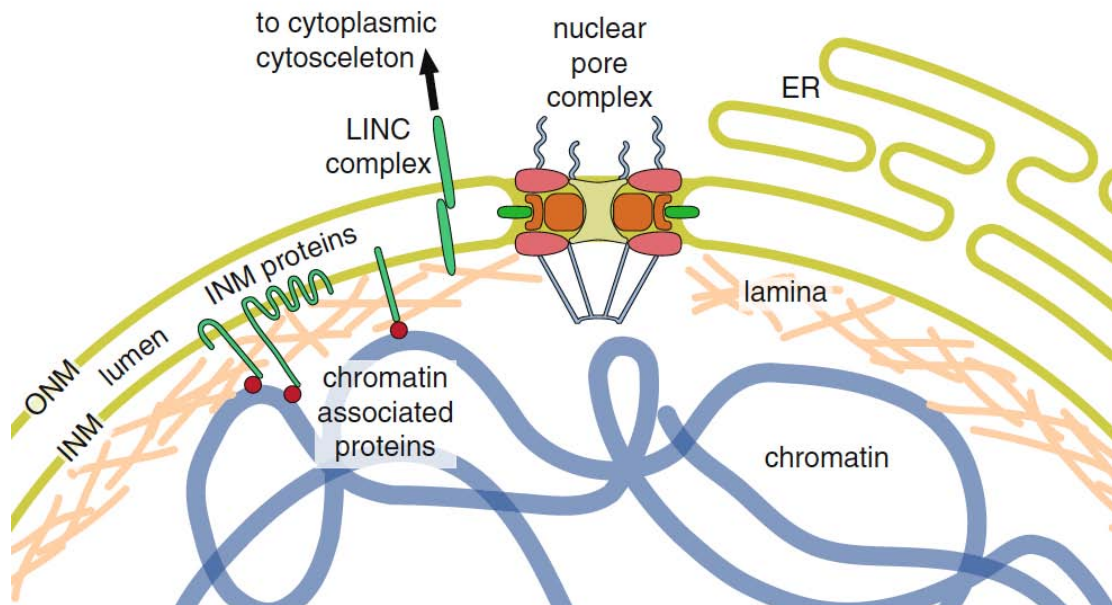


**Fig. 1.3.1. Overview of the nuclear envelope.** The two phospholipid-bilayers of the NE are separated by a luminal space, which is continuous with the ER network. The ONM and INM are connected at the nuclear pores. The INM is enriched by a set of integral membrane proteins that connect the nuclear envelope to chromatin directly or indirectly via chromatin-associated proteins and the nuclear lamina. The chromatin is connected to the cytoplasmic cytoskeleton through the LINC complex (Schooley et al., 2012).

## 1.3.2 The LINC complex

### 1.3.2.1 Nesprins and SUN domain proteins

The LINC complex is composed of inner and outer nuclear membrane proteins, providing a physical link between the nucleus and the cytoskeletal (Fig. 1.3.2.1). It has diverse functions in nuclear positioning, chromatin organization, and mechanotransduction (Chang et al., 2015). The core components of LINC complex are Nesprins (KASH domain proteins) and SUN domain proteins (Kim et al., 2015; Lombardi et al., 2011). Emerin and Lamin A/C, other NE proteins have been also

considered as peripheral components of the LINC complex (Ostlund et al., 2009; Stewart et al., 2007).

Nesprins are C-terminal Klarsicht, ANC-1 and Syne Homology (KASH) domain proteins, located at the ONM. In mammals, four nesprin isoforms have been identified: nesprin-1, 2, 3, 4. Nesprin 1 and 2 contain N-terminal actin-binding domains, whereas nesprin 3 binds to intermediate filaments through plectin, and nesprin 4 to kinesin-1 (Kim et al., 2015). It has been shown that nesprin 1 and 2 play important roles in maintaining nuclear architecture, sensing mechanical forces and regulating gene expression (Guilluy et al., 2014; Lombardi et al., 2011; Zhang et al., 2010). Nesprin's KASH domain consists of a transmembrane region followed by a conserved stretched of around 35 amino acids protruding into the perinuclear space. This domain interacts with SUN domain proteins, allowing a proper localization of nesprins in the NE (Razafsky and Hodzic, 2009; Starr and Fridolfsson, 2010).

SUN domain proteins are type-II transmembrane proteins with a conserved C-terminal SUN domain localizing in the perinuclear space and an N-terminus facing the nucleoplasm. In mammals, five SUN domain proteins have been identified: SUN1, 2, 3, 4, 5. Among them, SUN1 and 2 are widely expressed. The C-terminal region of SUN domain interacts directly with KASH domain, whereas its N-terminal region binds to A-type lamins (Fridkin et al., 2009; Razafsky and Hodzic, 2009). SUN domain proteins are essential to a wide range of cellular processes (Kim et al., 2015). SUN1 is required for tethering telomeres to the NE, and together with KASH5, they mediate proper pairing of chromosomes during meiosis (Horn et al., 2013). SUN1/2 double knockout mice die shortly after birth and can be rescued by expressing Sun1 gene, suggesting that SUN proteins play critical but redundant roles (Lei et al., 2009). Importantly, KASH domain proteins are recruited by SUN domain proteins, and the KASH-SUN interaction is essential for bridging the NE. This model suggests a mechanism by which the LINC complex can sense signals bidirectionally at the NE (Starr and Fridolfsson, 2010; Tzur et al., 2006).

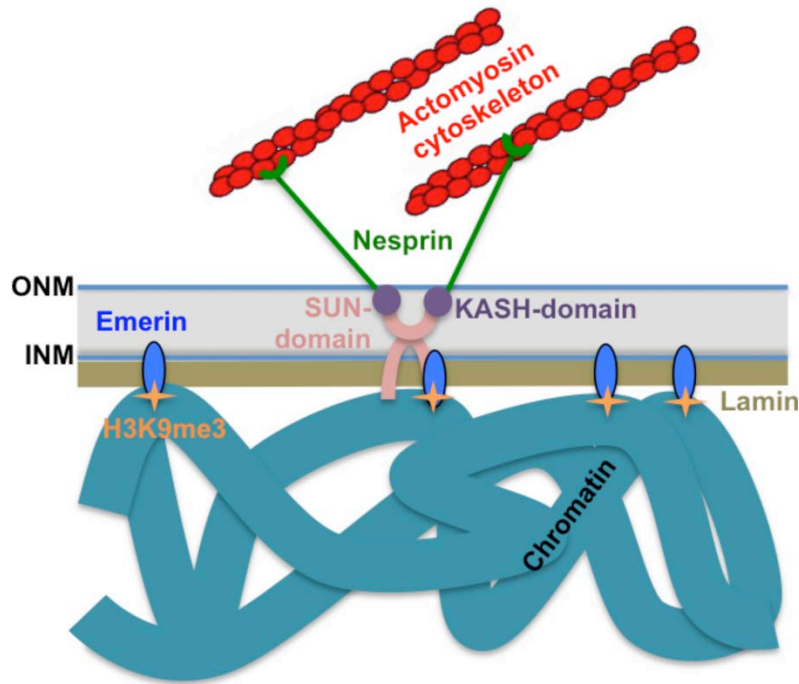


**Fig. 1.3.2.1.** *The LINC complex acts as a bridge linking the chromatin to the cytoskeleton. This complex consists of KASH domain, SUN domain proteins, emerin and lamin A/C. Nesprin, a KASH domain protein, spans the ONM and interacts with the cytoskeleton networks. SUN domain protein and emerin at the INM interact directly with lamin A/C and heterochromatin.*

### 1.3.2.2 Emerin

Emerin (Emd) is a well-conserved type II transmembrane protein consisting of 254 amino acids. The main sequence of Emd is composed of an N-terminal LEM domain, a region rich in hydrophobic amino acids containing the nuclear localization signal, and a C-terminal transmembrane region. After synthesis, Emd is inserted into the ER system and diffused to the continuously linked-ER ONM. Emd is a relative small protein ~29 kDa (34 kDa observed molecular weight), which allows it to diffuse freely through the NPC, where the INM and ONM are integrated. At the INM, Emd binds to lamins for proper localization and function (Ostlund et al., 2009; Wolff et al., 2001).

Emd principally localizes at the INM where it interacts with lamins, barrier-to-autointegration factor (BAF) and chromosome through its LEM domain. Additionally, Emd also interacts with nuclear myosin I, nuclear  $\alpha$ II-spectrin,  $\beta$ -catenin, actin, etc (Holaska and Wilson, 2007; Markiewicz et al., 2006). Emd is ubiquitously expressed, and has been reported to have multiple functions, including transcriptional regulation, cell signaling, and maintaining nuclear and chromatin architecture (Berk et al., 2013; Koch and Holaska, 2014; Lammerding et al., 2005). Emd knockout mice show no overt pathology, but defects in muscle regeneration and subtle defects in motor coordination (Melcon et al., 2006). Interestingly, failure to express or altered the localization of Emd in human leads to Emery-Dreifuss Muscular Dystrophy (EDMD) which, particularly affects tissues that experience mechanical loads, resulting in progressive skeletal muscle weakening, contractures of major tendons and potentially fatal cardiac conduction defects (Holaska and Wilson, 2006; Koch and Holaska, 2014).

Furthermore, Emd has been shown to reside at the interface between the nucleus and the cytoplasm, where it binds to other ONM proteins (Crisp and Burke, 2008; Salpingidou et al., 2007), as well as to F-actin, and promotes the polymerization of actin (Holaska et al., 2004). Recent study suggested that Emd regulates mechanical reinforcement of isolated nuclei. Force strongly induces Emd phosphorylation, and Emd-deficient-nuclei fail to adapt to force (Guilluy et al., 2014). Together, Emd is predicted to play a role in anchoring cortical nuclear actin-myosin networks near the NE to provide structural rigidity to the nuclear envelope and to transmit mechanical forces from the cytoplasm to the nucleus (Koch and Holaska, 2014).

### **1.3.3 Chromatin architecture**

The whole human genome consists of 23 chromosome pairs, in total about 2 meters physical length of naked DNA. How can this much DNA be packed within the nucleus with an average diameter of 6  $\mu$ m. To achieve this highly compacted order, the DNA helix is wrapped 1.7 turns (146 base pairs) around histone proteins, forming nucleosomes. The nucleosome structure is highly dynamic and is subjected to change by chromatin remodelling complexes. The activity of these complexes is associated with the regulation of gene expression, according to the needs of the cell. The string of

nucleosomes is further compacted into a 30 nm chromatin fiber. This shortens DNA about 40-fold relative to naked DNA. In interphase nuclei, it has been suggested that there are at least two higher levels of compacting beyond the 30 nm chromatin fiber (Fig. 1.3.3.1) (Alberts et al., 2007; Pollard and Earnshaw, 2007).

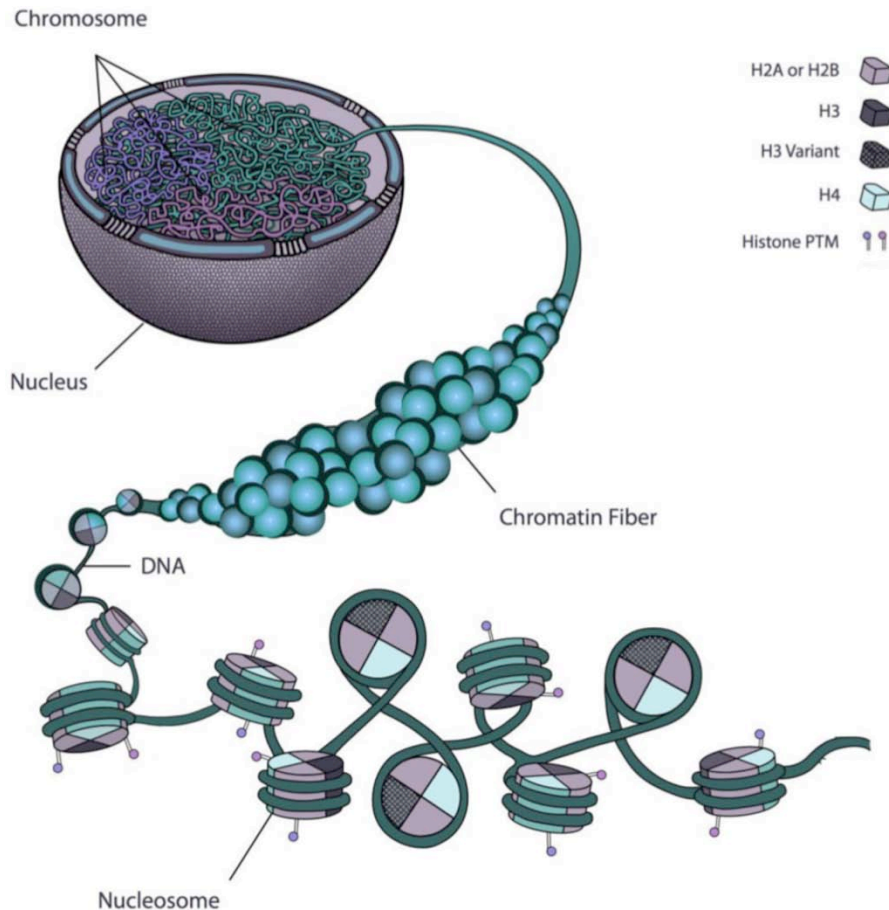


**Fig. 1.3.3.1. DNA packaging in the nucleus.** DNA wraps around the histone core to form a nucleosome. Nucleosomes cluster together into 30 nm chromatin fiber. The DNA packaging allows DNA to fit inside the nucleus. (Rosa and Shaw, 2013).

Based on structural and functional criteria, chromatin is divided into two types: a highly condensed form, called heterochromatin, and a less condensed form, known as euchromatin. Euchromatin contains all actively transcribed genes. Heterochromatin represents a special compact structure of chromatin. There are two types of heterochromatin: constitutive and facultative heterochromatin. Constitutive

heterochromatin is mainly associated with gene-poor regions and repetitive genetic elements, which are packaged close to the nuclear periphery. In contrast, facultative heterochromatin is a special term to describe compact genomic regions that can change their conformation to an “open” state in certain developmental stages or in a specific cell type. The formation of heterochromatin mainly relies on epigenetic mechanisms. The eukaryotic euchromatin and heterochromatin are spatially segregated within the nucleus, and play important roles in regulation of genome functions. Most nuclei have euchromatin residing toward the nuclear interior, while heterochromatin tends to localize at the nuclear periphery. In mammals, genome-wide analysis showed that lamin-bound heterochromatin builds up to 40% of the genome, and organizes into called lamin-associated domains (LADs) that span from several kilobases up to megabases. Importantly, euchromatin and heterochromatin segments are alternating, which require an orientational folding of chromosome, indicating that the organization of chromosomes is non-random and correlates with the functional segments. During interphase, each chromosome occupies a distinct region of the nucleus, known as chromosome territory, providing a basic feature of nuclear architecture (Fig. 1.3.3.2A) (Alberts et al., 2007; Allis and Jenuwein, 2016; Oberdoerffer and Sinclair, 2007; Saksouk et al., 2015a; Solovei et al., 2016; Towbin et al., 2012).

Several recent studies on three-dimensional (3D) structure of the mammalian genomes have gained more insight into chromatin dynamics and functions. At the megabase scale, the genome can be divided into two compartments: A and B (approximately 3-5 Mb each) (Fig. 1.3.3.2B). The A compartments are associated with open chromatin regions (mostly euchromatin), while the B compartments associate with closed chromatin. These two compartment alternate along chromosomes, and tend to interact with other same type compartments throughout the genome. They are cell-type specific and the changes are associated with gene expression, meaning that they are rather gradients than simply two states. The A and B compartments contribute to the genome maintenance, gene expression regulation, and transmission of genetic information (Dekker et al., 2013; Fortin and Hansen, 2015; Gonzalez-Sandoval and Gasser, 2016).

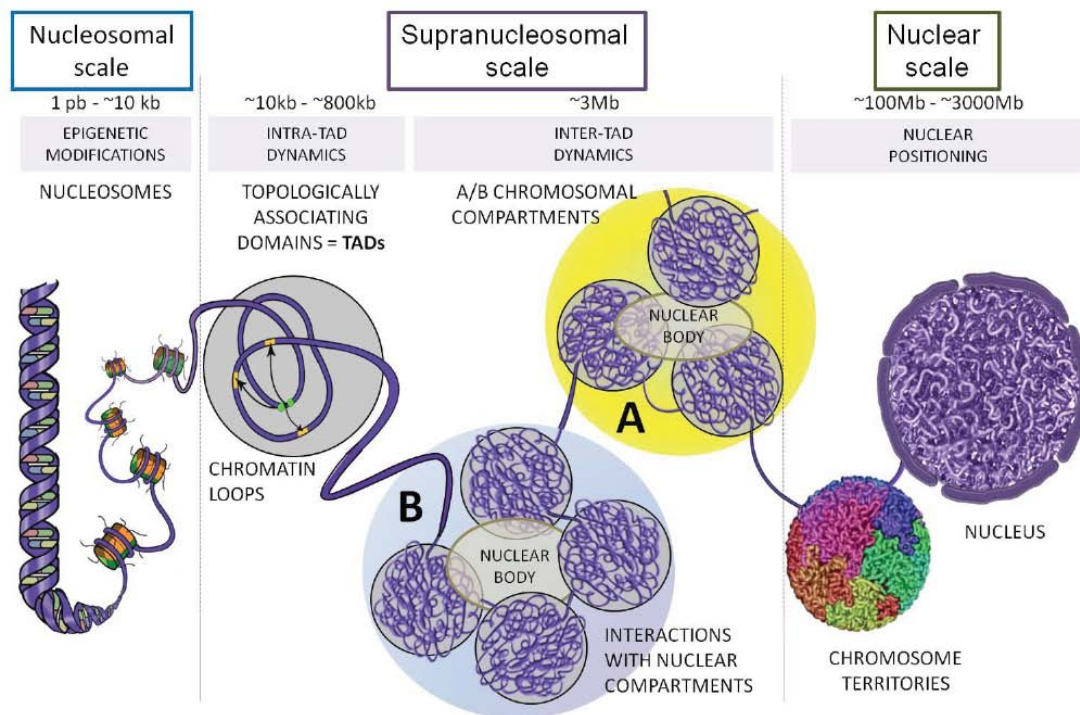


**Fig. 1.3.3.2. Chromosome territories and genome compartments.** Chromosome conformation capture profiles revealed that the mammalian chromatin is organized into topologically associating domains (TADs). A TAD is referred as a hard-wired unit of chromosome. Groups of adjacent TADs form either active (A) or inactive (B) compartments. These compartments alternate along chromosomes. Each chromosome occupies a specific region within the nucleus, known as chromosome territory (Dekker et al., 2013; Ea et al., 2015).

Within a compartment, chromatin itself folds into building blocks, known as topologically associating domains (TADs), which often span to hundreds of kilobases (500-800 kb). TADs can be defined as boundary elements or linear units of chromatin that fold into 3D structures. They serve as functional platforms for physical looping interactions between genes and proximal as well as distal regulatory elements, e.g. enhancer-promoter interactions. TADs are enriched with several genomic elements such as CTCF (a transcriptional repressor), especially at TADs boundaries. It has been suggested that in some cases, CTCF-bound sites may act as boundary elements, but further experiments are required. Unlike A/B compartments, TADs are conserved in their positioning patterns across cell types. TADs can be active or inactive, which is defined by chromatin environment. The mechanism ensuring the chromatin

arrangement within TADs, and how TADs works together and how they integrate with other epigenetic marks to regulate nuclear architecture and functions are not yet understood (Ciabrelli and Cavalli, 2015; Dekker et al., 2013; Fortin and Hansen, 2015; Gonzalez-Sandoval and Gasser, 2016; Pope et al., 2014; Solovei et al., 2016).

### **1.3.4 Epigenetic regulation of chromatin dynamics**

Epigenetics is defined as the study of heritable changes in genome function that occur without alterations the DNA sequence. The epigenetic marks ensure cell identity, and determine whether, when and how particular genetic information will be expressed. Therefore, epigenetic processes are critical for development and differentiation. The molecular basis of epigenetic processes is complex and involves many factors such as chromatin modifications, nucleosome remodeling and histone variants. Importantly, epigenetic marks are inherited across generations; however, they are reversible upon environmental signals (Allis and Jenuwein, 2016; Avgustinova and Benitah, 2016; Probst et al., 2009).

As mentioned, DNA in the nucleus is highly folded and compacted by histones into nucleosomes, a unit of chromatin fiber. Each nucleosome contains an octamer of core histones: an H3-H4 tetramer and two H2A-H2B dimers. Each histone harbors a flexible N-terminal tail protruded from the histone core. The histone tail is important for interactions both inside and outside of nucleosome, and is subjected to a variety of post-translational modifications (PTMs), including methylation (me), acetylation (ac), ubiquitination (ub), phosphorylation (ph), and SUMOylation (su) (Fig. 1.3.4). These modifications have essential roles in regulation of chromatin structure, and therefore affect gene expression, silencing and many other DNA processes such as replication, recombination and repair machinery. The complexity of possible combinations of PTMs of histones and the correlation impacts on genomic functions led to the proposal of the histone code hypothesis, emphasizing the important role of epigenetic marks to the genetic code (Bannister and Kouzarides, 2011; Campos and Reinberg, 2009; Jenuwein and Allis, 2001; Pollard and Earnshaw, 2007).

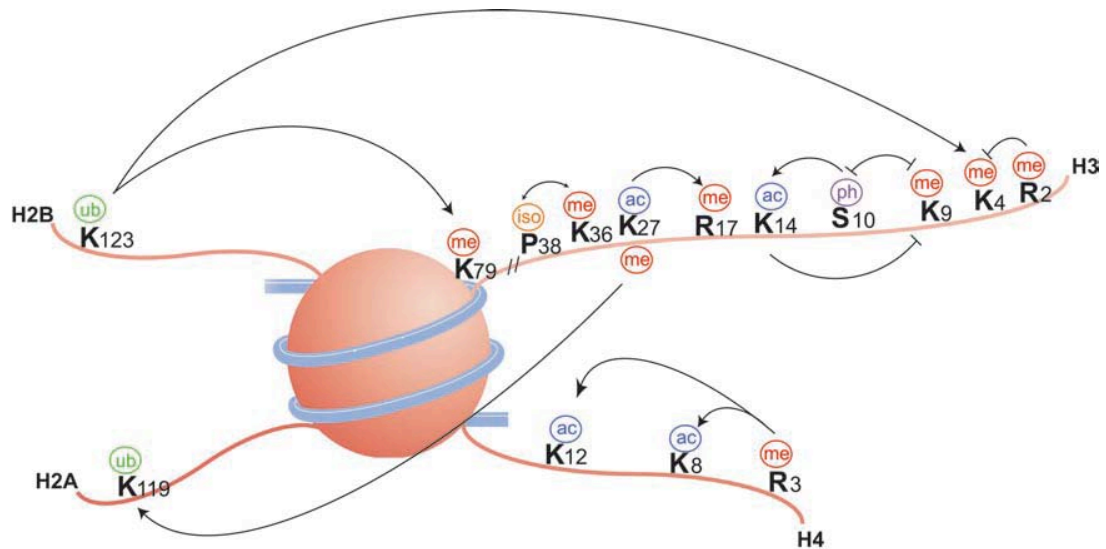


**Fig. 1.3.4. Schematic of histone PTMs and their interactions.** Histone PTMs can interact and regulate other modifications. A positive regulation is indicated by an arrow head, whereas negative effect is represented by a flat head (Bannister and Kouzarides, 2011).

### 1.3.4.1 Polycomb repressive complexes

Polycomb group (PcG) proteins were first discovered in *Drosophila melanogaster* as repressors of *Hox* genes. Genome-wide studies in vertebrates, including humans, revealed widespread roles of PcG in epigenetic silencing machinery that is essential for gene regulation for normal development, cell identity, and a wide-range of cancers. Furthermore, PcG proteins also participate in regulating nuclear architecture, such as looping and long-range interactions between TADs, thereby regulating gene expression at multiple scales. In mammals, most PcG proteins belong to two transcriptional repressive complexes: PRC1 and PRC2 (Blackledge et al., 2015; Entrevan et al., 2016).

A mammalian PRC1 contains RING1A/B that ubiquitinates lysine 119 (K119) on H2A (Fig. 1.3.4.1A), and other subunits, like the chromobox homolog (Cbx), one of six polycomb ring fingers. The subunit composition is responsible for recruitment to target genes and the catalytic activity of PRC1. The presence of multiple different PcG complexes indicates the overlapping and redundant functions of PRC1. Genetic studies showed that it is indeed the case. Most PRC1 knockout mice survive during early

embryogenesis but show restricted phenotypes at later stages. Although PRC1 has been shown to repress transcription and promote chromatin compaction, its mechanism is not yet clear (Di Croce and Helin, 2013; Lanzuolo and Orlando, 2012; Laugesen and Helin, 2014).

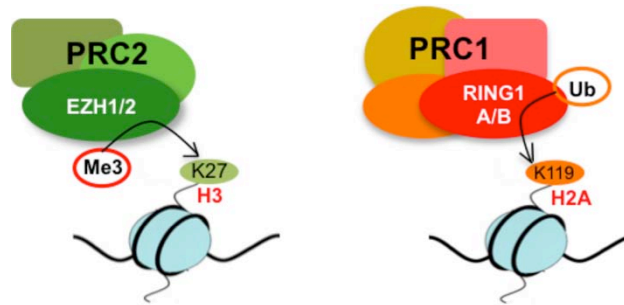


**Fig. 1.3.4.1A. Schematic representation of PcG proteins.** PRC1 has a core of 4 subunits, in which RING1A/B is responsible for ubiquitination of K119 on H2A. The core subunits of PRC2 contain EZH1/2, which methylates K27 on H3. H3K27me3 and H2AK119Ub are important to establish and maintain the polycomb-mediated gene repression, and to promote chromatin compaction.

The core subunits of PRC2 consist of the SET-domain-containing component EZH2 (and to a lesser extent the paralog protein EZH1), the Zinc finger protein SUZ12, and the WD40 protein EED. The core complex interacts with several additional factors, such as RBBP4, JARID2 or non-coding RNA. Different partners affect PRC2 activity or its recruitment to target genes. A signature activity of PRC2 is to catalyse the mono-, di- and tri-methylation on K27 of H3 (H3K27me1/2/3) by the EZH2 subunit (Fig. 1.3.4.1A). Current data shows that the establishment of H3K27me1/2 is very fast, whereas H3K27me3 is relatively slow and requires stable binding of PRC2. Therefore, H3K27me3 occupancy is usually overlapped with a PRC2 binding signal. H3K27me3 is a hallmark for gene repression and highly enriched at promoter regions of tissue-specific genes, which normally have CpG-rich sequences. It is demonstrated to be critical for normal development, gene expression and cell identity. Misregulation of PRC2 has a global effect on H3K27me3 and can lead to embryonic lethality, and many kinds of cancers. In spite of its essential roles, the genes encoding PRC2 components are often mutated. Misregulation of PRC2 activity has been thought not to change the transcription programs, but rather alter the thresholds for gene activation. This implies that the chromatin is more sensitive to environmental stimuli, and therefore regulation of chromatin states are critical during fate transitions. Interestingly, genome-wide

studies revealed overlaps between signals for H3K27me3 and H3K4me3 – a marker for active transcription – on some tissue-specific promoters, forming so called bivalent domains (Fig. 1.3.4.1B). The bivalency is considered to poise RNA polymerase at developmental or lineage genes, thus allowing their timely activation while remaining inactive in the absence of differentiation signals (Becker et al., 2016; Di Croce and Helin, 2013; Jadhav et al., 2016; Laugesen and Helin, 2014; Richly et al., 2011; Simon and Kingston, 2013; Voigt et al., 2013).

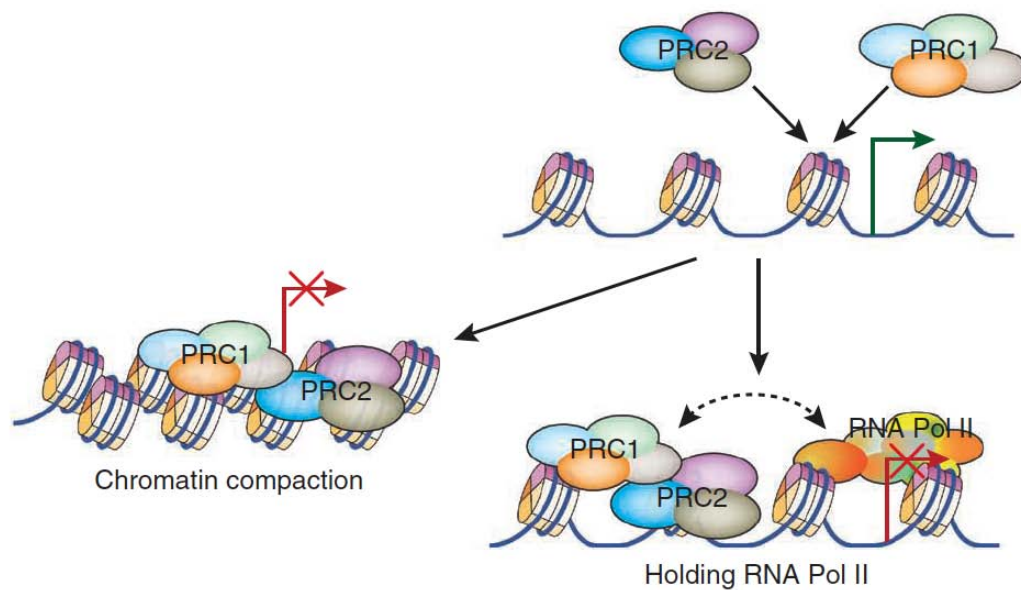


**Fig. 1.3.4.1B. Functions of PcG proteins.** The binding of PRCs contributes to gene repression in two ways: 1) it causes chromatin compaction, and 2) it interferes with transcription process by pausing RNA polymerase II at the promoter region, known as bivalent promoter (Di Croce and Helin, 2013).

Several studies have shown that PcG can interact with histones, DNA and RNA, which potentially might play roles in recruitment. Some studies found that the role of PRC2 is to block initial transcription, whereas other studies demonstrated that PRC2 is recruited upon transcriptional repression, and is required for maintaining the silencing state of target genes (Laugesen and Helin, 2014; Riising et al., 2014). It has been also proposed that the recruitment of PRC1 depends on PRC2, because the CBX subunit of PRC1 has high affinity with H3K27me3. This led to the classical model in which PRC2 is

recruited onto target genes to catalyse H3K27me<sub>3</sub>, which then facilitates the recruitment of PRC1, resulting in silencing and chromatin compaction. However, this model has been challenged in recent years for several reasons: 1) not all PRC1-bound locations require H3K27me<sub>3</sub>, and 2) the binding of PRC1 and subsequent ubiquitination of H2AK119 in some cases trigger the recruitment and stimulate H3K27me<sub>3</sub> activity of PRC2, suggesting a new hierarchy for PRC recruitment under certain circumstances. Collectively, although there are several proposal models, no study has been so far able to pin out a clear recruitment mechanism of PcG proteins (Blackledge et al., 2015; Laugesen and Helin, 2014; Schwartz and Pirrotta, 2014; van den Boom et al., 2016).

#### **1.3.4.2 H3K9 methylation**

Among the epigenetic mechanisms, the formation of heterochromatin is important for chromatin stability and cell-type specific silencing of genes. H3K9me<sub>2/3</sub> together with H3K27me<sub>3</sub> are two important epigenetic marks controlling transcriptional repression. By using chromatin immunoprecipitation (ChIP) techniques, a genome wide distribution of these marks has been revealed. As mentioned, H3K27me<sub>3</sub> is enriched at facultative heterochromatin, in particular associated with tissue-specific genes, and is reversible. In contrast, H3K9me<sub>2/3</sub> is detected prominently at constitutive heterochromatin, and is considered to be a permanent repression signal. However, current studies have observed the enrichment of H3K9me<sub>2/3</sub> signal in some cell-type specific sites of facultative heterochromatin. These regions increase during differentiation in a cell-type specific manner. Importantly, although some developmental transcription factor genes are enriched for both H3K9me<sub>2/3</sub> and H3K27me<sub>3</sub>, most H3K9me<sub>2/3</sub>-containing facultative heterochromatin domains are distinct from the H3K27me<sub>3</sub> domains, indicating different roles of these repressive marks. Almost 40% of the genome is associated with the nuclear lamina through LADs, and these domains have been demonstrated to correlate with H3K9 methylation from worms to human. H3K9 methylation is therefore thought to provide a signal to trigger perinuclear anchoring (Becker et al., 2016; Gonzalez-Sandoval and Gasser, 2016; Hawkins et al., 2010; Kim and Kim, 2012; Lawrence et al., 2016; Towbin et al., 2012).

In mammals, methylation of H3K9 in constitutive heterochromatin, pericentromeric and telomeric regions is mainly catalyzed by Suppressor of Variegation 3-9 homolog 1 and 2 (SUV39H1 and 2). Other methyltransferases, including SET domain bifurcated 1 (SETDB1) and Euchromatic Histone-Lysine N-Methyltransferase 1 and 2 (EHMT1/2) can also methylate H3K9 and are mostly found in euchromatic regions. Also here, the mechanism of methyltransferase recruitment remains unclear (Dejardin, 2015; Kim and Kim, 2012; Peters et al., 2003). Various proteins have been shown to interact with heterochromatin, in particular binding specifically to different level of methylation H3K9. Among them, heterochromatin protein 1 (HP1) isoforms are most extensively studied. Together with H3K9me<sub>2/3</sub>, HP1 isoforms are found to occupy constitutive heterochromatin as well as LADs. It has been suggested that both HP1 and H3K9 methylation are essential to establish heterochromatin domains in mammals. However, although HP1 and H3K9 methylation signals overlap, recent data shows that HP1 is not required for SUV39H recruitment, H3K9me<sub>3</sub> spreading and tethering methylated H3K9 to nuclear lamina, suggesting that the perinuclear anchoring of LADs is mediated by a novel class of uncharacterized factors (Bickmore and van Steensel, 2013; Dejardin, 2015; Towbin et al., 2012).

### **1.3.5 RNA polymerase II**

Eukaryotic nuclei have three RNA polymerases: RNA polymerase (RNAP) I, II and III. They share a common structure and some similar subunits, but they transcribe different DNA types. RNAPI and III transcribe genes encoded for transfer RNA, ribosomal RNA, and various small RNA, whereas RNAPII is responsible for the synthesis of all messenger RNA (mRNA) as well as many non-coding RNA. RNAPII consists of twelve subunits, of which RPB1 is the largest. RPB1 has a unique carboxyl-terminal domain (CTD), which is not required for catalyzing the synthesis of RNA. The CTD consists of 26 (yeast) or 52 (human) unusual tandem repeats of the consensus heptapeptide sequence Tyr<sup>1</sup>-Ser<sup>2</sup>-Pro<sup>3</sup>-Thr<sup>4</sup>-Ser<sup>5</sup>-Pro<sup>6</sup>-Ser<sup>7</sup>. The CTD acts as a binding scaffold for many nuclear factors involving in all steps of the transcription process, such as initiation, elongation, termination, as well as the processing of nascent

RNA (Hahn, 2004; Phatnani and Greenleaf, 2006; Pollard and Earnshaw, 2007; Suh et al., 2013).

All the amino acids within the CTD are highly subjected to various PTMs, including phosphorylation, glycosylation, *cis-trans* isomerization and ubiquitination. The roles of all PTMs are far from being understood. Among them, phosphorylation of CTD has been studied extensively. The pattern of CTD phosphorylation is highly dynamic, and its state correlates to the transcription cycle. CTD phosphorylation recruits factors that regulate chromatin states and RNA processing, thus integrating transcription with genome architecture and stability. Importantly, RNAPII can exist across active and inactive genes with different state of CTD phosphorylation suggesting the crucial role of CTD PTMs for controlling gene expression state (Fig. 1.3.5) (Brookes and Pombo, 2009; Phatnani and Greenleaf, 2006).

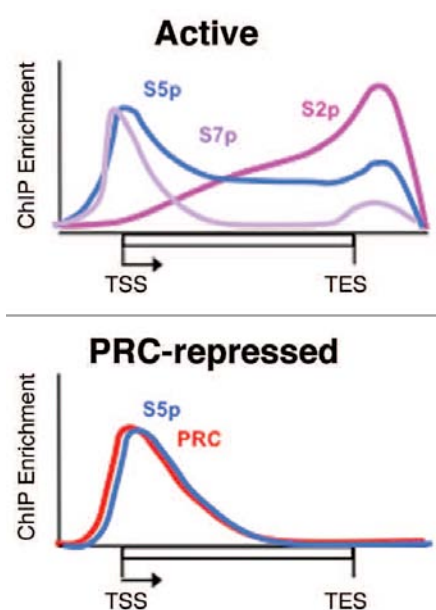


**Fig. 1.3.5 Phosphorylation of RNAPII CTD during transcription.** Average ChIP profile for different RNAPII phosphorylation states. Active genes are associated with S5p and S7p enrichment peaks near TSS, where as S2p level is increasing throughout the gene bodies. For bivalent promoters, S5p is highly enriched around TSS and overlapped with PRC, but no signal from S2p. TSS, transcription start site; TES, transcription end site (Brookes and Pombo, 2009).

RNAPII is recruited to promoter regions in a hypophosphorylated state. During transcriptional initiation, the CTD becomes phosphorylated at Ser5 (S5p) by

transcription factor (TF) IIIH. S5p plays direct and important role in recruiting and facilitating the capping enzyme, synthesizing the 5'-cap structure on the nascent RNA. It also contributes in the recruitment of other factors involving in the transition process from initiation to elongation state of RNAPII, early transcription termination, as well as histone modification. Shortly after promoter escape, the level of S5p decreases. Beside S5p, TFIIH can also phosphorylate S7, which is known to be required for 3'-end processing of non-coding RNA, however, the role of S7p at the gene body regions is still controversial. One study suggested that this mark contributes in recruiting the positive transcription elongation factor (P-TEFb), which phosphorylate S2 of CTD. S2p increases throughout productive elongation state of RNAPII. This mark helps in the recruitment of splicing and polyadenylation factors, as well as H3K36 histone methyltransferases, promoting compatible chromatin remodelling for a stable transcription process (Brookes and Pombo, 2009; Suh et al., 2013; Tietjen et al., 2010).

The presence of RNAPII at promoter regions of PRC-repressed genes in association with S5p (bivalent promoters) has been recently discovered and a focus of attention. This phenomenon is referred as promoter-proximal pausing of RNAPII. The poised state is a late step of the transcriptional initiation process, but instead of entering to the elongation state, the polymerase is stalled by negative factors, such as PRC2. This state is associated with the production of approximately 20 – 50 nucleotides nascent transcripts from these poised promoters. Further activation factors are required for the poised RNAPII to continue to transcribe. This phenomenon can occur both at highly active or at less transcribed genes. Studies of the pausing phenomenon have brought more insight to its functions within recent years. It is proposed as a checkpoint for transcription to ensure that the nascent RNA is protected and matures into fully functional mRNA. Moreover, establishment of poised RNAPII helps to maintain an open and accessible chromatin structure as a primed state for transcriptional bursting in response to signalling. Genome wide analysis showed a widespread of pausing RNAPII state in transcriptional regulation and its important roles during development, signalling and response to environmental stress (Adelman and Lis, 2012; Brookes and Pombo, 2012; Jadhav et al., 2016; Voigt et al., 2013).

### **1.3.6 Function of actin during transcription process**

Actin and myosin have been studied extensively for their roles in generating cytoskeleton and transduced mechanic forces in the cytoplasm. Interestingly, actin is constantly shuttled between the cytoplasm and the nucleus specifically in a complex with cofilin driven by importin-9 (IPO9), and vice versa in a complex with profilin by exportin-6 (XPO6). The cytoplasmic and nuclear pools of actin are dynamically connected, and the shuttling rate depends on the available of G-actin (Dopie et al., 2012; Stüven et al., 2003). Although the conformation of nuclear actin is unclear, it is suggested that a nuclear-base mechanism exists to regulate nuclear actin polymerization between monomeric G-actin and short oligomeric actin or even long actin fibers. The functions of each nuclear actin form are still uncharacterized, although cells treated with actin polymerization inhibitors exhibit disrupted nuclear actin functions. Since actin is present both in the cytoplasm and the nucleus, it is proposed to function as a sensor to transduce extrinsic stimuli to the genome and mediate gene expression (Dopie et al., 2012; Percipalle and Visa, 2006; Visa and Percipalle, 2010).

In 1984, for the first time, Jockush and Chambon showed a potential role of actin in gene transcription. Since 1998, several independent laboratories have reported that actin is indeed involved in many nuclear processes. G-actin has been identified as a structural component of ATP-dependent chromatin remodeling complexes, but its function within these complexes is unknown (Zhao et al., 1998). Actin can also be detected in ribonucleoprotein particles, and found at sites of active transcription. Importantly, actin has been shown to associate with all three RNA polymerases, and to be directly involved in transcriptional elongation (Kukalev et al., 2005; Percipalle, 2013). Collectively, although the role of nuclear actin is far from understood, it has been suggested to play various functions in the nucleus. Importantly, the nuclear actin pool is linked to the cytoplasmic actin, suggesting a novel role of nuclear actin in generating cellular responses to mechanical force-induced regulation of cytoplasmic actin remodeling.

## **2. Aims of the thesis**

Mechanotransduction is the process by which mechanical stimuli are sensed by the cell or its subcompartments, converted into biochemical signals, resulting in changes in cell behavior that can regulate a number of cellular signaling pathways. However, the molecular mechanisms underlying this process remain unclear. This study aimed to understand the role of extrinsic mechanical force in regulating epidermal progenitor cell (EPC) fate decisions as well as the responsible mechanosensitive pathways. In particular, I want to understand:

1. What is the impact of force on EPCs during their differentiation?
2. How can force be transmitted into the nucleus to drive transcriptional responses?
3. What is the biological consequence of mechanical force on skin homeostasis?

### 3. Methods

#### 3.1 Cell culture of EPCs

EPCs (human primary epidermal keratinocytes, CellnTec HPEKp) were grown in epithelial growing medium (CellnTec CnT-PR). EPCs were maintained on Collagen-I pre-coated 10 cm dish at a density of 25000 viable cells/cm<sup>2</sup> in a humidified chamber at 37°C and 5 % CO<sub>2</sub> until reach 70 – 90% confluent. To get single cell suspension, EPCs were rinsed once with 1X PBS and subjected to accutase cell detachment solution (Sigma A6964) for 10 min at 37°C. Detached EPCs were suspended in 3 volumes (V) of CnT-PR medium, followed by centrifugation at 300 x g for 5 min at room temperature (RT). For storage, EPCs were resuspended in CnT-PR medium with 10 % dimethyl sulfoxide (DMSO; Sigma C6164) at the concentration of 1 x 10<sup>6</sup> viable cells/ml. Cells were frozen down in cryovials (Thermo 368632) using freezing container (Thermo 5100-0001). EPCs were stored in liquid nitrogen tanks. For thawing, EPCs were thawed in 37°C water bath, subsequently diluted in 10 V of CnT-PR so that the final concentration of DMSO is less than 1 %. EPCs were then placed on the pre-coated 10-cm dish as described.

#### ***Collagen-I coating medium***

0.02 M        HEPES pH 7,3 (1 M stock, Roth 9105.4)  
0.25 ml        Collagen-I, rat tail 3 mg/ml (EMD Millipore 08-115)  
filled up with MEM (Spinners modified, Sigma M8167) to 25 ml.

#### ***10X PBS***

80 g        NaCl (Roth 3957.2)  
2 g        KCl (Roth 6781.1)  
14.4 g       Na<sub>2</sub>HPO<sub>4</sub> x H<sub>2</sub>O (Roth T877.1)  
2 g        KH<sub>2</sub>PO<sub>4</sub> (Roth 3904.1)  
filled up with milli-Q H<sub>2</sub>O to 1 L, adjusted pH to 7.4  
***1X PBS*** was diluted from 10X PBS with milli-Q water

### 3.2 Mechanical straining

For mechanical straining, EPCs were placed on a Collagen-I pre-coated silicon elastomeric membrane culture plate (Bioflex BF-3001U; FlexCell International Corporation) until 70 % confluent. After which, cells were switched to keratinocyte differentiation medium and exposed to extrinsic biaxial cyclic mechanical strain using the Flexcell Tension System (FX4000T; FlexCell International Corporation). The strain's parameters were set to 10 % elongation at 100 mHz frequency.

#### *Keratinocyte differentiation medium*

110 ml        *Ham's F12 (PAA E15-016)*  
5 ml         *Pen/Strep (100x, Gibco 15140-122)*  
50  $\mu$ l       *Hydrocortison (5 mg/ml, Calbiochem 386698)*  
5  $\mu$ l         *Cholera Toxin (1mg/ml, Sigma C8052)*  
1.8 mM      *CaCl<sub>2</sub> (stock 100 mM, Roth T885.2)*  
*filled up with MEM to 500 ml, and sterile filtered.*

### 3.3 RNA sequencing analysis and bioinformatics

RNA was isolated using the RNeasy Plus Mini Kit (QIAGEN 74134). After quantification and quality control of total RNA (Agilent 2200 TapeStation; RIN=10 for all samples), total RNA amounts were adjusted to equal levels after which ERCC ExFold RNA Spike-In Mixes (Ambion) were added to all samples according to the manufacturer's instructions. Libraries were prepared with NEBNext Ultra Directional RNA Library Prep Kit (New England Biolabs) followed by sequencing with HiSeq 2500 (Illumina) from 3 biological replicates. After preprocessing and read mapping, read counts were normalized to ERCC reference RNAs after which differential gene expression was analyzed using the DESeq2 R library (R 3.2.0, DESeq2 version 1.8.1). Alternatively, differential gene expression was analyzed directly using DESeq2 without ERCC reference RNAs.

The quality of the data was analyzed using fastqc (version 0.11.2) after which adapters were removed using cutadapt (version 1.5). To allow the mapping of the spike-Ins, the

ERCC sequences were added to the human genome and were indexed together. The fastq files were subsequently mapped to the combined ERCC and Homo sapiens genome (build GRCh37) using the tophat2 algorithm (version v2.0.13) allowing unique mapping. Reads were counted from the bam files on exon-level based on the gene annotation from Ensembl using the feature counts algorithm from the SubRead software package (version 1.4.2), resulting in a read count for each gene. To correct for potential transcriptional bias the normalization size factors of the ERCC samples were calculated using DESeq2 (R 3.2.0, DESeq2 version 1.8.1). The count data was then normalized by the same size factors to estimate the effective library size. After calculating the gene dispersion across all samples, the comparison of two different conditions resulted in a list of differentially expressed genes. Genes with an adjusted p-value  $\leq 0.05$  were considered significant. Estimation of global polyA+ RNA expression was carried out using the erccdashboard package (Bioconductor).

Gene set enrichment analysis was performed on a pre-ranked gene list (ranked according to log<sub>2</sub> fold change) and compared to the Broad Institute Molecular Signatures Database collection of chemical and genetic perturbations (C2 CGP, a total of 3395 gene sets) using the web-based tool available from the Broad Institute. Enrichments with an FDR value  $< 0.25$  were considered significant. Gene set enrichment analysis was performed on a pre-ranked gene list (ranked according to log<sub>2</sub> fold change) and compared to the Broad Institute Molecular Signatures Database collection of chemical and genetic perturbations (C2 CGP, a total of 3395 gene sets) using the web-based tool available from the Broad Institute. Enrichments with an FDR value  $< 0.25$  were considered significant.

### **3.3 Chemical treatments**

Where indicated, EPCs were treated with 5,6-dichlorobenzimidazole 1- $\beta$ -D-ribofuranoside (DRB; 100  $\mu$ M; Sigma D1916) for 12 h. Blebbistatin (10  $\mu$ M; Sigma B0560) or Cytochalasin D (100 nM; Sigma C8273) were added directly prior to mechanical straining. The vehicle DMSO was used as a control for all treatments.

### **3.4 Biochemical fractionations, immunoprecipitation and western blotting**

#### **3.4.1 Preparation of histones**

Cells were harvested in 1X phosphate buffered saline (PBS) by scraping, followed by centrifugation at 1000 x g for 10 min at 4°C. The pellet was resuspended in lysis buffer (0.5% Triton X-100 (Roth 3051.2) in 1X PBS with protease inhibitors). Cells were lysed for 30 min on ice and followed by centrifugation at 2000 x g for 10 min at 4°C. The pellet was rinsed once with lysis buffer after which histones were extracted overnight in 0.2 N HCl (Sigma H1758) at 4°C. Samples were neutralized by adding 1/5 volume of 1 M NaOH (Merk 106482) and cleared by centrifugation max speed for 10 min at 4°C. Histones were analyzed by western blot.

#### **3.4.2 Determining G- to F-actin ratio**

Cells were harvested in cytoskeleton-stabilizing lysis buffer. After centrifugation at 4°C for 60 min at 150 000 x g, the supernatant was collected as the G-actin fraction. The pellet was solubilized in actin depolymerizing buffer, followed by sonication and used as the F-actin fraction. Samples were analyzed by western blot.

##### ***Cytoskeleton-stabilizing lysis buffer***

<i>50 mM</i>	<i>PIPES, pH 6.9 (Sigma P8203)</i>
<i>50 mM</i>	<i>NaCl (Roth 3957.2)</i>
<i>5 mM</i>	<i>MgCl<sub>2</sub> (Roth KK36.3)</i>
<i>5 mM</i>	<i>EGTA (Sigma E3889)</i>
<i>0.2 mM</i>	<i>DTT (Sigma 43815)</i>
<i>0.1%</i>	<i>NP40 (Sigma I18896)</i>
<i>0.1%</i>	<i>Tween 20 (Sigma P1379)</i>
<i>5%</i>	<i>glycerol (Roth 7533.3)</i>
<i>1 mM</i>	<i>ATP (Cayman Chemical I4498)</i>
	<i>EDTA-free protease inhibitors cocktail (Roche 04693159001)</i>

##### ***Actin depolymerizing buffer***

<i>50 mM</i>	<i>PIPES, pH 6.9 (Sigma P8203)</i>
<i>5 mM</i>	<i>MgCl<sub>2</sub> (Roth KK36.3)</i>

10 mM *CaCl<sub>2</sub>* (Roth T885.2)  
5 μM *Cytochalasin D* (Sigma C8273)  
*EDTA-free protease inhibitors cocktail* (Roche 04693159001)

### 3.4.3 Nuclear fractionation

Cells were harvested in 1X PBS by scraping and centrifuged at 1000 x g for 10 min at 4°C. The cell pellet was incubated at -80°C for 45 min, and subsequently resuspended in ice-cold buffer A. Samples were vortexed for 30 s and centrifuged at 2000 x g for 10 min at 4°C. The supernatant was collected as the cytoplasmic fraction. The pellet containing the nuclei was resuspended in ice-cold buffer B, and homogenized by passing through a 20 G needle. After rotation for 90 min at 4°C, insoluble material in the nuclear fraction was removed by sedimentation at maximum speed for 30 min at 4°C. Samples were analyzed by western blot.

#### ***Buffer A***

10 mM *HEPES* (1 M stock, Roth 9105.4)  
1.5 mM *MgCl<sub>2</sub>* (Roth KK36.3)  
10 mM *KCl* (Roth 6781.1)  
0.5 mM *DTT* (Sigma 43815)  
0.05% *NP40, pH 7.9* (Sigma I18896)  
*EDTA-free protease inhibitors cocktail*

#### ***Buffer B***

5 mM *HEPES* (1 M stock, Roth 9105.4)  
1.5 mM *MgCl<sub>2</sub>* (Roth KK36.3)  
0.2 mM *EDTA* (Roth CN06.3)  
0.5 mM *DTT* (Sigma 43815)  
26% *glycerol* (Roth 7533.3)  
500 mM *NaCl* (Roth 3957.2)  
*pH was adjusted to 7.9*  
*EDTA-free protease inhibitors cocktail*

### 3.4.5 Immunoprecipitation

Cells were harvested in IP lysis buffer and cleared by centrifugation max speed for 5 min at 4°C. After which the supernatant was split equally into 2 parts for immunoprecipitation, and 10% of cell lysate was kept as input. Antibodies against Emerin (Leica Emerin-CE; 1:100, Cell Signaling 2659; 1:100) were added to the cell lysate and incubated for 3 h at 4°C. Isotype-matched IgG antibodies (Cell Signaling 2759 and 5415) were used as a negative control. Lysates were then incubated with pre-washed protein G-agarose beads (Roche 11243233001) for 30 min at 4°C. After 3x washing with IP lysis buffer, proteins were eluted by laemmli buffer at 95°C for 10 min and analyzed by western blotting.

#### *IP lysis buffer*

150 mM	NaCl (Roth 3957.2)
50 mM	Tris-HCl, pH 7.4 (1 M Stock, Roth 9090.3)
1 mM	EDTA pH 8.0 (Roth CN06.3)
0.5%	Triton X-100 (Roth 3051.2)
<i>EDTA-free protease inhibitors cocktail</i>	
<i>Phosphatase Inhibitor Cocktail (Roche 04906837001)</i>	

#### *4x laemmli buffer*

125 mM	Tris-HCl, pH 6.8
4 %	SDS (Roth CN30.1)
50 %	glycerol
0.2 %	bromphenol blue (Roth T116.1)
5 %	2-mercaptoethanol (Roth 4227.3), freshly added prior to use

### 3.4.6 Western blotting

#### **Equipments**

Electrophoresis chambers: Mini-PROTEAN Tetra Cell System, Biorad

Protein transfer system: Trans-Blot Turbo Transfer System, Biorad

Developing system: Curix 60, Agfa

Microplate spectrophotometer: TECAN Infinite M200

### **Quantification of protein concentration**

Protein concentration was determined using Bradford assay (self-made). In principle, coomassie dye binds to protein under acidic condition, thereby results in an absorbance shift of the dye. The coomassie-bound protein has a maximum absorbance at 595 nm. Protein concentration is calculated according to a series of protein standard (albumin, Pierce 23209). The absorbance was measured using a spectrophotometer.

### **SDS-polyacrylamide gel electrophoresis**

This method is used to separate a mixture of denatured and negatively charged protein based on their molecular weight. The gels were cast as described below. After polymerization, denatured samples were loaded, and electrophoresis was carried on at 120 V. Samples were denatured in Laemmli buffer (stock 4x) at 95°C for 10 min.

### **Western blotting**

Separated proteins by SDS-PAGE were transferred onto a Polyvinylidene fluoride membrane (Immobilon-P PVDF transfer membrane, Millipore IPVH00010). The PVDF membrane was activated by incubation in methanol for 10 min, followed by washing in blotting buffer. The membrane and SDS gel were assembled into a sandwich and transferred onto the turbo blot machine. Proteins were transferred at 25 V, 0.3 A for 60 min at RT. After transfer, the membrane was stained with Ponceau red solution (Sigma P7170) to check the quality of transferred process. The membrane was then washed in TBS-T and blocked with 5% milk (Roth T145.2) or bovine serum albumin (BSA, Serva 11930.03) in TBS-T, according to primary antibody instruction for 30 min. Then, specific primary antibodies were applied overnight at 4°C. The membrane was then washed with TBS-T several times and subjected to secondary antibodies conjugated with HRP for 30 min at RT, followed by washing steps with TBS-T. Protein signals were detected using chemiluminescence HRP substrate (Millipore WBKLS0500) and exposed on X-ray film (Thermo 34089).

### **Bradford solution**

100 mg                      *Coomassie Brilliant Blue G250 (Sigma 27815)*

50 ml                        *Ethanol (Sigma 32205)*

100 ml                      *Phosphoric acid (Roth 2608.1)*

*filled up to 1000 ml with milli-Q water*

*filtered through Whatman #1 paper*

### **10x SDS Running buffer**

30.3 g                        *Tris base (Roth 4855.3)*

144.2 g                      *glycine (Roth 3908.3)*

50 ml                        *20 % SDS*

*filled up to 1000 ml with milli-Q water*

### **Stacking gel**

2.75 ml                      *milli-Q water*

3.5 ml                        *0,5 M Tris-HCl, 0,4 % SDS, pH 6,8*

0.8 ml                        *acrylamide (Roth 3029.1)*

93.8 µl                      *10 % APS (Roth 9592.1)*

9.8 µl                        *TEMED (Roth 2367.1)*

### **Separating gel**

2 ml                         *milli-Q water*

5.4 ml                        *acrylamide*

8.4 ml                        *1.5 M Tris-HCl, 0.4 % SDS, pH 8.8*

135 µl                        *10 % APS*

13,5 µl                        *TEMED*

### **10X blotting buffer**

30.3 g                        *Tris base*

144.1 g                      *glycine*

*filled up to 1000 ml with milli-Q water, store at 4°C*

*1X blotting buffer was diluted from 10X blotting buffer and supplemented with 20 % methanol (Sigma 32213), stored at 4 °C*

### **10X TBS**

60.5 g      *Tris base*

87.6 g      *NaCl*

*filled up to a final volume of 1000 ml distilled water and adjusted pH to 7.5*

*1X TBS was diluted from 10X TBS and 0.1 % Tween20 was added*

### **Primary antibodies**

<b>Name</b>	<b>Company</b>	<b>Cat. No.</b>	<b>Dilution</b>
<i>Actin</i>	<i>Sigma</i>	<i>A2066</i>	<i>1:1000</i>
<i>Emerin</i>	<i>Leica</i>	<i>Emerin-CE</i>	<i>1:5000</i>
<i>GAPDH</i>	<i>Calbiochem</i>	<i>1001</i>	<i>1:10000</i>
<i>H3K27me3</i>	<i>Cell Signaling</i>	<i>9733</i>	<i>1:5000</i>
<i>H3K9me2,3</i>	<i>Cell Signaling</i>	<i>5327</i>	<i>1:5000</i>
<i>Lamin A/C</i>	<i>Cell Signaling</i>	<i>4777</i>	<i>1:1000</i>
<i>Loricrin</i>	<i>Covance</i>	<i>PRB-145P</i>	<i>1:1000</i>
<i>NMIIA</i>	<i>Covance</i>	<i>PRB-440P</i>	<i>1:1000</i>
<i>P-MLC (Thr18/Ser19)</i>	<i>Cell Signaling</i>	<i>3674S</i>	<i>1:1000</i>
<i>Periplakin</i>	<i>Santa Cruz</i>	<i>sc50449</i>	<i>1:1000</i>
<i>RNAPII-S2p</i>	<i>Abcam</i>	<i>ab5095</i>	<i>1:1000</i>
<i>Total H3</i>	<i>Cell Signaling</i>	<i>3638</i>	<i>1:5000</i>
<i>Transglutaminase 1</i>	<i>Abcam</i>	<i>ab103814</i>	<i>1:1000</i>

### **Secondary antibodies**

<b>Name</b>	<b>Conjugate</b>	<b>Company</b>	<b>Cat. No.</b>
<i>Goat anti-mouse IgG</i>	<i>HRP</i>	<i>BioRad</i>	<i>170-6516</i>
<i>Goat anti-rabbit IgG</i>	<i>HRP</i>	<i>BioRad</i>	<i>170-6515</i>

## **3.5 FACS analysis of apoptosis and proliferation**

Fluorescence-activated cell sorting (FACS) is a method to detect and quantify a specific cell type from a mixed cell suspension. In principle, cells can be detected by their size, expression of genetically engineered fluorescent proteins or cell surface markers.

Apoptotic cells were detected by incubation with Annexin-V-FITC antibodies (Abcam 14085; 1:100) for 30 min at 4°C. This method is based on the binding of Annexin-V to phosphatidyl serine (PS) at the outer cellular membrane. In normal cells, PS resides at the cytoplasmic side of the plasma membrane, however, in apoptotic cells, PS is translocated to the outer surface of cellular membrane, thus can be detected by Annexin-V, followed by FACS using a FACSCanto II cytometer equipped with FACSDiva Software (BD).

For measuring proliferation, 5-ethynyl-2'-deoxyuridine (EdU, Invitrogen E10187) was added to the culture medium at the onset of straining. EdU is a nucleoside analog of thymidine and is incorporated into DNA during DNA synthesis. It can be detected in a reaction with azide, catalyzed by copper-I, known as “click” reaction. The product is a stable triazole ring, conjugated to a fluorophore. Single-cell suspensions were incubated in EdU staining solution for 30 min at room temperature, followed by FACS. Cell viability was assessed by FVD eFluor506 (eBioscience 65-0866; 1:1000).

#### ***EdU staining solution***

<i>100 mM</i>	<i>Tris pH 8.5</i>
<i>1 mM</i>	<i>CuSO<sub>4</sub></i>
<i>100 mM</i>	<i>ascorbic acid</i>
<i>0.5 μM</i>	<i>488-Azide (Invitrogen A10266)</i>

### **3.6 qPCR**

Quantitative real-time polymerase chain reaction (q-PCR) is a PCR-based method that detects and visualizes the amplified DNA product using fluorescent dyes in real time. This method was used to quantitatively measure gene expression at the RNA level. Firstly, RNA was isolated using the RNeasy Plus Mini Kit (QIAGEN 74134). After quantification and quality control, cDNA was synthesized using the High-Capacity cDNA Reverse Transcription Kit (Applied Biosystems 4368814). qPCR was performed on the StepOne Plus Real Time PCR System (Applied Biosystems 4376600) or CFX384 Touch Real Time PCR Detection System (Bio-Rad 1855485) using the DyNAmo ColorFlash SYBR Green Mix (Thermo F416). Gene expression

changes were calculated following normalization to *S26* or *Gapdh* using the comparative Ct (cycle threshold) method with primer efficiency correction.

Efficiency (E) was calculated from the slopes of a cDNA dilution (1:5, 1:10, 1:20) calibration curve according to the equation:  $E = 10^{(-1/\text{slope})}$

The calculation of the ratio was made according to the equation:

$$\text{Ratio} = ((E_{\text{target}})^{\Delta\text{Ct}_{\text{target}}(\text{control-sample})}) / ((E_{\text{reference}})^{\Delta\text{Ct}_{\text{reference}}(\text{control-sample})})$$

$\Delta\text{Ct}$  = crossing point difference of cyclic threshold

#### ***cDNA synthesis reaction (Applied Biosystems 4368814)***

2  $\mu\text{l}$             10x RT Buffer  
2  $\mu\text{l}$             10x random primer  
0.8  $\mu\text{l}$         25x dNTPs (100 mM)  
1  $\mu\text{l}$             reverse transcriptase  
0.5  $\mu\text{g}$         RNA  
*adjusted to 20  $\mu\text{l}$  with RNase-free water*

#### ***cDNA synthesis program***

25 °C        10 min  
37 °C        2 h  
85 °C        5 min  
*hold at 4 °C, cDNA was stored at -20 °C*

#### ***qPCR reaction***

*(Measurements were always performed in triplicates or quadruplicates)*

5  $\mu\text{l}$             2X SYBR Green (DyNAmo Color Flash, Thermo F-416)  
0.5  $\mu\text{l}$         primers (10  $\mu\text{M}$ )  
0.5  $\mu\text{l}$         cDNA (diluted 1:5)  
4  $\mu\text{l}$             nuclease-free water

**List of oligonucleotides used for qPCR**

<i>Species</i>	<i>Target</i>	<i>Forward</i>	<i>Reverse</i>
<i>h</i>	<i>CRCT1</i>	<i>TCGGAGTTTGCCCCGTAAG</i>	<i>AAATCACATCGGGGTCAGGG</i>
<i>h</i>	<i>EMD</i>	<i>ATTCCCAGATGCTGACGCTT</i>	<i>TGATGCTCTGGTAGGCACTG</i>
<i>h</i>	<i>EZH2</i>	<i>TCATGCAACACCCAACACTT</i>	<i>TTGGTGGGGTCTTTATCCGC</i>
<i>h</i>	<i>FLG</i>	<i>GAGGGCACTGAAAGGCAAAA</i>	<i>CTTCCGTGCTGAGAGTGTCT</i>
<i>h</i>	<i>HOXA5</i>	<i>TCTCGTTGCCCTAATTCATCTTT</i>	<i>CATTCAGGACAAAGAGATGAACAGAA</i>
<i>h</i>	<i>HOXA9</i>	<i>CTGTCCCACGCTTGACACTC</i>	<i>ATAGGGGCACCGCTTTTTCC</i>
<i>h</i>	<i>HOXA13</i>	<i>GGAACGGCCAAATGTACTGC</i>	<i>ATTCGTGGCGTATTCCCGTT</i>
<i>h</i>	<i>HOXD10</i>	<i>GAAGATGAACGAGCCCGTGA</i>	<i>GAGCCAATTGCTGGTTGGTG</i>
<i>h</i>	<i>IPO9</i>	<i>ATGCCACTTGTTGCTCCTGT</i>	<i>GAACTGCTGTACCACGGGAA</i>
<i>h</i>	<i>KRT14</i>	<i>GAGGACGCCACCTCTCCTCCT</i>	<i>CGAAGGACCTGCTCGTGGGTG</i>
<i>h</i>	<i>LCE1A</i>	<i>CCTAGAAGAGCAGACTCGGG</i>	<i>GGGCATCTCAGCCACTCTTG</i>
<i>h</i>	<i>LOR</i>	<i>CTCACCTTCCTGGTGCTTT</i>	<i>GGGTGGGCTGCTTTTTCTGA</i>
<i>h</i>	<i>PPL</i>	<i>GAGAATGGAAGGAGCAGCCA</i>	<i>GGGTCATTCTACTTCCGGC</i>
<i>h</i>	<i>S26</i>	<i>GCGAGCGTCTTCGATGCCTATGT</i>	<i>GGGGGTGTTCCGGTCCTTGCG</i>
<i>h</i>	<i>SOX1</i>	<i>CAGCCTTAGGTTTCCCTCG</i>	<i>AGGCTCACTTTTGACGGAC</i>
<i>h</i>	<i>SOX2</i>	<i>GGCAGAGAAGAGAGTGTGGC</i>	<i>CGCCGCCGATGATTGTTAT</i>
<i>h</i>	<i>SPRR2D</i>	<i>TCGTTCCACAGCTCCACTTG</i>	<i>CAGGCCACAGGTTAAGGAGA</i>
<i>h</i>	<i>TGM1</i>	<i>ACACCCCAAGAGACTAGCAG</i>	<i>GCAAAAATGAAAGGCGTGTCG</i>
<i>h</i>	<i>XPO6</i>	<i>CGGTACTTACGGCAGAGCTT</i>	<i>TTCTCCGCCGTGATGTTCAA</i>
<i>m</i>	<i>Cret1</i>	<i>ACTGCACTTTGATGTTCA</i>	<i>CAGGAGGCCTGTTTTGAA</i>
<i>m</i>	<i>Flg</i>	<i>TGGCCGCAACTCAACCAA</i>	<i>GGATCCGGCCTTTCCAGAAT</i>
<i>m</i>	<i>HoxA9</i>	<i>AGTTCTCTCCTTGGCGGTTG</i>	<i>AATGGGCTACCGACCCTAGT</i>
<i>m</i>	<i>HoxA11</i>	<i>CTCACCGACCGTCAAGTCAA</i>	<i>CCCTCCCAATTCCAGTAGGC</i>
<i>m</i>	<i>HoxA13</i>	<i>GAACGGCCAAATGTACTGCC</i>	<i>CTGAAGGATGGGAGACGACG</i>
<i>m</i>	<i>HoxB13</i>	<i>CCAGCCTATGGCCAGTTACC</i>	<i>GACTGTTGGCTCTGCAAAC</i>
<i>m</i>	<i>HoxD10</i>	<i>CAGGAGAAGGAAAGCAAAGAGG</i>	<i>CAATTCCAGCGTTTGGTGCT</i>
<i>m</i>	<i>Gapdh</i>	<i>GGTGTGAACGGATTTGGCCGATTG</i>	<i>CCGTTGAATTTGCCGTGAGTGGAGT</i>
<i>m</i>	<i>K14</i>	<i>ATCGAGGACCTGAAGAGCAA</i>	<i>TCGATCTGCAGGAGGACATT</i>
<i>m</i>	<i>Lcel1a</i>	<i>CACTTTAGACAAACCATTTCAGGAGAA</i>	<i>CCAAGAAGACAAACCCAGCAA</i>
<i>m</i>	<i>Lcelc</i>	<i>AGATCTCAAACATTCTATGCAGAGGA</i> <i>A</i>	<i>TCACAAAATACTGAAGAAGAAAGGGA</i> <i>TT</i>
<i>m</i>	<i>Lcell</i>	<i>CATGAAGGCTTCAGACAAGCAAT</i>	<i>TTGGAATCACAGAAGGAGATGAGAC</i>

<i>m</i>	<i>Lce1m</i>	<i>AGCATTGACTGAAGACCTGCAA</i>	<i>GCAAAGCCAATGCATCTCAGA</i>
<i>m</i>	<i>Lor</i>	<i>AAGTAAGGTCACCGGGTTGC</i>	<i>GGGAAGGGGCGCTTAAAATG</i>
<i>m</i>	<i>Myh9</i>	<i>GTCCACTCGGAAGAACCAGC</i>	<i>TGGAAGGCACCCATACCAAC</i>
<i>m</i>	<i>Ppl</i>	<i>CCGAGAGTCAACTGGGACAC</i>	<i>CACTGTTCTGCTCCTTGTCTT</i>
<i>m</i>	<i>Sox1</i>	<i>GTACAGCCCCATCTCCAAC</i>	<i>CTCCGACTTGACCAGAGATCC</i>
<i>m</i>	<i>Sox2</i>	<i>TAGAGCTAGACTCCGGGCGATGA</i>	<i>TTGCCTTAAACAAGACCACGAAA</i>
<i>m</i>	<i>Sprr1a</i>	<i>TCTCTGAGTATTAGGACCAAGTGC</i>	<i>CTTGGTTTTGGGGGCACAAG</i>
<i>m</i>	<i>Sprr2f</i>	<i>GAGAACCTGATCCTGAGGCTT</i>	<i>CACACCGAGGGAGAACAAGG</i>
<i>m</i>	<i>Tgml</i>	<i>CTGGCGGCAAGAATATGTGC</i>	<i>AGGTTCGTTGCGCCAATCTGT</i>

### 3.7 ChIP analyses

Chromatin immunoprecipitation (ChIP) is a method to detect a transcription factor, cofactor, or any protein associated with DNA. The associated DNA sites can be identified by qPCR method. In brief, 10<sup>6</sup> EPCs were crosslinked by 1% formaldehyde (Roth 7398.1) for 10 min at 37°C, followed by quenching with glycine to a final concentration of 0.125 M. Subsequently cells were rinsed twice with ice-cold 1X PBS and harvested in 1 ml ChIP lysis buffer by using a cell scraper. Cells were subjected to sonication (Covaris M220 ultrasonicator) at 15% of duty factor in 12 min at 4°C to fragment DNA (200-800 bp). After centrifugation (max speed for 10 min at 4°C), the supernatant was split equally into 2 parts for immunoprecipitation. 10% of cell lysate was kept as input. 4 µg antibody were added to cell lysate and an isotype-matched IgG (Cell Signaling 2759 and 5415) was used as a negative control. Samples were rotated gently overnight at 4°C.

Nest day, samples were incubated with ChIP-Grade Protein A/G magnetic beads (Thermo 26162) for 1 h at 4°C, and subsequently washed 2 times for 5 min each in following buffers: high salt washing buffer, LiCl washing buffer and TE buffer. Chromatin was then eluted in 200 µl of elution buffer for 20 min rotation at RT. After which, immunoprecipitated DNA and input DNA were decrosslinked with NaCl (50 mM final concentration) at 65°C overnight.

1  $\mu$ l of RNaseA (Thermo EN0531) was added and incubated at 37°C for 1 hour, followed by 1  $\mu$ l of Proteinase K (QIAGEN 19131) at 55°C for 30 min. 5  $\mu$ l of ChIP DNA binding buffer (~ 1000  $\mu$ l, Zymo Research D5201) was mixed well with each sample and loaded on Zymo spin column (Zymo Research C1003). After centrifugation (max speed, 1 min), the column was washed once with DNA wash buffer (Zymo Research D4003-2). After which, DNA was eluted by 50  $\mu$ l of milli-Q water, and stored at -20°C.

ChIP DNA was analyzed by qPCR. Fold enrichment was calculated by first normalizing ChIP DNA to input DNA to get the enrichment as percentage of input. This was then normalized to the percentage input of a negative control gene region (intergenic region of chromosome 10 for RNAPII-S2p-ChIP, S26 for H3K27me3- and H3K9me2,3-ChIP; intergenic region of chromosome 5 for H3K27me3-ChIP in mouse) to correct for experiment-to-experiment variation. RNAPII-S2p antibody (ab5095) was from Abcam, H3K27me3 (9733), H3K9me2,3 (5327) and isotype-specific IgG control (2729 and 5415) were from Cell Signaling.

% input was calculated according to the equation:

$$\% \text{ input} = 2^{-\Delta C_t} \times 100$$

$$\Delta C_t = C_t_{\text{ChIP DNA}} - (C_t_{\text{input}} - DF)$$

$$DF \text{ (dilution factor)} = \log_2 (10\%)$$

***ChIP Lysis Buffer:***

50 mM                      *Tris-HCl, pH 8.0*

10 mM                      *EDTA, pH 8.0*

1%                              *SDS (stock 20%)*

*EDTA-free protease inhibitors cocktail (Roche 04693159001)*

***ChIP dilution buffer:***

20 mM                      *Tris-HCl, pH 8.0*

2 mM                        *EDTA, pH 8.0*

150 mM                      *NaCl*

1%                              *TritonX-100*

**High salt washing buffer:**

20 mM	Tris-HCl, pH 8.0
2 mM	EDTA, pH 8.0
500 mM	NaCl
1%	TritonX-100
0,1%	SDS

**LiCl washing buffer:**

0,25 M	LiCl (Roth P007.1)
10 mM	Tris-HCl, pH, 8.0
1 mM	EDTA, pH 8.0
1%	NP40
1%	deoxycholic acid (Roth 3484.3)

**TE buffer**

10 mM	Tris-HCl, pH 8.0
1 mM	EDTA, pH 8.0

**Elution buffer (fresh):**

0,1 M	NaHCO <sub>3</sub> (Roth 6885.1)
1%	SDS

**3.8 FAIRE**

Formaldehyde-Assisted Isolation of Regulatory Elements (FAIRE) is a method to determine nucleosome-depleted regions in the genome. Cells were fixed in 1% formaldehyde for 10 min after which cells were lysed in ChIP lysis buffer and sonicated (see 3.6). An aliquot of the lysate (10%) was collected from which crosslinks were reversed and input DNA was purified by using Zymo-Spin column. Phenol/chloroform was added to the remaining lysate and the sample was rigorously vortexed for 10 s, followed by centrifugation at max speed for 5 min. The aqueous phase was collected and the FAIRE DNA was purified. FAIRE enrichment was

analyzed by qPCR and normalized to the input DNA of the specific target gene (see 3.6). Primers against intergenic regions on chromosomes 10 and 19 were used as negative controls.

**List of oligonucleotides used for ChIP qPCR and FAIRE-qPCR**

<i>Species</i>	<i>Target</i>	<i>Forward</i>	<i>Reverse</i>	<i>Application</i>
<i>h</i>	<i>ACTIN</i>	<i>ACATCTCTTGGGCACTGAGC</i>	<i>AGGGCAGTTGCTCTGAAGTC</i>	<i>H3K27me3</i>
<i>h</i>	<i>ACTIN</i>	<i>CGGACTCGTCATACTCCTGC</i>	<i>GTCCCCTCCCTCCTCAGAT</i>	<i>RNAPII-S2p,</i> <i>FAIRE</i>
<i>h</i>	<i>B2M</i>	<i>GGGGCACCATTAGCAAGTCA</i>	<i>GCTGGAGGCACATTAAGGCT</i>	<i>H3K27me3</i>
<i>h</i>	<i>B2M</i>	<i>CTGGCTTGGAGACAGGTGAC</i>	<i>GACTCACGCTGGATAGCCTC</i>	<i>RNAPII-S2p</i>
<i>h</i>	<i>CDKN2a</i>	<i>TGAAAACCTCCCAGGAAGCC</i>	<i>GATCCAGGTGGGTAGAGGG</i> <i>T</i>	<i>H3K27me3</i>
<i>h</i>	<i>CDKN2a</i>	<i>GCTTTGGAAGCTCTCAGGGT</i>	<i>GCACCAGAGGCAGTAACCAT</i>	<i>RNAPII-S2p</i>
<i>h</i>	<i>Chr10</i> <i>(LADs)</i>	<i>AGGCCAGTG TAGGTCATTGC</i>	<i>GTGGTTTCCGAGGCTCTTCA</i>	<i>RNAPII-S2p,</i> <i>FAIRE,</i> <i>H3K9me2,3</i>
<i>h</i>	<i>Chr19</i> <i>(LADs)</i>	<i>CCTCCAGCCCCTACCATAGA</i>	<i>TGCAACTGTCCCACACTGTT</i>	<i>FAIRE,</i> <i>H3K9me2,3</i>
<i>h</i>	<i>CRCT1</i>	<i>GTGCATCCCCGTCATCATCT</i>	<i>TATGCGATAAGCCTGCTGGG</i>	<i>H3K27me3,</i>
<i>h</i>	<i>CRCT1</i>	<i>GCCAGGCTGACTTG TACTACT</i>	<i>GCGCTCTGTTGAGAGGACAT</i>	<i>RNAPII-S2p,</i> <i>FAIRE</i>
<i>h</i>	<i>GAPDH</i>	<i>CACAGTCCAGTCCTGGGAAC</i>	<i>TAGTAGCCGGGCCCTACTTT</i>	<i>H3K27me3</i>
<i>h</i>	<i>GAPDH</i>	<i>GGGAGGTAGAGGGGTGATGT</i>	<i>ATGGCATGGACTGTGGTCTG</i>	<i>RNAPII-S2p,</i> <i>FAIRE</i>
<i>h</i>	<i>HOXA13</i>	<i>AGTGGGGACAGGTCAGGTAA</i>	<i>GAGGCTCCAAGAAACACCCA</i>	<i>H3K27me3</i>
<i>h</i>	<i>HOXA13</i>	<i>TTGGGGGTTGACGTTTGACA</i>	<i>ACTGGCATTTCCTCTCCCG</i>	<i>RNAPII-S2p,</i> <i>FAIRE</i>
<i>h</i>	<i>HOXD10</i>	<i>GGTAGACTCCCCATTTGCC</i>	<i>TCACCCCGGATTAGGGTTCT</i>	<i>H3K27me3</i>
<i>h</i>	<i>HOXD10</i>	<i>ATGCAAACCTGTGGACTGCT</i>	<i>TGGTGGTGAAGGAGCAAGT</i> <i>G</i>	<i>RNAPII-S2p,</i> <i>FAIRE</i>
<i>h</i>	<i>KLK8</i>	<i>CCAGACTGCTGGATCTCGAC</i>	<i>GATACAGACATCAGGCCCCCG</i>	<i>H3K27me3</i>

<i>h</i>	<i>KLK8</i>	<i>TGGCTCCCAATCCGTAGAGA</i>	<i>CACACATCCCTCATTGCCCT</i>	<i>RNAPII-S2p, FAIRE</i>
<i>h</i>	<i>LCE1A</i>	<i>AGAGGGAGCTTCACTAGGCA</i>	<i>GAGCTTCCCAGATGGCTGTA</i>	<i>H3K27me3</i>
<i>h</i>	<i>LCE1A</i>	<i>TTCAGCTCCTGAACACCCAC</i>	<i>TGACACTGCAGCAGGAAGA G</i>	<i>RNAPII-S2p, FAIRE</i>
<i>h</i>	<i>LOR</i>	<i>AGGTTTAGAGCATTGCCCCG</i>	<i>ACTGCTGGGAGCTAGGAAGT</i>	<i>H3K27me3</i>
<i>h</i>	<i>LOR</i>	<i>GAGGATGGCGATGTTGCCTA</i>	<i>TGGAAGGGGAGAAGAGAGC A</i>	<i>RNAPII-S2p, FAIRE</i>
<i>h</i>	<i>PPL</i>	<i>TGTGGCTGTGCTCATTCTGT</i>	<i>GCCATTGGTCCCAGATCTCC</i>	<i>H3K27me3</i>
<i>h</i>	<i>PPL</i>	<i>TGAGGGAGAGACATGGCAGA</i>	<i>GCCTGAAGGGGTACAGGAA C</i>	<i>RNAPII-S2p, FAIRE</i>
<i>h</i>	<i>Major satellite 1</i>	<i>CACTGTGAGATGAATGCAAACG</i>	<i>GGCTGTGGTGCAAAAGGAAA TG</i>	<i>H3K9me2,3</i>
<i>h</i>	<i>Major satellite 2</i>	<i>GCTGGCAGATTCCACAGAAAC</i>	<i>AATTGGATCGCTTGGATGCC</i>	<i>H3K9me2,3</i>
<i>h</i>	<i>S26</i>	<i>TGCTGGAGGGAAGGTGAATC</i>	<i>AGCATTACAGACCCAGGATGG</i>	<i>FAIRE</i>
<i>h</i>	<i>SOX1</i>	<i>GCCTCCTTAACTGTGGCCT</i>	<i>ACTCTGCCCTGTCTTTCGTG</i>	<i>H3K27me3</i>
<i>h</i>	<i>SOX1</i>	<i>ATCCTCTCCGTCTCCCTCC</i>	<i>ATCATGCTGTACATCGGGGC</i>	<i>RNAPII-S2p, FAIRE</i>
<i>h</i>	<i>SOX2</i>	<i>TTGAAACTGGGGCAAGGTT</i>	<i>ACACGGTTTCTGAGCCAACA</i>	<i>H3K27me3</i>
<i>h</i>	<i>SOX2</i>	<i>TTGTCTGGAGACGGAGAAGC</i>	<i>GGGCAGCGTGTACTTATCCT</i>	<i>RNAPII-S2p, FAIRE</i>
<i>h</i>	<i>TGM1</i>	<i>ATGAAGAAGCTGCAAGGGCA</i>	<i>CTGGGCAGGATGAGTTCCA G</i>	<i>H3K27me3</i>
<i>h</i>	<i>TGM1</i>	<i>GTGAGTACCATCCAACCGGA</i>	<i>TGCACCACCTGTCTTGTGAG</i>	<i>RNAPII-S2p, FAIRE</i>
<i>m</i>	<i>Crct1</i>	<i>TCTGCCTAGCAGGTGTCAAGTT C</i>	<i>GCTACATTCTGGCTGCATCC TACT</i>	<i>H3K27me3</i>
<i>m</i>	<i>Chr5</i>	<i>AGGCTCTTGTGGCTTCCAGAT</i>	<i>CACCTGGCCCTGTCCTGTA</i>	<i>H3K27me3 (negative control)</i>
<i>m</i>	<i>Flg</i>	<i>TCCCTTTTACAGGTGCATACACA C</i>	<i>CCTCCTTATCACTGGTTGAG TATTGTT</i>	<i>H3K27me3</i>
<i>m</i>	<i>Lce1m</i>	<i>AGCATTGACTGAAGACCTGCAA</i>	<i>GCAAAGCCAATGCATCTCAG A</i>	<i>H3K27me3</i>

<i>m</i>	<i>Tgm1</i>	CTGCTAACCTGTCTCCAGCC	CCATCCCTGTGTCGTAGAGC	H3K27me3
----------	-------------	----------------------	----------------------	----------

### 3.9 RNAi

siRNAs targeting Ezh2 (ID: s4916 and s4918), Xpo6 (ID: s23301 and s23303), Ipo9 (ID: s31299 and s31301), Emd (ID: s4646 and s225840) and negative control siRNA (AM4635) were from Ambion (Silencer Select). Transfections were performed using Lipofectamine RNAiMax (Invitrogen 13778075) according to manufacturer's instructions.

In brief, EPCs were seed until 70% confluent with CnT medium in a 6-well plate format. Prior to transfection, cells were changed into MEM (Spinners modified) medium, supplemented with 0.292 g/l L-glutamin (Gibco 25030). 7 µl of lipofectamine RNAiMAX reagent was diluted in 150 µl of OptiMEM (Gibco 11058-021). 3 µl of siRNA mix (10 µM) was diluted in 150 µl of OptiMEM. After which, diluted lipofectamine RNAiMAX was added into diluted siRNA mix (1:1) and incubated for 5 min at RT. 300 µl of siRNA-lipix mix was then added to EPCs (1 well of 6-well plate). After 72 h of transfection, cells were harvested and analyzed.

### 3.10 Immunofluorescence and confocal microscopy

Cells were fixed in 4% paraformaldehyde (Sigma P6148) or ice-cold methanol, permeabilized with 0.3% Triton X-100 or 0.003% digitonin (Sigma D141) in PBS, and blocked in 5% BSA. Samples were subsequently incubated overnight in primary antibody in 1% BSA, followed by washing and incubation in secondary antibody. Nuclei were counterstained with 1 mg/ml DAPI (Roche 10236276001). Finally, samples were mounted in Elvanol. All fluorescence images were collected by laser scanning confocal microscopy (SP5X or SP8X; Leica) with Leica Application Suite software (version 2.7.3.9723), using 40x, 63x or 100x immersion objectives.

#### *Elvanol*

2.4 g

*Mowiol (Roth 0713)*

7.5 ml                      glycerol  
 11.7 ml                     milli-Q water

=> **stirred for 2 h at RT**

4.8 ml                      Tris-HCl, pH 8.5

=> **stirred at 53 °C until dissolved**

0.02 g                      Dabco (Roth 0718)

stored at -20 °C

### **Primary antibodies**

<b>Name</b>	<b>Company</b>	<b>Cat. No.</b>	<b>Dilution</b>
<i>Actin</i>	<i>Sigma</i>	<i>A5441</i>	<i>1:800</i>
<i>Emerin</i>	<i>Leica</i>	<i>Emerin-CE</i>	<i>1:500</i>
<i>H3K27me3</i>	<i>Cell Signaling</i>	<i>9733</i>	<i>1:500</i>
<i>Keratin 10</i>	<i>Covance</i>	<i>PRB-155P</i>	<i>1:750</i>
<i>Keratin 14</i>	<i>Progen</i>	<i>GP-CK14</i>	<i>1:500</i>
<i>Lamin A/C</i>	<i>Abcam</i>	<i>ab133256</i>	<i>1:500</i>
<i>Loricrin</i>	<i>Covance</i>	<i>PRB-145P</i>	<i>1:500</i>
<i>NMIIA</i>	<i>Covance</i>	<i>PRB-440P</i>	<i>1:500</i>
<i>RNAPII-S2p</i>	<i>Abcam</i>	<i>ab24758</i>	<i>1:500</i>
<i>Transglutaminase 1</i>	<i>Abcam</i>	<i>ab103814</i>	<i>1:500</i>

### **Secondary antibodies**

<b>Name</b>	<b>Conjugate</b>	<b>Company</b>	<b>Cat. No.</b>
<i>Goat anti-guinea pig IgG</i>	<i>A488</i>	<i>Invitrogen</i>	<i>982288</i>
<i>Goat anti-mouse IgG</i>	<i>A488</i>	<i>Invitrogen</i>	<i>A11001</i>
<i>Goat anti-mouse IgG</i>	<i>A568</i>	<i>Invitrogen</i>	<i>A11004</i>
<i>Goat anti-mouse IgM</i>	<i>A488</i>	<i>Invitrogen</i>	<i>A21042</i>
<i>Goat anti-rabbit IgG</i>	<i>A488</i>	<i>Invitrogen</i>	<i>A11008</i>
<i>Goat anti-rabbit IgG</i>	<i>A568</i>	<i>Invitrogen</i>	<i>A11011</i>

Nascent RNA was detected by using 5-Ethynyl Uridine (EU) incorporation (Click-iT RNA Alexa Fluor 488 Imaging Kit, Thermo Fisher C10329), according to manufacturer's instruction. EU is incorporated to newly synthesized RNA. Detection of global RNA synthesis through EU incorporation is followed the "click" reaction (see 3.4).

For nuclear imaging, fields were randomly selected based exclusively on the presence of nuclei, as assessed by DAPI staining, not on actin, RNAPII-S2p or H3K27me3 levels. Images were collected with the same settings for control and treated cells. Areas of interest were generated using automated thresholding of the DAPI staining, after which mean fluorescence intensities of RNAPII-S2p or H3K27me3 stainings were quantified within the areas of interest from equatorial confocal planes where the intensity of DAPI staining was the highest.

For quantification of nuclear localization of Emd, maximum projections of confocal planes through the entire nucleus were used. Areas of interest were generated based on DAPI staining, after which the mean intensity of Emd and Lamin A/C were quantified within this area. All image analyses were carried out using ImageJ software.

For analysis of perinuclear F-actin, cells were initially fixed in 0.5% Triton X-100 and 0.2% Gluteraldehyde (Serva 23115) in cytoskeleton buffer for 1 min, followed by post-fixation in 2% Gluteraldehyde for 5 min. Autofluorescence was quenched by NaBH<sub>4</sub> (1 mg/ml, Sigma 71321) for 5 min. Samples were incubated with primary antibody against Lamin A/C (Abcam ab133256; 1:500) overnight at 4°C, followed by washing and incubation in secondary antibody and A488-conjugated phalloidin (Invitrogen A12379). Finally, samples were mounted in elvanol.

#### ***Cytoskeleton buffer***

<i>10 mM</i>	<i>MES (Roth 4256.2)</i>
<i>150 mM</i>	<i>NaCl</i>
<i>5mM</i>	<i>Glucose (Roth HN06.3)</i>
<i>5 mM</i>	<i>MgCl<sub>2</sub></i>
<i>pH was adjusted to 6.1</i>	

### **3.11 Chromosome FISH**

Kreatech whole chromosome probes against chromosome 1 (KBI-30001R) and chromosome 18 (KBI-30018G) were from Leica Biosystems. Cells were fixed twice in fresh ice-cold Carnoy's fixative (3:1, methanol : glacial acetic acid (Roth 3738.2)) for 2 min and subsequently air-dried. Samples were then pre-treated for 15 min in 2X SSC at 37°C, followed by dehydration in a graded ethanol series (70-100%). Probes for Chr1 and 18 were diluted 5-fold with FISH hybridization buffer (Kreatech; Leica Biosystems), and applied to the sample. Samples and probes were co-denatured on a hot plate at 75°C for 10 min, then hybridized at 37°C overnight in a moist chamber. Samples were then washed in 0.4X SSC (Promega G329A), 0.3% Triton X-100 for 2 min at 72°C without agitation, followed by 2X SSC, 0.1% Triton X-100 for 1 min at room temperature. Samples were subsequently dehydrated in a graded ethanol series (70-100%) and air-dried at room temperature. Finally, a DAPI counterstain was added and the sample were mounted on glass coverslip and imaged using a confocal microscope (Leica SP8, 63x objective). Full z-scans through entire nuclei were obtained.

For quantification of images, 3D projections of entire nuclei were created using Imaris 8.1.2 software. Nuclear and chromosome volumes were measured from the 3D raw images using the Surface Detection algorithm and used to calculate the percentage of chromosome volume in respect to nuclear volume. Chromosome positions were measured by determining centres of chromosome mass, and measuring the distance of this to the centre of mass of the nucleus using a custom made MatLab script.

### **3.12 Mouse strains**

To obtain an epidermis-restricted deletion of the *Myh9* gene, mice expressing Cre under the control of the Keratin 14 promoter were crossed with floxed *Myh9* mice<sup>37</sup>. Controls were littermates of *Myh9*-deficient mice. Genders were distributed randomly between genotypes. Mice were analyzed at embryonic stage E16.5 or as newborns (P0). All animal experiments were performed according to institutional guidelines and animal licence of the State Office North-Rhine Westphalia. No statistical method was

used to predetermine sample size, and the experiments were not randomized. As the phenotype of Myh9-deficient mice was obvious, it was not meaningful to blind investigators to genotype allocation during experiments and outcome assessment.

### **3.13 Histology**

Hematoxylin/eosin staining of paraffin-embedded skin sections was performed using standard protocols. This method is a standard histological method that allows detection of several distinct tissue structures. The principle is based on the application of hemalum, an oxidation product of haematoxylin. Hemalum colors nuclei in blue. Eosin serves as a counterstain and colors eosinophilic structures, mainly structures that are basic, in different shades of red. Images were taken with a Leica DM4000 light microscope using a 20x objective.

For hematoxylin (Shandon Gill3 Hematoxylin) and eosin (Shandon Eosin Y, Aqueous) staining, paraffin sections were deparaffinized (2 x 5 min Xylol) followed by rehydration (100 % isopropanol, 95 %, 75 %, 50 % ethanol, and milli-Q water; 5 min each). Sections were stained for 50 s with Hematoxylin and blued in tap water. Sections were counterstained for 10 sec with Eosin and subsequently washed in water. Sections were then dehydrated (50 %, 75 %, 95 % ethanol, isopropanol 2 min each), washed 2 x 2 min in Xylol, and finally mounted in Entellan (Merck 1.07961.0100).

### **3.14 Statistics**

Statistical analyses were performed using GraphPad Prism software (GraphPad, version 5.0). Statistical significance was determined by the Mann-Whitney U-test, unpaired t-test, Kruskal-Wallis ANOVA with Dunn's post hoc test, linear regression, or Spearman's rank correlation coefficient test as indicated in the corresponding figure legends. In all cases where a test for normally distributed data was used, normal distribution was confirmed with the Kolmogorov–Smirnov test ( $\alpha = 0.05$ ). All experiments presented were repeated at least in 3 independent experiments/biological replicates.

## 4. Results

### 4.1 Mechanical strain represses global transcription

#### 4.1.1 Mechanical strain has no major impact on cell growth

To understand how mechanical forces are sensed and transmitted to control cell fate, EPCs were exposed to biaxial cyclic mechanical strain. A strain at 10% elongation and 100 mHz was used as it is in the range of physiological strain *in vivo* that has been measured in certain epithelium-covered tissues. Measurements of strain in living skin are technically challenging, and therefore reports on strain experienced in this tissue are limited and partially conflicting (Blanchard et al., 2009; Evans et al., 2013).

Therefore, we first examined whether strain at 10%-100 mHz had any impact on cell growth or viability. 5-ethynyl-2'-deoxyuridine (EdU) was added to the culture medium prior to strain for a period of 12 h to study the effect of strain on cell proliferation. FACS analysis of EdU incorporation showed no significant differences in proliferating rate of strained cells compared to control (Fig. 4.1.1A). Furthermore, Annexin-V staining also revealed that strain did not induce apoptosis in EPCs (Fig. 4.1.1B). However, these results did not exclude the possibility that strain can lead to nuclear deformation as previously described in fibroblasts (Haase et al., 2016). To address this, nuclear shape and volume were quantified in order to detect any deformation, which may cause by strain. As expected, strained cells showed no differences in nuclear shape and volume compared to control (Fig. 4.1.1C), indicating that mechanical strain at 10%-100 mHz did not cause nuclear deformation or damage. Importantly, strain also did not lead to detachment of EPCs from the monolayer (Fig. 4.1.1D). Taken together, these results indicate that mechanical strain at 10%-100 mHz does not induce changes in cell density, proliferation, apoptosis or gross nuclear structure, excluding the possibility that strain-induced damage and suggesting that it is in the physiological range of epidermis.

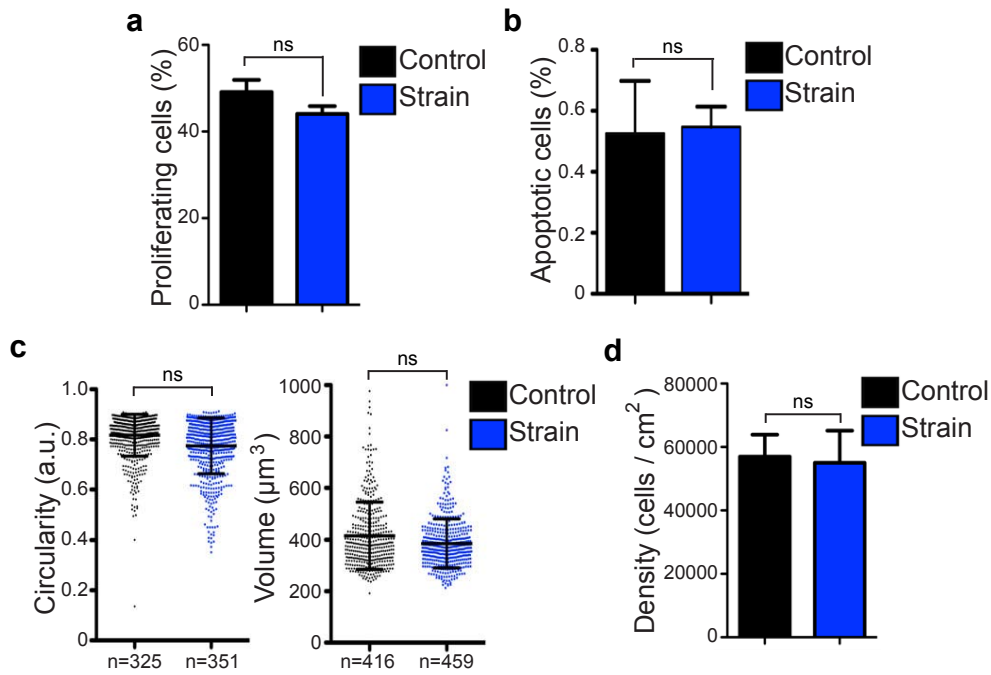


**Figure 4.1.1. Mechanical strain has no impact on cell growth or viability.** *a.* FACS analysis of proliferating cells (EdU incorporation) shows no differences after 12 h of strain (mean + SD,  $n=3$ , ns=not significant, Mann-Whitney). *b.* FACS analysis of apoptotic cells (Annexin-V) shows no differences after 12 h of strain (mean + SEM,  $n=6$ , ns=not significant, Mann-Whitney). *c.* Quantification of nuclei shows no significant differences in circularity and volume after 12 h of strain (mean  $\pm$  SD,  $n>300$  nuclei from 4 independent experiments, ns=not significant, Mann-Whitney). *d.* Quantification of cell density shows no differences after 12 h of strain (mean + SD,  $n=5$ , ns=not significant, Student's *t*-test).

#### 4.1.2 Mechanical strain represses global transcription

To identify mechanosensitive pathways, EPCs were exposed to 12 h of strain followed by a genome wide transcriptional analysis using next generation sequencing (RNA-seq). External RNA controls consortium (ERCC) spike-in RNA mixtures were included in proportion to the concentration of RNA in samples (Fig. 4.1.2A). This method has been tested as a robust and accurate approach to quantify differential gene

expression and global changes in messenger (m)RNA levels (Jiang et al., 2011; Loven et al., 2012). Similar amounts of total RNA in control and strained samples were subjected to sequencing. The sequencing data was analyzed by the MPI-AGE bioinformatics core facility, using RNA spike-in normalization method. Strikingly, no genes were found significantly upregulated ( $q$ -value  $< 0.05$ ), whereas nearly 4000 downregulated genes were detected in the strained condition (Fig. 4.1.2B). Interestingly, by performing regression analysis with the ERCC-dashboard package, we also observed a drop in the level of poly-A RNA to 85% of control cells in response to strain (Fig. 4.1.2C), suggesting strain-induced global downregulation of mRNA transcription. To confirm such an effect, nascent RNA were quantified by incorporation of 5-ethynyl-uridine (EU) into EPCs (Jao and Salic, 2008). Quantitative analysis of EU incorporation using immunofluorescence showed a reduction in the levels of nascent RNA after 12 h of strain to approximately 85% of control levels (Fig. 4.1.2D). These results indicate that mechanical strain significantly represses transcription.

In order to uncover potential signaling pathways responsible for this global transcriptional repression, we performed Gene Set Enrichment Analysis (GSEA) (Subramanian et al., 2005). The analysis was carried out on a pre-ranked gene list according to  $\log_2$  fold change from RNA-seq, using a Broad Institute Molecular Signatures Database collection of chemical and genetic perturbation. GSEA analysis revealed that genes known to carry H3K27me3 as well as genes regulated by the PRC2 were most significantly over-represented in the dataset (Fig. 4.1.2E, Appendix Table 1). Collectively, these results suggest that mechanical strain at 10%-100 mHz induces transcriptional repression that might be regulated by a PRC2 and H3K27me3-dependent epigenetic mechanism.

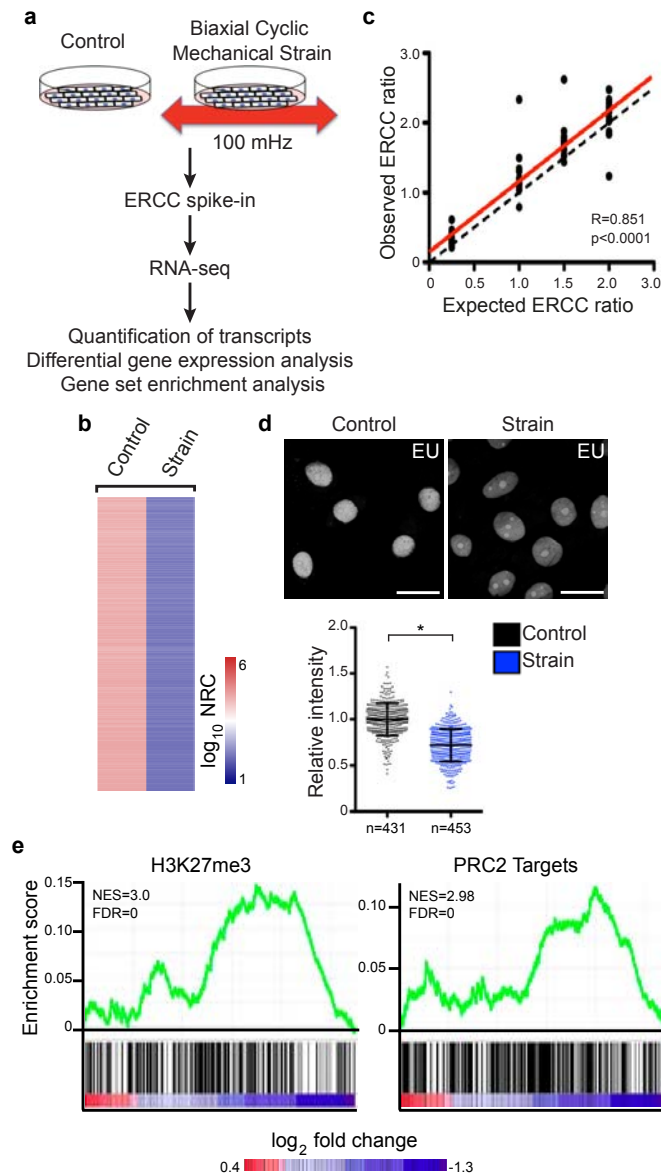


**Figure 4.1.2. Mechanical strain represses global transcription in a PRC2 dependent manner.** *a.* Strategy to identify mechanosensitive gene signatures. *b.* Heat map of normalized read counts (NRC) from RNA-seq (mean,  $n=3$ ). *c.* Estimation of global mRNA expression changes from ERCC spike-ins (black dots = data points, dotted black line = the expected ratio). Regression analysis with the ERCC-dashboard package (red solid line) indicates a drop of polyA RNA levels to 85% of control cells in response to strain ( $n=3$ ). *d.* EU incorporation assay shows reduced levels of nascent RNA upon 12 h of strain (scale bars 25  $\mu\text{m}$ ). Quantification shows mean  $\pm$  SD,  $n>400$  nuclei from 4 independent experiments,  $*p=0.02$ , Mann-Whitney. *e.* GSEA shows enrichment of genes marked by H3K27me3 or defined as PRC2 in downregulated genes.

### **4.1.3 Mechanical strain mediates H3K27me3 and RNAPII-S2p occupancy**

To validate the hypothesis that strain repressed global transcription through increasing PRC2 and H3K27me3-mediated gene silencing, global levels of H3K27me3 and an active form of RNAPII, marked by the phosphorylation of serine 2 (RNAPII-S2p), were analyzed using immunofluorescence and western blotting. These analyses showed that strain lead to an increased signal of H3K27me3 and a decrease in RNAPII-S2p (Fig. 4.1.3.1A, B). Consistent with previous reports on the negative relationship between PRC occupancy and transcriptional elongation (Brookes et al., 2012; Brookes and Pombo, 2009), Spearman's rank correlation coefficient analysis showed a negative correlation between H3K27me3 and RNAPII-S2p signals in single cells (Fig. 4.1.3.1C). These experiments confirm that strain leads to enhanced PRC2 and reduced RNAPII-S2p activity.

To further investigate the effect of strain on H3K27me3 and RNAPII-S2p at the single gene level, chromatin immunoprecipitation (ChIP) was used to determine the occupancy of these two marks on genes found downregulated in the RNA-seq data, as well as on other known PRC2 target genes, in EPCs after 12 h of strain. The results showed increased occupancy of H3K27me3 at promoters of lineage-specific PRC2 target genes such as LOR, TGM1, CRCT1, LCE1A (Consortium, 2012) and CDKN2A, previously shown to be a PRC2 target in EPCs (Ezhkova et al., 2009) (Fig. 4.1.3.2A). A small but consistent enrichment of H3K27me3 was also detected at promoters of actively transcribed genes (ACTB, B2M, KLK8, GAPDH), as well as non-lineage-specific PRC2 target genes (HOX, SOX) (Fig. 4.1.3.2A). As expected, RNAPII-S2p ChIP analysis showed an opposite effect to H3K27me3, a decrease on RNAPII-S2p at gene bodies of these genes (Fig. 4.1.3.2B).

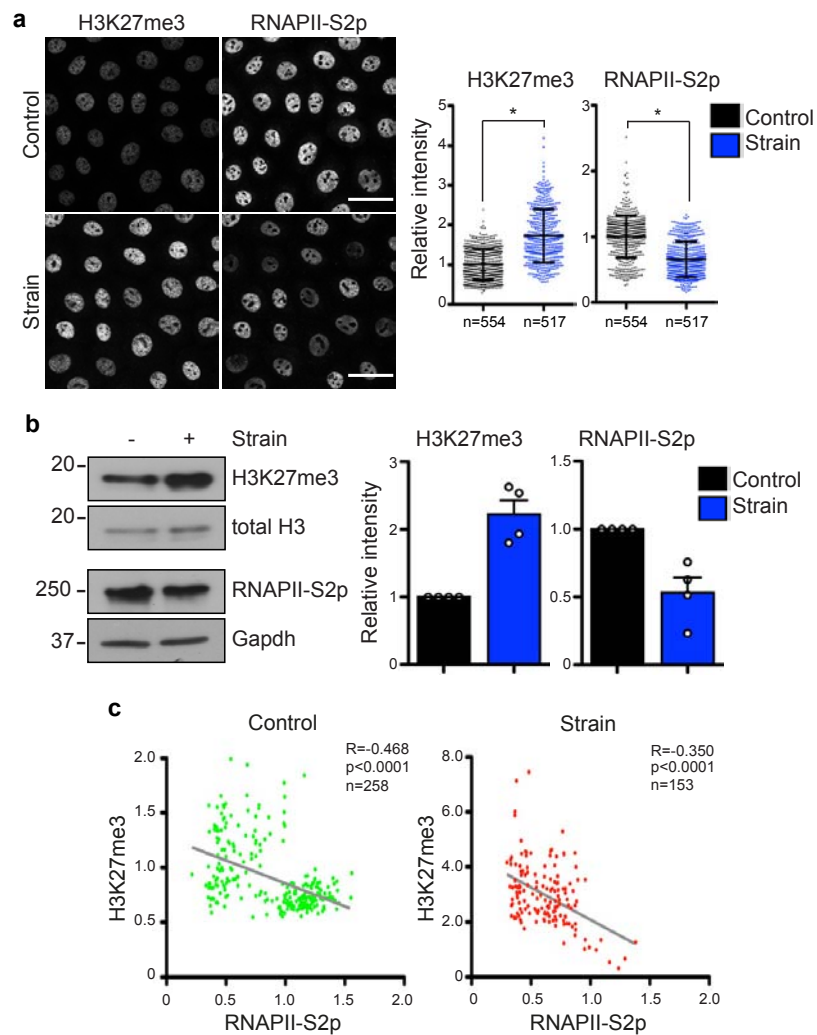


**Figure 4.1.3.1. The effect of strain on H3K27me3 and RNAPII-S2p. a.** Immunostaining of cells exposed to 12 h of strain shows increased H3K27me3 and a parallel decrease in RNAPII-S2p (scale 40  $\mu$ m, mean  $\pm$  SD,  $n \geq 400$  cells from 4 independent experiments,  $**p=0.0075$ ,  $*p=0.021$ , Mann-Whitney). **b.** Western blot analyses show increased H3K27me3 and decreased RNAPII-S2p levels in cells exposed to 12 h of strain. Quantifications show mean + SEM from 4 independent experiments. **c.** Scatter plots display a negative correlation between RNAPII-S2p and H3K27me3 signal in single cells ( $R$ =Spearman's rank correlation coefficient,  $n > 150$  cells from 3 independent experiments).

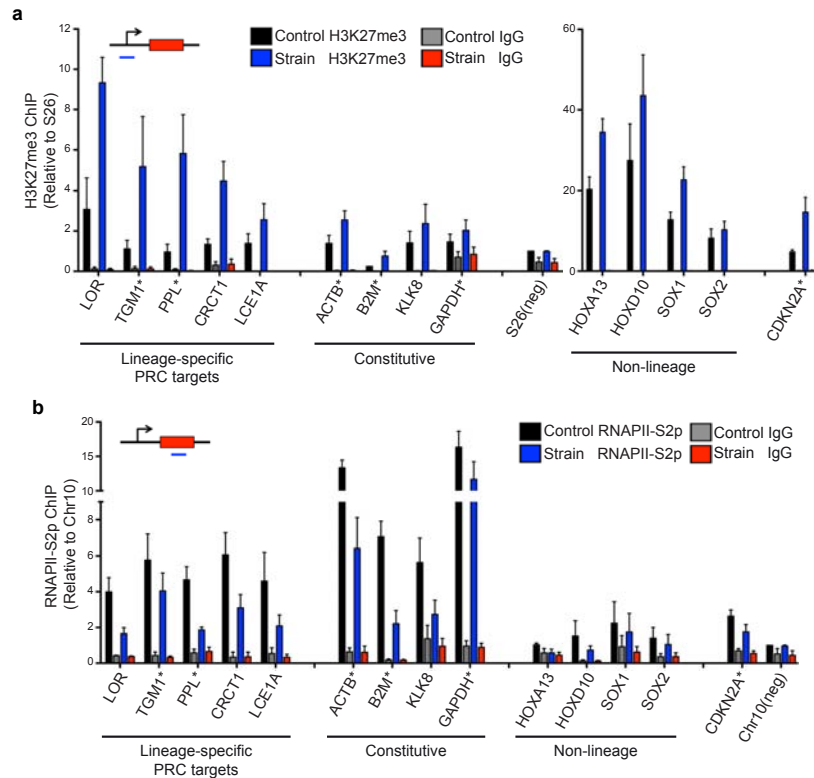


**Figure 4.1.3.2. ChIP analyses of H3K27me3 and RNAPII-S2p after 12 h of strain. a.** H3K27me3-ChIP shows increased H3K27me3 levels at promoters of PRC2 target genes as well as at constitutively expressed genes after 12 h of strain (mean + SEM, n=4). **b.** RNAPII-S2p-ChIP displays decreased levels of this mark at gene bodies of strain-induced enrichment of H3K27me3 genes (mean + SEM, n=3), \*downregulated in RNA-seq.

Moreover, time scale experiments of mechanical strain after 3, and 6 h revealed that the decrease in RNAPII-S2p occupancy was already visible after 3 h, while the increase of H3K27me3 became evident after 6 h (Fig. 4.1.3.3A-D). These results suggest that mechanical strain first attenuated RNAPII activity, followed by the recruitment of PRC2 to promoters of silenced genes to trimethylate H3K27. This is in line with a previous study showing that inhibition of transcription is sufficient to recruit PRC2 to specific target genes (Rising et al., 2014).

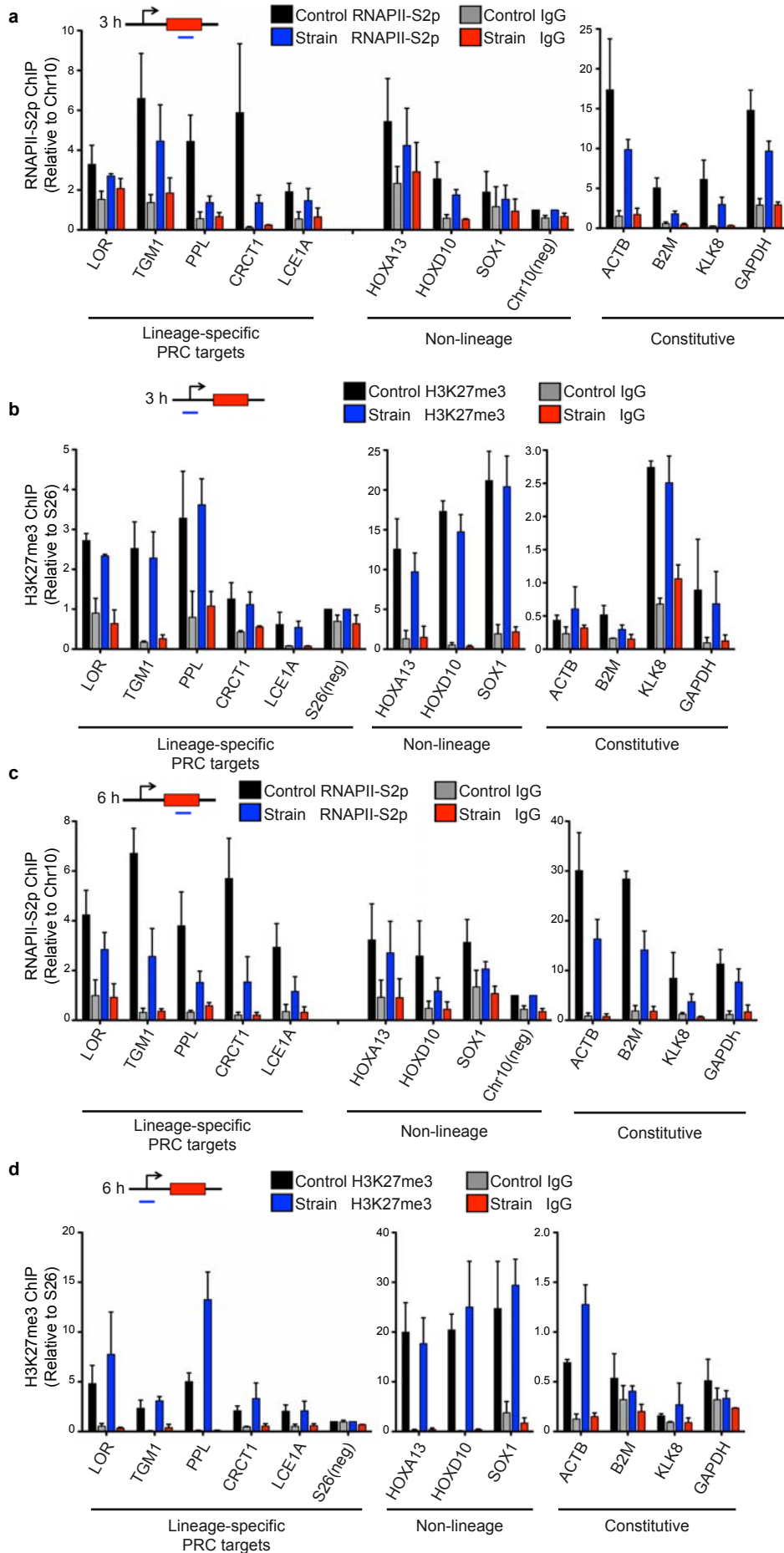


**Figure 4.1.3.3. Strain first attenuates RNAPII activity, followed by enrichment of H3K27me3.** *a.* ChIP-qPCR for RNAPII-S2p reveals that decreased occupancy of RNAPII-S2p at gene bodies of PRC2 target genes as well as on constitutively expressed genes can be detected already after 3 h of strain (mean + SEM, n=3 independent experiments). *b.* H3K27me3-ChIP shows no changes of this mark after 3 h of strain (mean + SEM, n=3 independent experiments). *c.* Strain further reduces the occupancy of RNAPII-S2p after 6 h (mean + SEM, n=3 independent experiments). *d.* Enrichment of H3K27me3 at promoters becomes visible only after 6 h of strain (mean + SEM, n=3 independent experiments).

As EPCs were exposed to a relatively long period of strain for 12 h, it was of great interest to know if the strain-induced H3K27me3 occupancy was stable or reversible. To answer this question, EPCs were exposed to strain for 12 h, followed by returning them to an unstrained state. ChIP-H3K27me3 data revealed that the enrichment of H3K27me3 at promoter region of silenced genes after 12 h of strain was fully restored to control levels 24 h post strain (Fig. 4.1.3.4). This indicates that the effects of strain on transcription are transient, in agreement with previous reports that all epigenetic histone marks are in principle reversible (Tsukada et al., 2006; Whetstine et al., 2006).

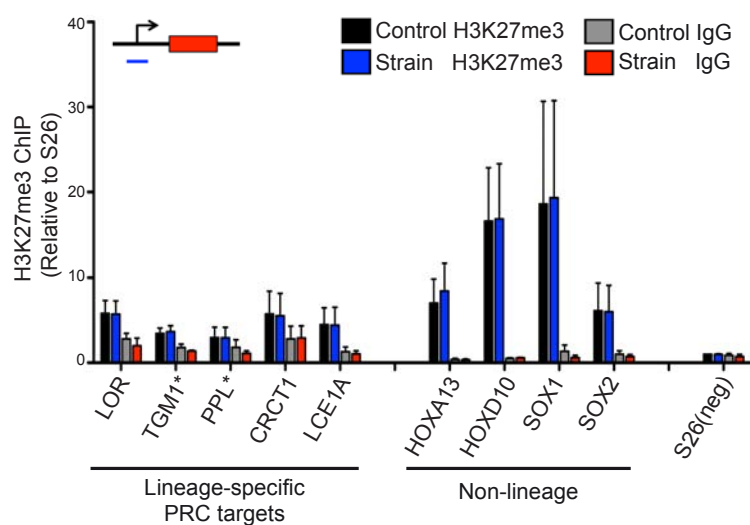


**Figure 4.1.3.4. Enrichment of H3K27me3 upon strain is reversible.** H3K27me3-ChIP shows no differences in H3K27me3 occupancy at promoters of PRC2 target genes in 24 h unstrained cells after 12 h of strain (mean + SEM, n=3).

#### 4.1.4 Mechanical strain induces chromatin remodeling

As nucleosome remodeling and positioning play an essential role in regulating transcriptional elongation and promoter-proximal pausing of RNAPII, and thus gene expression (Bai and Morozov, 2010; Struhl and Segal, 2013), we next asked if changes in H3K27me3 and RNAPII-S2p upon strain were accompanied by changes in nucleosome remodeling and positioning. Formaldehyde-assisted isolation of regulatory elements (FAIRE) analysis can be used to identify chromatin states, FAIRE separates open and closed chromatin states by crosslinking and subsequent differential sedimentation of nucleosome occupied and unoccupied DNA fragments. (Giresi et al., 2007). FAIRE analysis revealed a reduction in open chromatin sites of lineage-specific PRC2 target genes as well as constitutive genes in strained EPCs compared to control cells (Fig. 4.1.4). Non-lineage genes such as HOX and SOX were used as negative control in FAIRE, the result showed no enrichment in gene body of these genes. Interestingly, strain further enhanced negative enrichment of these regions (Fig. 4.1.4). In summary, the data so far showed that in response to biaxial cyclic mechanical strain,

EPCs first attenuated transcription, followed by enhanced H3K27me3 occupancy. These processes are associated with chromatin remodeling and compaction.

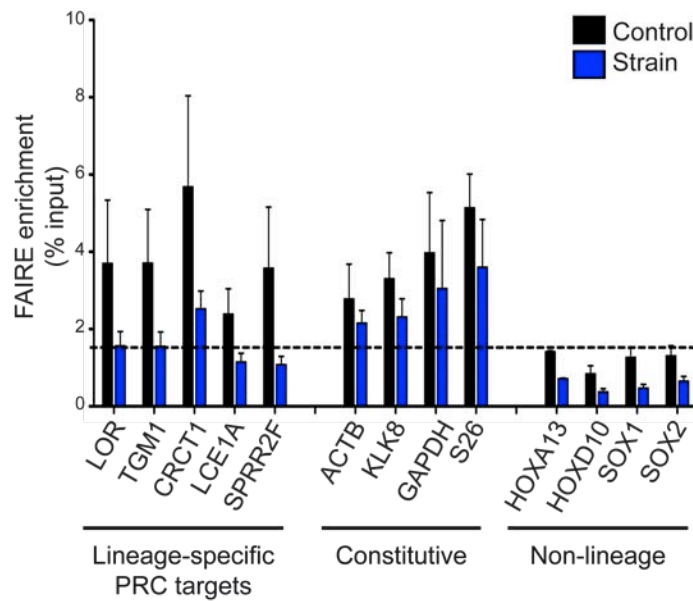


**Figure 4.1.4.** FAIRE-qPCR shows decreased open chromatin (dotted line) in cells subjected to strain for 12 h (mean + SEM, n=3).

## 4.2 Mechanosensory complex of Emd-Actin-NMIIA

### 4.2.1 Strain induces enrichment of H3K27me3 in an actomyosin dependent manner

To further understand how forces can be transmitted to the nucleus to impact chromatin states, we next analyzed changes in the actomyosin cytoskeleton, a structure that plays a central role in generating and sensing mechanical forces (Hoffman et al., 2011; Provenzano and Keely, 2011). Consistent and in agreement with a previous report (Guolla et al., 2012), mechanical strain led to increase NMII activity, marked by the phosphorylation of its light chain, after 3 h of strain, when changes in RNAPII-S2p occupancy were first recorded (Fig. 4.2.1A). Immunofluorescence analysis at this time point also revealed an increased level of F-actin stress fibers (Fig. 4.2.1B). Surprisingly, strain led to the accumulation of F-actin around the nucleus, and this accumulation extended to cover the ER (Fig. 4.2.1C). The perinuclear F-actin

polymerization was also accompanied by an enrichment of NMIIA around the nucleus upon strain (Fig. 4.2.1D). Furthermore, analysis of the free G- to F-actin ratio showed a drop in the monomeric G-actin pool and an increase in F-actin pool after 3 h of strain (Fig. 4.2.1E). The effect of strain on reducing of G-actin was offset by blebbistatin (Bleb) – an inhibitor of NMII ATPase activity (Kovacs et al., 2004) (Fig. 4.2.1E). These results suggest that strain induces extensive F-actin polymerization in a myosin II-dependent manner.

To verify whether the observed increase in global levels of H3K27me3 upon strain was downstream of strain-induced myosin activity, EPCs were treated with Bleb and exposed to strain. Western blotting of a purified histone fraction showed that blocking myosin activity prevented the strain-induced increase in H3K27me3 (Fig. 4.2.1F). Together, these data indicate that strain induces enrichment of H3K27me3 in a myosin-dependent manner.

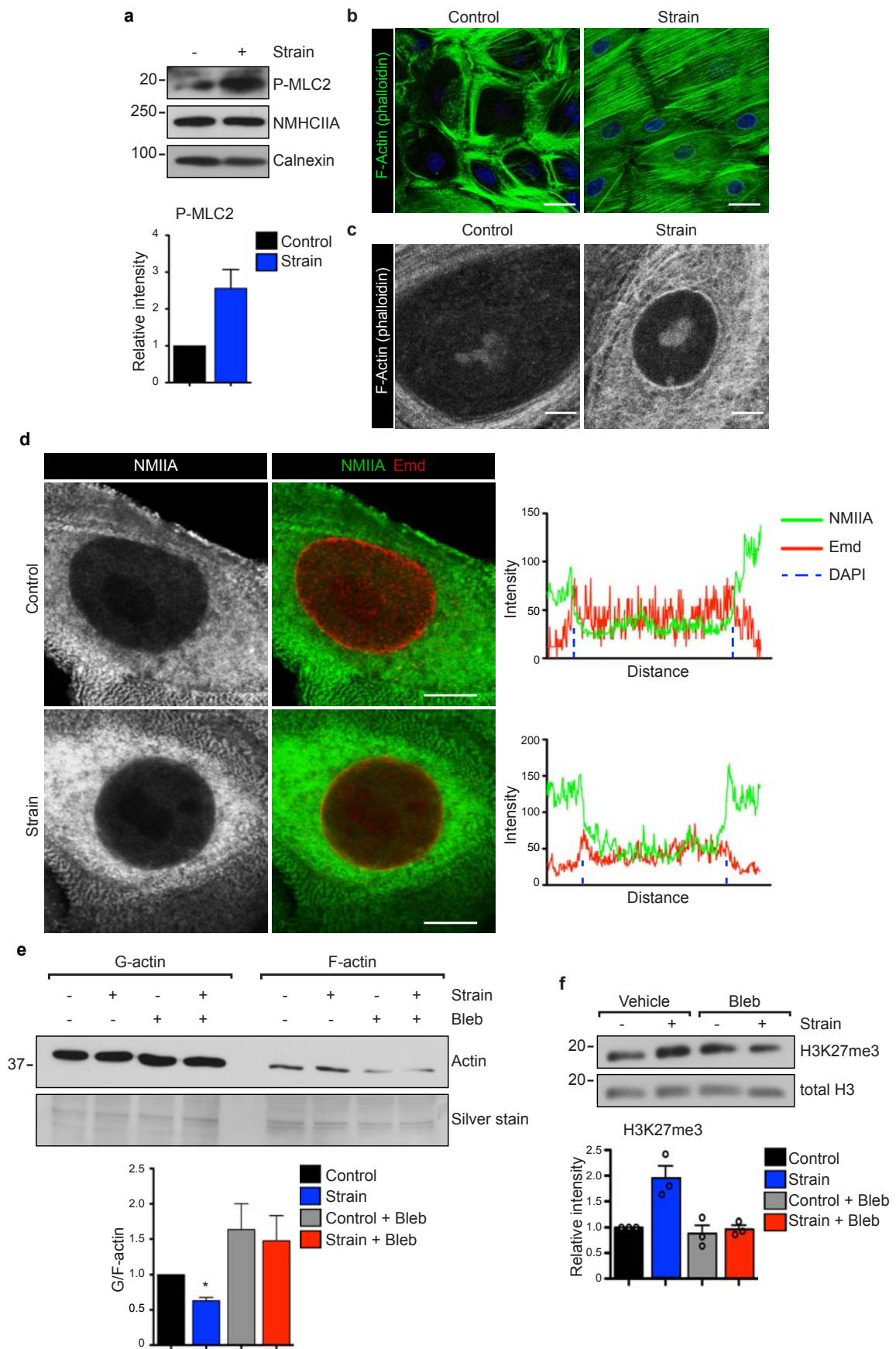


**Figure 4.2.1. Strain induces F-actin polymerization and enhances myosin II activity.**

**a.** Western blot analysis reveals an increase of NMIIA activity upon strain, marked by phosphorylated of its light chain (P-MLC2). Heavy chain of NMIIA (NMHCIIA) and calnexin are used as loading controls. Graph shows quantification (mean + SEM, n=5). **b.** Immunostaining of the actin cytoskeleton shows increased F-actin stress fibers upon 3 h of strain (scale bars 25  $\mu$ m). **c.** Immunofluorescence analysis shows accumulation of F-actin around the nucleus after 3 h of strain (scale bar 5  $\mu$ m). **d.** Immunostaining of NMIIA and Emd reveals the accumulation of NMIIA around the nucleus upon 3 h of strain (scale bars 7.5  $\mu$ m). Right panels show line scans through the nucleus. **e.** Western blot analysis of G- and F-actin fractions shows that strain decreases G/F-actin ratio in an NMII-dependent manner. Silver staining of SDS-PAGE gel is used as loading control (lower panel). Quantification of G/F actin ratio shows mean + SEM, n=5 (\* $p$ <0.05, Kruskal-Wallis/Dunn's). **f.** Western blot of purified histones shows increased levels of H3K27me3 upon 12 h of strain. This increase is abolished by the NMII inhibitor blebbistatin (Bleb). Quantification shows mean + SEM, n=3.

**4.2.2 Strain induces enrichment of Emd at the outer nuclear membrane to control localized actin remodeling**

Emd has been shown to be phosphorylated in response to extrinsic forces applied to isolated nuclei, and to be essential in the mechanical reinforcement of the nuclei to this force, suggesting that Emd could play an important role in transmitting mechanical forces from the cytoplasm to the nucleus (Guilluy et al., 2014). To investigate the role of Emd in response to strain, we first performed immunofluorescence staining of Emd in EPCs upon strain. By using two different permeabilization reagents: digitonin and triton X-100, the population of Emd at the outer or the inner nuclear membrane can be observed, respectively (Griffis et al., 2003). The results showed that strain induced an enrichment of Emd at the ONM and the endoplasmic reticulum that is continuous with the ONM, and a corresponding decrease of Emd at the INM (Fig. 4.2.2A-B). Lamin A/C was used as a control for the INM accessibility after permeabilization. Importantly, strain did not change total protein levels of either Emd or lamin A/C (Fig.

4.2.2C). These results indicate that mechanical strain leads to redistribution of Emd from the INM to the ONM.

As strain was observed to induce the formation of a perinuclear F-actin ring, we next asked if the enhancement of actin polymerization upon strain depends on Emd. This seemed plausible as Emd has been shown to bind actin and to possess actin capping activity (Holaska et al., 2004). Emd-depleted cells were exposed to mechanical strain for 3 h, followed by F-actin staining. The staining showed that depletion of Emd prevented the formation of perinuclear F-actin ring in response to mechanical strain (Fig. 4.2.2D), indicating that Emd is required for strain-induced localized F-actin remodeling.

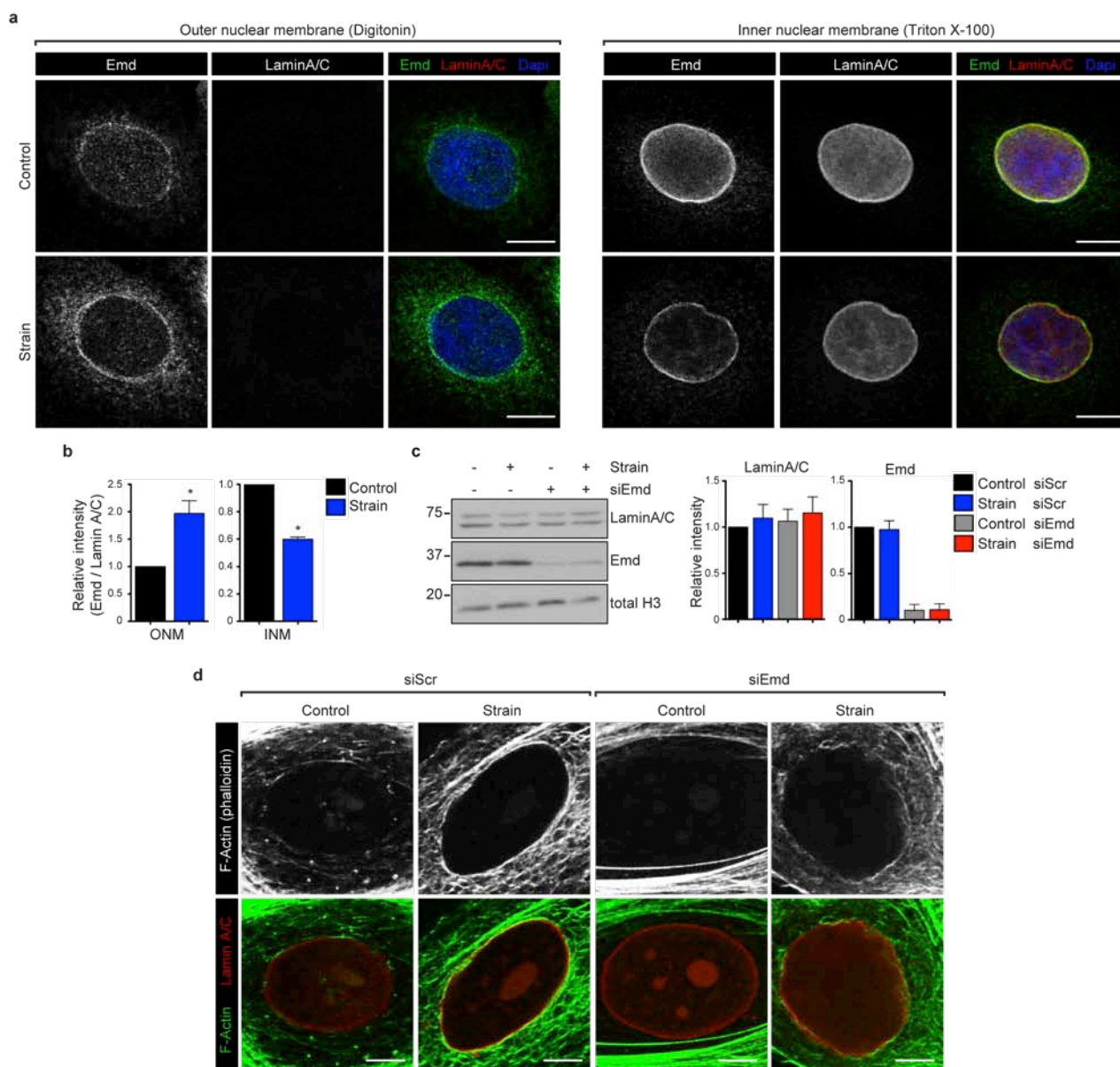


**Fig. 4.2.2. Strain induces localized F-actin remodeling in an Emd-dependent manner.** *a.* Immunostaining of Emd at the ONM in digitonin-permeabilized cells (left panel) and at the INM in Triton-X-permeabilized cells (right panel), scale bars 10  $\mu$ m. Lamin A/C was used as control for the INM accessibility. The results show that strain induces an enrichment of Emd at the ONM and a corresponding decrease of Emd at the INM. *b.* Quantification of the intensity ratio of Emd and LaminA/C at the ONM and INM reveals the redistribution of Emd from the INM to the ONM (mean + SEM,  $n=4$  independent experiments with >50 cells/experiment,  $*p<0.05$ , Mann-Whitney). *c.* Western blot analysis of total protein levels of LaminA/C and Emd upon strain. Depletion of Emd (siEmd) results in efficient reduction of this protein, and has no

effect on LaminA/C levels (mean + SEM, n=5). **d.** Immunofluorescence analysis shows accumulation of F-actin around the nucleus upon 3 h of strain. Depletion of Emd (*siEmd*) prevents actin polymerization at this site. Scale bars 5  $\mu$ m.

### 4.2.3 Emd-actin-NMIIA complex functions as a nuclear force sensor

Our results so far revealed that strain had a major effect on actin, NMIIA and Emd, leading to accumulation of these proteins around the nucleus. We next assessed if strain would promote interactions between Emd, actin and NMIIA. Emd immunoprecipitation experiments showed co-precipitation of Emd, lamin A/C, actin and NMIIA (Fig. 4.2.3). Interestingly, strain increased interactions between Emd, actin and an active form of NMIIA (P-MLC2) (Fig. 4.2.3). In contrast, strain decreased an interaction between Emd and lamin A/C (Fig. 4.2.3), which further supported our observation that strain reduces Emd levels at the INM. These data confirm that: 1) Emd can bind to actin and NMIIA. 2) Strain further strengthens interactions between Emd, actin and active NMIIA at the ONM. 3) Strain decreases Emd-bound lamin A/C at the INM. Together, the results suggest that an Emd-actin-NMIIA complex is established upon strain that might serve as a sensor to transmit mechanical forces into the nucleus.

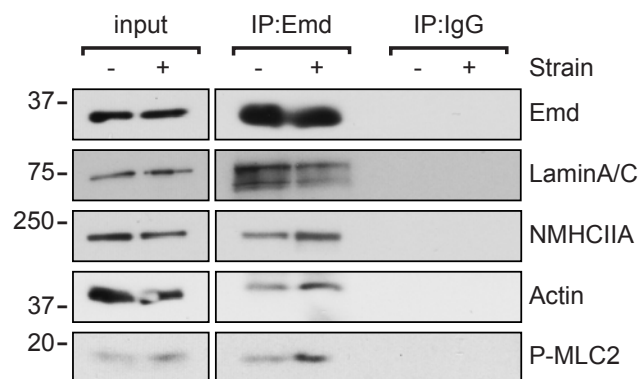


**Fig. 4.2.3. Emd-actin-NMIIA complex.** Co-immunoprecipitation of Emd shows interactions between Emd, actin, NMIIA and Lamin A/C. Strain further enhances Emd-

*bound actin, NMIIA and P-MLC but decreases Emd-bound lamin A/C. Unspecific IgG was used as negative control.*

#### **4.2.4 Strain regulates RNAPII-S2p and H3K27me3 occupancy through Emd-actin-NMIIA complex**

To test whether Emd relocation was important for force-mediated effects on transcriptional silencing, Emd-depleted EPCs were exposed to 12 h of strain, followed by immunofluorescence analysis of RNAPII-S2p and H3K27me3. Depletion of Emd alone did not alter global RNAPII-S2p and H3K27me3 levels compared to control cells, as shown by immunofluorescence analysis (Fig. 4.2.4). However, a combination of Emd depletion and mechanical strain prevented strain from repressing transcription and enhancing H3K27me3 occupancy (Fig. 4.2.4), indicating that Emd is required to transmit the effects of force on chromatin.

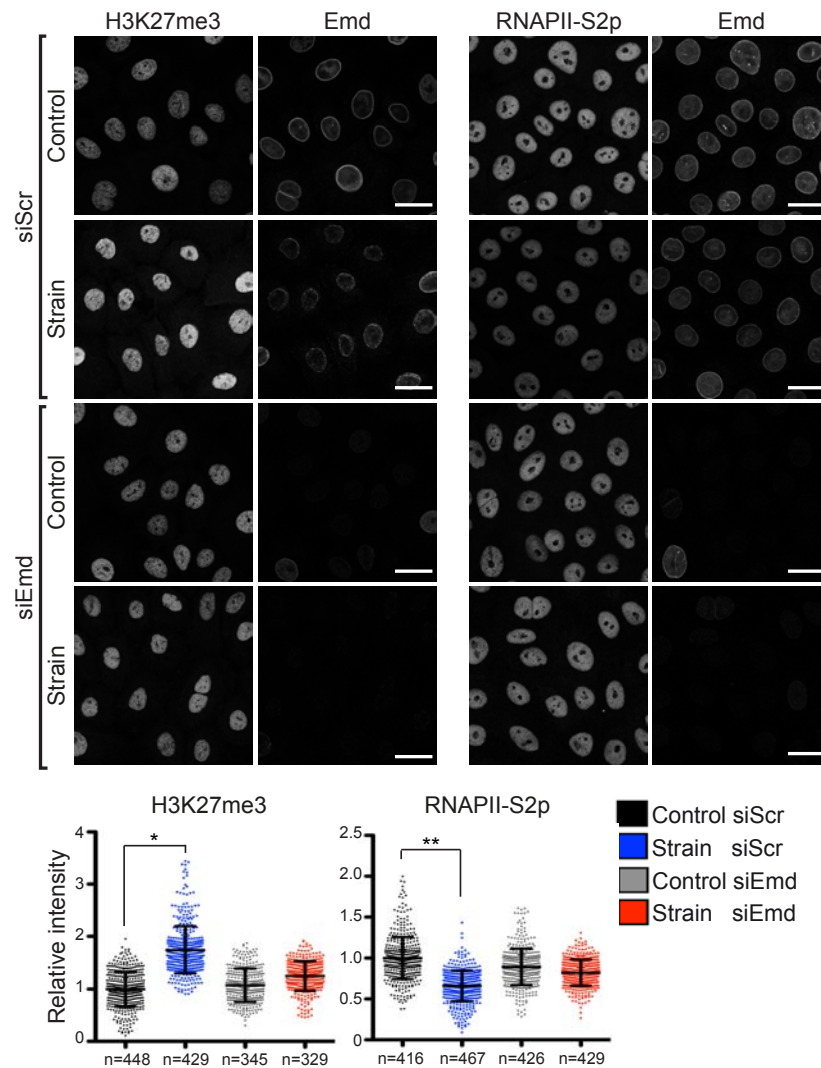


**Fig. 4.2.4. Emd mediates the effect of strain on H3K27me3 and RNAPII-S2p.** Immunofluorescence analysis of H3K27me3 and RNAPII-S2p shows that depletion of Emd blocks the effect of strain on increasing H3K27me3 accumulation and a corresponding decrease in RNAPII-S2p levels (scale bars 25  $\mu$ m, mean  $\pm$  SD,  $n > 300$  nuclei from 3 independent experiments, \* $p < 0.05$ , \*\* $p < 0.01$ , Kruskal-Wallis/Dunn's).

### **4.3. Strain induces global chromatin reorganization**

#### **4.3.1 Strain reduces H3K9me<sub>2,3</sub> levels**

Previous studies reported that Emd plays a role in tethering heterochromatin to the nuclear lamina through H3K9 methylation (Demmerle et al., 2012; Towbin et al., 2013). As we had observed that strain reduces Emd at the INM, we asked if this could impact on the methylation of H3K9 as well as the tethering of heterochromatin to the NE. Consistently with previous reports on Emd and H3K9me, western blot analysis of Emd-depleted cells showed reduced levels of H3K9me<sub>2,3</sub> compared to control cells (Fig. 4.3.1A). Analysis of the histone fraction also revealed a decline in H3K9me<sub>2,3</sub> signal in cells exposed to 12 h of strain. Importantly, a combination of Emd depletion and strain induced only a minor additive decrease in H3K9me<sub>2,3</sub> levels (Fig. 4.3.1A), suggesting that strain reduces H3K9me<sub>2,3</sub> through Emd.

Time-scale experiments followed by H3K9me<sub>2,3</sub> ChIP revealed that the loss of H3K9me<sub>2,3</sub> upon strain became first visible after 6 h of strain. As changes in transcription were first detected after 3 h of strain, suggesting that the loss of H3K9me<sub>2,3</sub> is not the cause for the transcriptional repression. Interestingly, decreased H3K9me<sub>2,3</sub> levels were detected on LADs and major satellites (Fig. 4.3.1B-C), implying that mechanical strain may alter global chromatin structure.

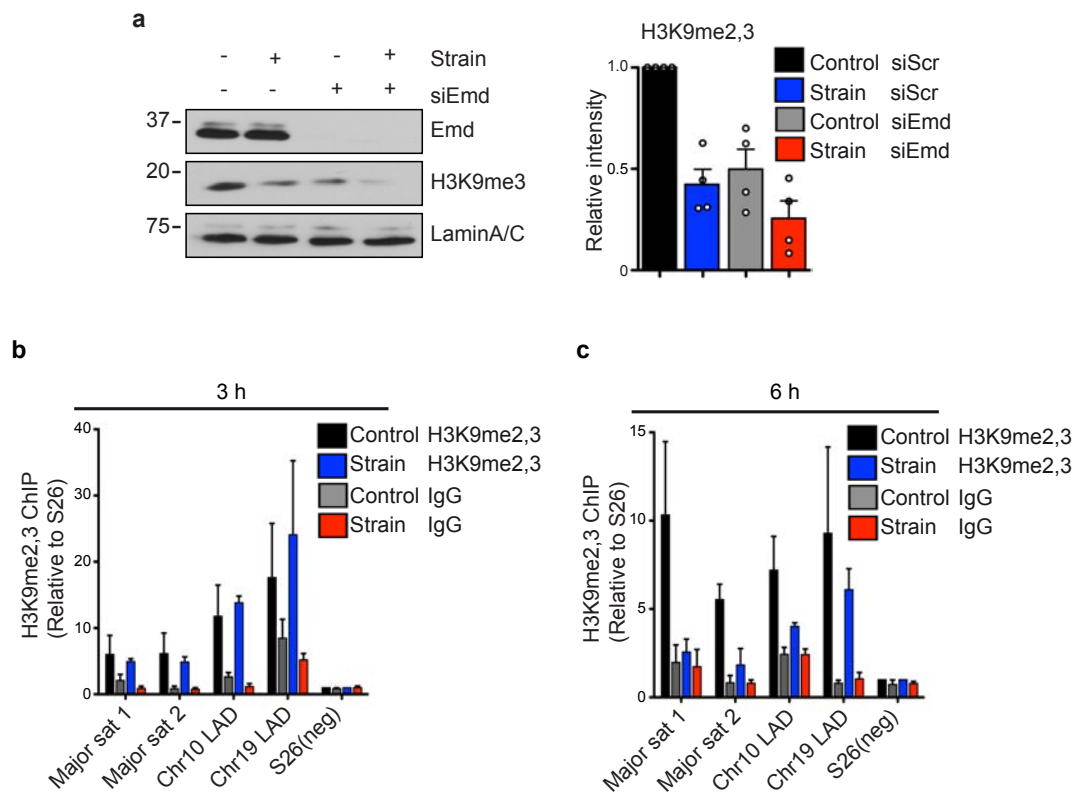


**Fig. 4.3.1. Strain reduces H3K9me2,3.** *a.* Western blot analysis of nuclear fractions shows a decrease in H3K9me2,3 levels both in Emd-depleted cells (siEmd) and in cells exposed to 12 h of strain. Quantification (right panel) represents 4 independent experiments (mean + SEM). *b.* No differences in H3K9me2,3 levels at major satellites and LADs can be detected after 3 h of strain (mean + SEM,  $n=3$  independent experiments). *c.* ChIP-qPCR shows that strain decreases H3K9me2,3 levels after 6 h of strain (mean + SEM,  $n=3$  independent experiments).

### 4.3.2 Strain leads to a compensation between H3K9me<sub>2,3</sub> and H3K27me<sub>3</sub>

H3K9me<sub>2,3</sub> and H3K27me<sub>3</sub> are repressive histone marks for constitutive and facultative heterochromatin, respectively (Venkatesh and Workman, 2015). Our results so far showed that mechanical strain impacts both of them. On one hand, strain induced H3K27me<sub>3</sub> occupancy at promoters of PRC2 target genes as well as constitutive transcribed genes. On the other hand, strain reduced H3K9me<sub>2,3</sub> occupancy on constitutive heterochromatin. We next asked whether strain would induce a switch from H3K9me<sub>2,3</sub> to H3K27me<sub>3</sub> on constitutive heterochromatin regions, as it was previously reported that these two repressive marks can compensate to ensure genome stability (Walter et al., 2016). To test this hypothesis, we performed ChIP experiments for H3K27me<sub>3</sub> and H3K9me<sub>2,3</sub> in cells exposed to 12 h of strain, and observed enrichment of H3K27me<sub>3</sub> at regions where H3K9me<sub>2,3</sub> was lost (Fig. 4.3.2A-B). Consistently, no changes in transcription levels from these regions were detected (Fig. 4.3.2C). These data indicate that an epigenetic switch from H3K9me<sub>2,3</sub> to H3K27me<sub>3</sub> upon strain is sufficient to maintain gene silencing at these regions.

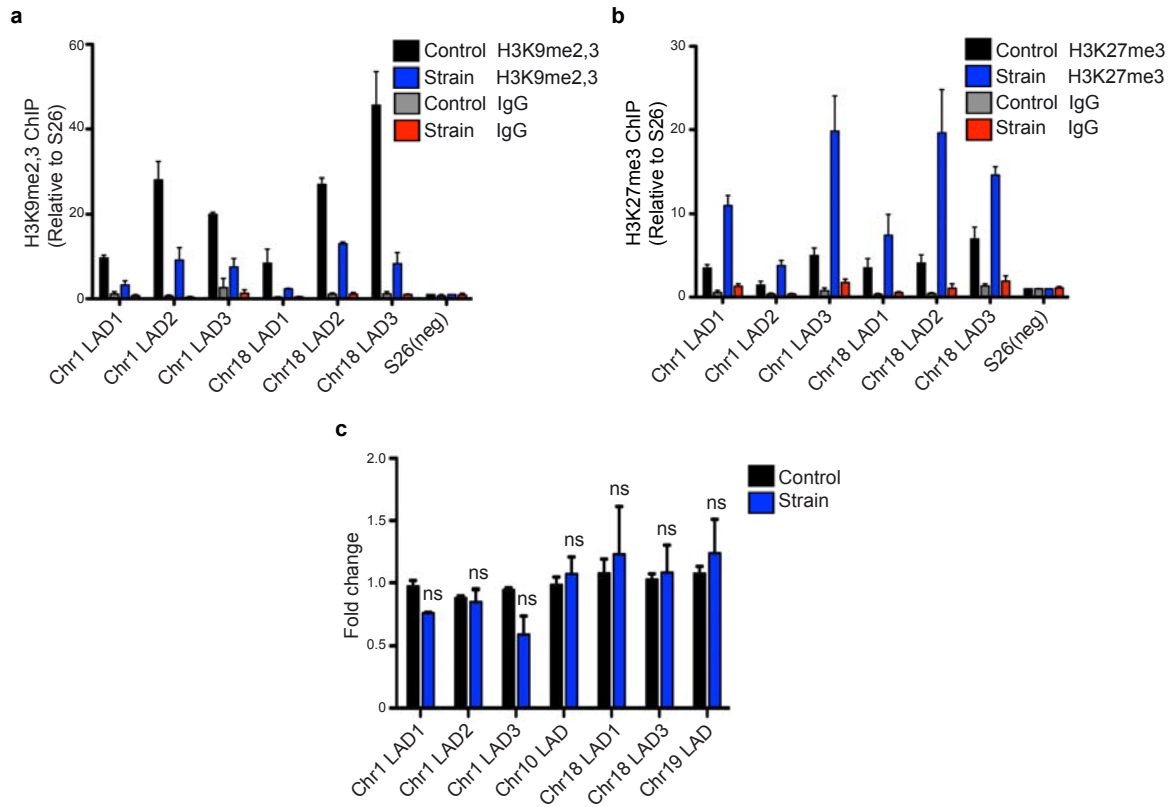


**Fig. 4.3.2. Compensation between H3K9me2,3 and H3K27me3 upon strain.** *a.* ChIP-qPCR reveals reduced occupancy of H3K9me2,3 on LADs upon 12 h of strain (mean + SEM,  $n=3$  independent experiments). *b.* ChIP-qPCR shows that LADs acquire H3K27me3 after 12 h of strain (mean + SEM,  $n=3$  independent experiments). *c.* qPCR analysis shows no differences in gene expression levels at LADs after 12 h of strain (mean + SEM,  $n=3$  independent experiments, ns=not significant, Mann-Whitney).

### 4.3.3 Strain induces global chromatin reorganization

Although the switch from H3K9me<sub>2,3</sub> to H3K27me<sub>3</sub> can ensure longstanding genome stability, H3K9me<sub>2,3</sub>-enriched chromatin is often viewed as a more static compacting structure compared to H3K27me<sub>3</sub> (Saksouk et al., 2015b; Walter et al., 2016). We therefore asked if this epigenetic switch would be accompanied by rearrangements of chromatin structure; for example, to a less condensed form of chromatin. To investigate this, fluorescence *in situ* hybridization (FISH) chromosome painting was used to visualize chromosome structure. Chromosome 1 contains the epidermal differentiation complex (EDC), a locus that harbors a large number of terminal differentiation genes for EPCs (Marenholz et al., 2001), and a heterochromatin-rich chromosome 18, the lowest gene-density chromosome in humans (Nusbaum et al., 2005) were chosen for this analysis. 3D analysis of chromosome 1 and 18 showed compact and distinct chromosome territories close to the nuclear periphery in control cells. In contrast, chromosome 1 and 18 of strained cells displayed dispersed territories, which were more centrally distributed (Fig. 4.3.3A-C). Interestingly, chromosome painting analysis of Emd-depleted cells also showed dispersed chromosome territories similar to strain. A combination of Emd depletion and mechanical strain did not further strengthen the effect (Fig. 4.3.3D), suggesting that strain-induced chromatin remodeling is mediated through Emd. Collectively, these data indicate that mechanical strain regulates chromatin rearrangement through Emd.

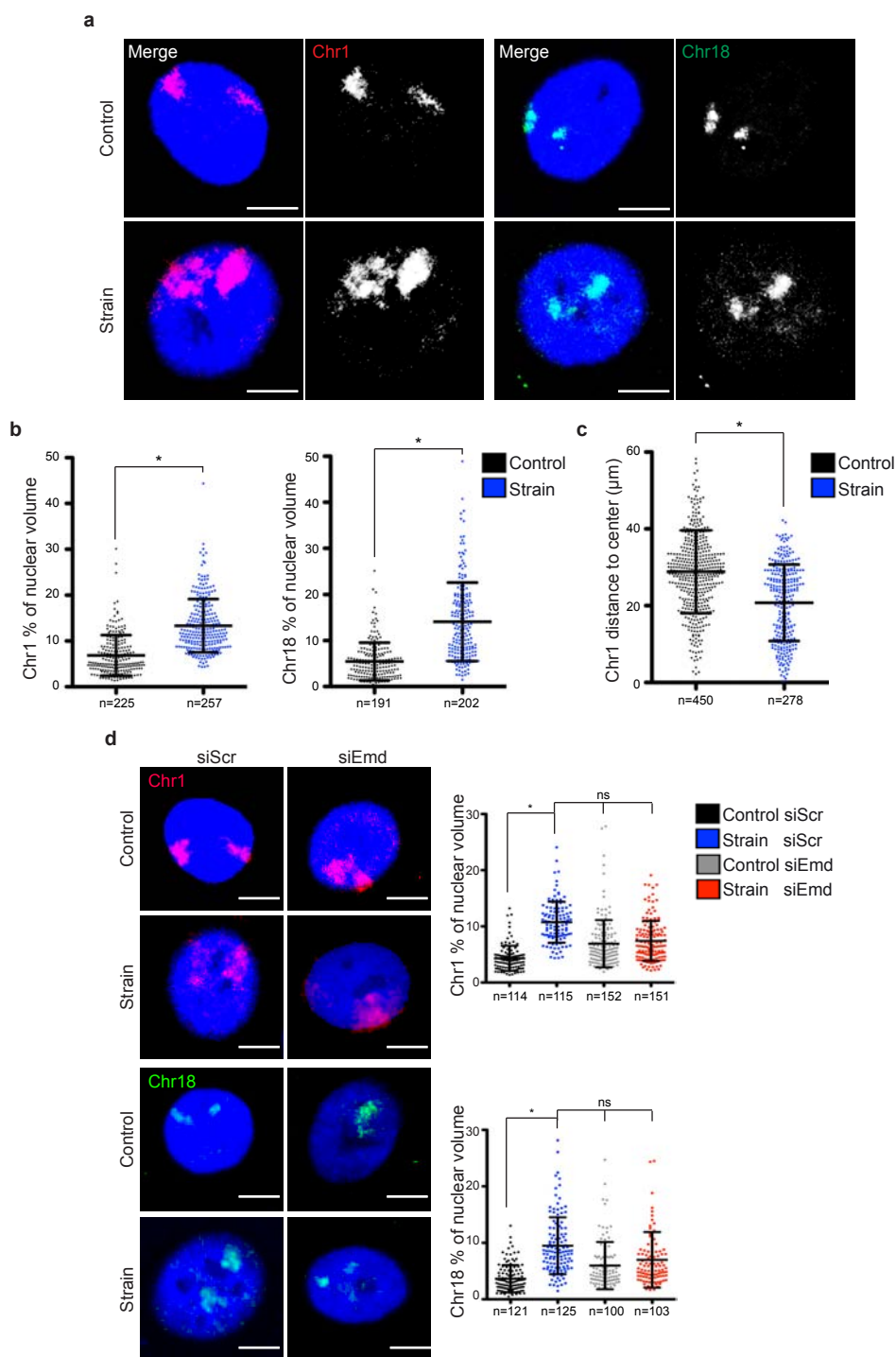


**Fig. 4.3.3. Strain induces chromatin remodeling.** *a.* Chromosome painting of Chr1 and 18 shows that strain induces diffused chromosome territories (scale bars 7.5  $\mu\text{m}$ ). *b.* Quantification shows the ratio of Chr1 and Chr18 volume to total nuclear volume (mean  $\pm$  SD,  $n \geq 150$  nuclei from 3 independent experiments,  $*p=0.05$ , Mann-Whitney). *c.* Quantification shows that strain leads to centrally located to the center of the nucleus (mean  $\pm$  SD,  $n \geq 150$  nuclei from 3 independent experiments,  $*p=0.05$ , Mann-

Whitney). **d.** *Chromosome painting of Chr1 and 18 show that both strain and depletion of Emd cause the chromosome domains more diffused (scale bars 5  $\mu$ m). Right panels show quantification (mean  $\pm$  SD,  $n > 120$  cells from 3 independent experiments,  $*p < 0.0237$ , Kruskal-Wallis/Dunn's).*

#### **4.4 Nuclear actin regulates transcription activity upon strain**

The switch from H3K9me<sub>2,3</sub> to H3K27me<sub>3</sub> on constitutive heterochromatin and the observed chromatin remodeling could partially explain for the strain-induced enrichment of H3K27me<sub>3</sub>; however, it could not account for increased H3K27me<sub>3</sub> occupancy at promoters of PRC2 target genes as well as constitutive actively transcribed genes, which had low or no signals of H3K9me<sub>2,3</sub> (Fig. 4.4) (Consortium, 2012). Therefore, the next step was to discover the mechanisms by which strain regulates transcribed genes.

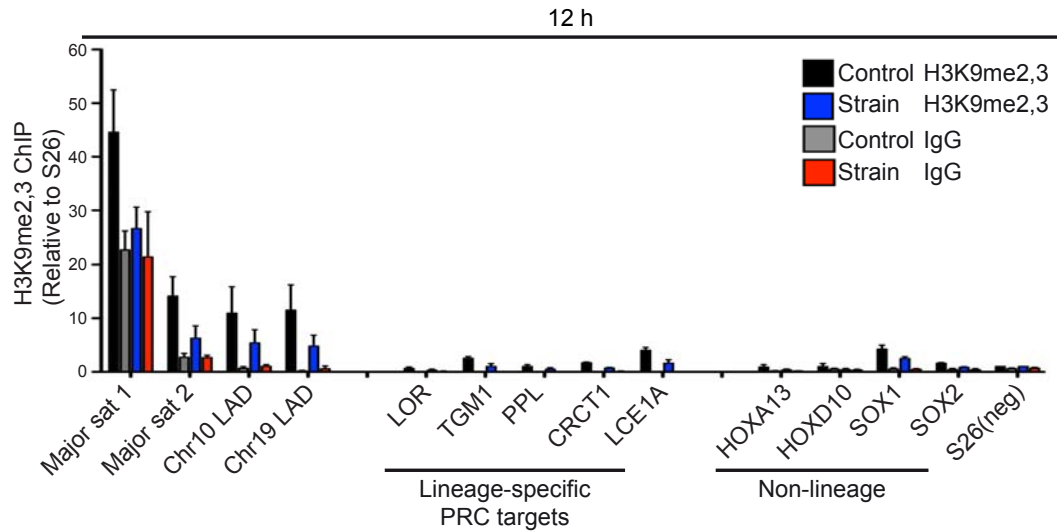
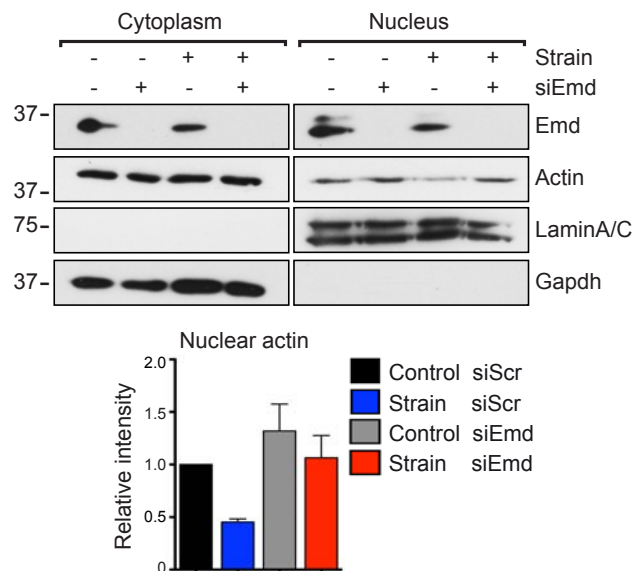


**Fig. 4.4. Different patterns of H3K9me2,3 enrichment on three different gene categories.** H3K9me2,3-ChIP reveals reduced levels of this mark on major satellites (Major sat) and LADs regions upon 12 h of strain. Low levels of H3K9me2,3 is detected at promoters of lineage and non-lineage PRC2 target genes (mean + SEM, n=3 independent experiments).

#### 4.4.1 Strain reduces nuclear actin levels in an Emd-dependent manner

We showed that strain induces a strong polymerization of actin around the nucleus (Fig. 4.2.1D). As nuclear actin has been reported to enhance RNAPII activity (Dopie et al., 2012; Hofmann et al., 2004; Kukalev et al., 2005), and play important role in the regulation of chromatin structure, and remodeling (Grosse and Vartiainen, 2013; Kapoor and Shen, 2014), we asked if strain-induced perinuclear F-actin ring would limit the availability of nuclear actin pool, resulting in transcriptional repression. To test this, nuclear fractions from EPCs exposed to 12 h of strain were analyzed. The results showed that strain indeed reduced nuclear actin levels to 50% of control levels (Fig. 4.4.1A-B). This reduction could be prevented by Emd-depletion (Fig. 4.4.1B),



confirming that Emd mediates the effect of strain.

**Fig. 4.4.1. Strain regulates nuclear actin levels through Emd.** Nuclear fractionation of cells exposed to 12 h of strain shows a decrease in nuclear actin levels in cells exposed to strain. Depletion of Emd prevents the strain-induced decrease in nuclear actin. Quantification shows mean + SEM, n=4 independent experiments.

#### **4.4.2 Accumulation of nuclear actin reverses the effect of strain on transcription and H3K27me3**

To investigate if the reduction in nuclear actin levels would impact transcription, we sought to alter nuclear actin pool. Because overexpression of nuclear actin is harmful for cells, an alternative approach was used to manipulate nuclear actin levels. It has been reported that actin can be shuttled from the cytoplasm to the nucleus specifically by importin-9 (IPO9), and vice versa by exportin-6 (XPO6) (Dopie et al., 2012; Stüven et al., 2003). As expected, nuclear actin levels were increased by depletion of XPO6 (Fig. 4.4.2A-B). Moreover, XPO6-depleted cells showed an opposite phenotype compared to strained cells. Immunofluorescence analysis of RNAPII-S2p showed that an accumulation of nuclear actin led to enhanced RNAPII activity and reduced H3K27me3 levels (Fig. 4.4.2C), in agreement with previous reports on nuclear actin and its role in regulatory of RNAPII activity (Hofmann et al., 2004; Kukalev et al., 2005). ChIP analysis of RNAPII-S2p from XPO6-depleted cells revealed increased signals of RNAPII-S2p at gene bodies of PRC2 target genes, both lineage and non-lineage, as well as actively transcribed genes (Fig.4.4.2D), whereas ChIP-H3K27me3 showed decreased occupancy of H3K27me3 at promoters of these genes (Fig. 4.4.2E), indicating that increasing availability of nuclear actin can reverse the effect of mechanical strain on transcriptional repression and PRC2 activity. As further evidence, inhibiting RNAPII elongation state by 5,6-dichlorobenzimidazole 1- $\beta$ -D-ribofuranoside (DRB) offset the effect of nuclear actin on H3K27me3 (Fig. 4.4.2F), strengthening our hypothesis that strain regulates H3K27me3 occupancy by suppressing of transcriptional elongation. Together, these data suggested that decreased nuclear actin levels upon strain attenuate RNAPII activity and this leads to increased H3K27me3 accumulation at promoters of silenced genes.

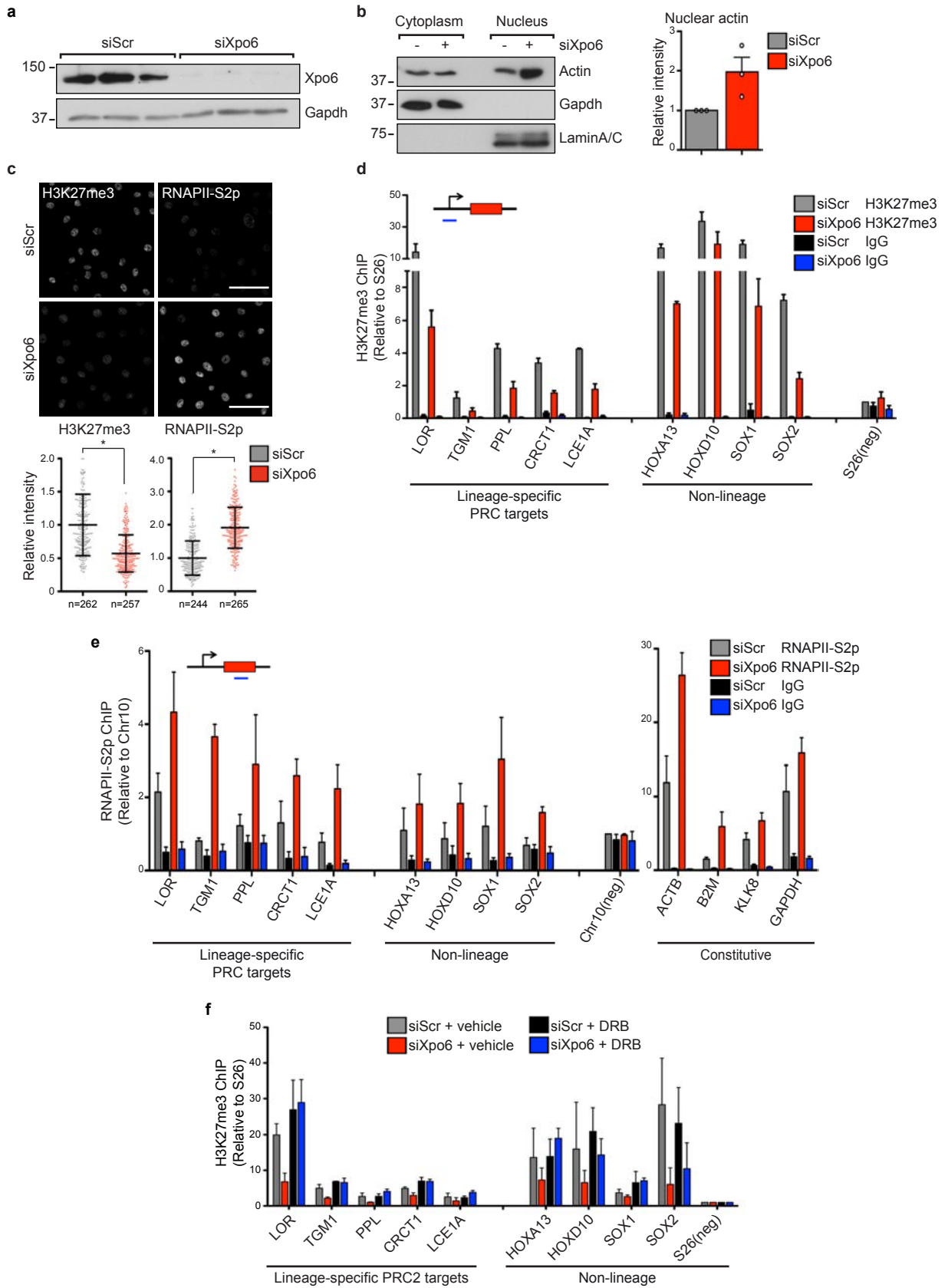


**Fig. 4.4.2. Nuclear actin mediates the effect of RNAPII-S2p on H3K27me3.** *a.* Western blot analysis shows an efficient depletion of Xpo6. *b.* Nuclear fractionation shows that depletion of XPO6 leads to increase nuclear actin levels. Quantification shows mean + SEM, n=3 independent experiments. *c.* Depletion of XPO6 results in decreased levels of H3K27me3 and a parallel increase in RNAPII-S2p (scale bars 50  $\mu$ m, mean  $\pm$  SD, n $\geq$ 200 cells from 4 independent experiments, \*p=0.021, Mann-Whitney). *d.* H3K27me3-ChIP shows that XPO6-depleted cells have decreased occupancy of this mark at promoters of PRC2 target genes (mean + SEM, n=3 independent experiments). *e.* RNAPII-S2p-ChIP shows that XPO6 depleting leads to increased occupancy of this mark on gene bodies of PRC2 target genes and constitutively expressed genes in Xpo6-depleted cells (mean + SEM, n=3 independent experiments). *f.* DRB treatment abolishes the effect of nuclear actin on H3K27me3 occupancy. (mean + SEM, n=3 independent experiments).

#### **4.4.3 Strain-induced chromatin remodeling is independent on nuclear actin-mediated transcription**

As nuclear actin is a component of chromatin remodeling complexes (Kapoor et al., 2013; Visa and Percipalle, 2010), we next investigated whether strain-induced chromatin rearrangements depend on nuclear actin. For this, H3K9me<sub>2,3</sub>-ChIP was performed in XPO6-depleted cells. The result showed that accumulation of actin in the nucleus did not alter H3K9me<sub>2,3</sub> occupancy on LADs and major satellites (Fig. 4.4.3), suggesting that strain-induced epigenetic switch on constitutive heterochromatin is independent of nuclear actin.

Collectively, these experiments indicate that the relocation of Emd upon strain has two parallel effects: 1) it mediates the switch from H3K9me<sub>2,3</sub> to H3K27me<sub>3</sub> on LADs and major satellites, thus inducing reorganization of chromatin. 2) Emd together with actin and NMIIA limit the availability of nuclear actin, thus repressing RNAPII-driven transcription, leading to increased H3K27me<sub>3</sub> occupancy at promoters of paused RNAPII-driven genes.

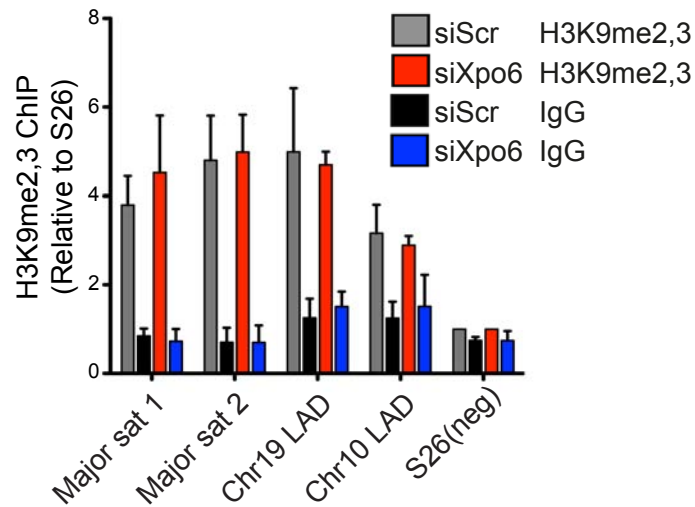


**Fig. 4.4.3. Strain-induced chromatin remodeling is independent on nuclear actin.** ChIP-qPCR shows no changes in H3K9me2,3 occupancy on LADs and major satellites (Major sat) upon Xpo6 depletion (mean + SEM, n=4 independent experiments).

## 4.5 Strain regulates EPC lineage commitment

### 4.5.1 Strain attenuates differentiation gene expression in a myosin dependent manner

To address the functional consequence of strain-induced chromatin remodeling, we studied the effect of forces on the expression of the lineage specific PRC2 target genes. Immunofluorescence analysis from EPCs exposed to strain revealed that strain prevented expression of Tgm1 protein, a marker for EPC differentiation (Fig. 4.5.1A) RT-qPCR analysis of EPC basal lineage specification and differentiation genes further showed that strained cells would not upregulate these genes in the presence of Ca<sup>2+</sup> as a differentiation signal after 24 h of strain (Fig. 4.5.1B-C). Importantly, strain did not change EPC lineage identity because Keratin 14 (K14), a basal lineage identity gene, was not altered. This is in agreement with previous reports showing that PRC2 selectively regulates terminal differentiation (Ezhkova et al., 2009).

Since myosin activity was required to increase H3K27me3 upon strain, we sought to confirm that it is also required to repress transcription of differentiation genes. To this end EPCs were exposed to 12h of strain in the presence of Bleb as an inhibitor for myosin activity. As expected, inhibition of myosin activity prevented the strain-induced suppression of EPC differentiation on both gene and protein levels (Fig. 4.5.1B-C).

To study whether strain-induced actin polymerization was required for repressing EPC differentiation cytochalasin D (CytoD) – an inhibitor of actin polymerization – was used (Casella et al., 1981). RT-qPCR analysis of EPC differentiation genes showed that CytoD-treated cells with or without strain expressed the same levels of differentiation genes as control cells (Fig. 4.5.1D), suggesting that actin polymerization and myosin activity are required for strain-induced repression of transcription.

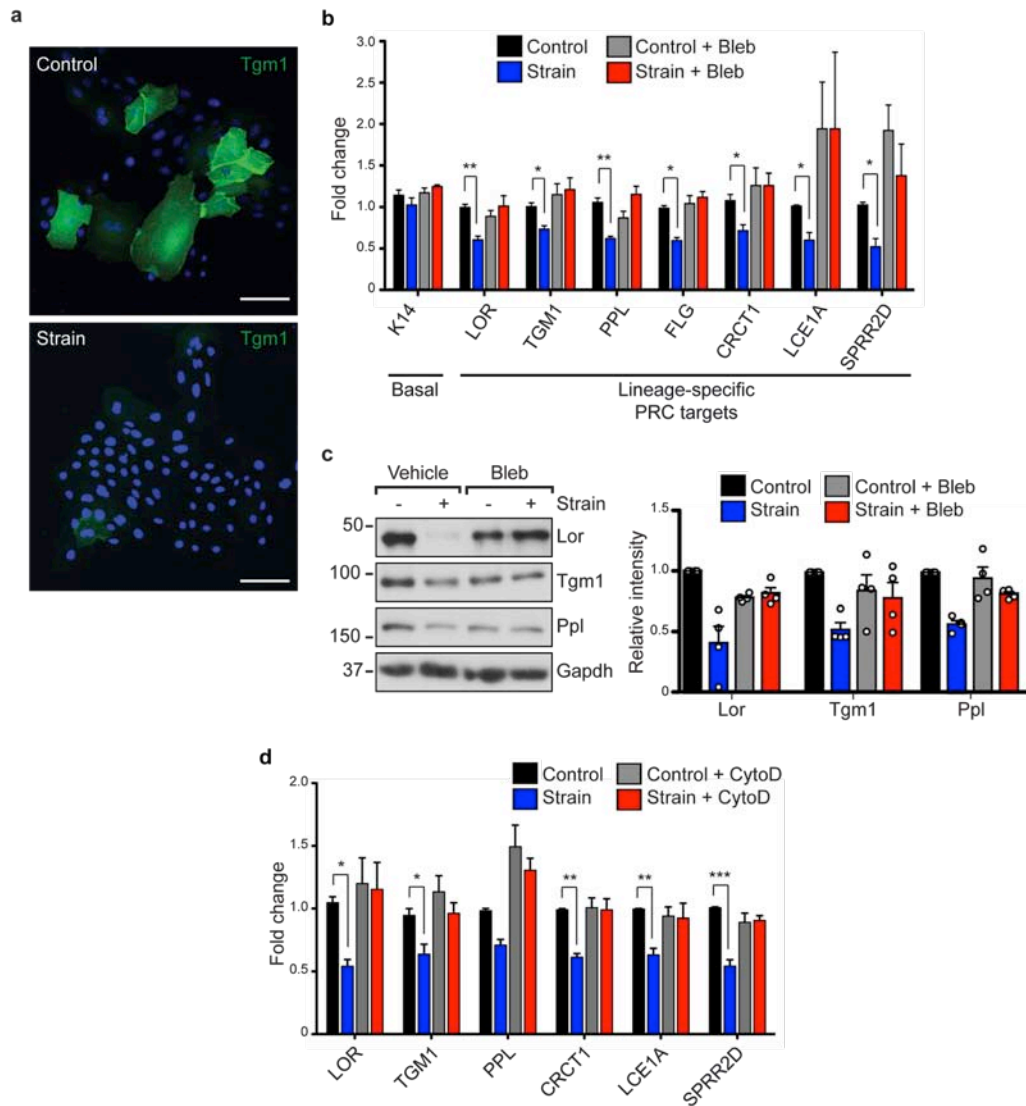


**Fig. 4.5.1. Force-mediated adjustment of transcription regulates EPC lineage commitment.** *a.* Immunofluorescence analysis of Transglutaminase 1 (*Tgm1*) reveals that strain decreases levels of *Tgm1* as a marker for EPCs differentiation (scale bars 100  $\mu$ m). *b.* qPCR of basal lineage specification and differentiation genes shows a myosin-dependent reduction in late differentiation genes upon strain (mean + SEM,  $n=5$  independent experiments,  $*p<0.1$ ,  $**p<0.01$ , Kruskal-Wallis/Dunn's). *c.* Western blot analysis shows a myosin-dependent reduction in the levels of late-differentiated proteins upon strain. Quantification shows mean + SEM,  $n=3$  independent experiments. *d.* qPCR analysis shows that disruption of F-actin stress fibers by CytoD treatment prevents repression of differentiation gene expression upon strain (mean + SEM,  $n=5$ ,  $*p<0.05$ ,  $**p<0.01$ ,  $***p<0.001$ , Kruskal-Wallis/Dunn's).

### 4.5.2 PRC2 activity is required for strain-repressed differentiation genes expression

To confirm that strain-induced repression of differentiation genes depends on PRC2 activity, Ezh2, the methyltransferase of the PRC2 complex, was knocked down prior to straining. ChIP-qPCR analysis of H3K27me3 showed that Ezh2-depleted cells failed to induce enrichment of H3K27me3 levels at promoters of lineage specific PRC2 target genes (Fig. 4.5.2A). RT-qPCR further revealed that without Ezh2, strained cells could not repress the expression of differentiation genes (Fig. 4.5.2B). These data confirm that PRC2 activity is required to mediate the effect of strain on gene expression.

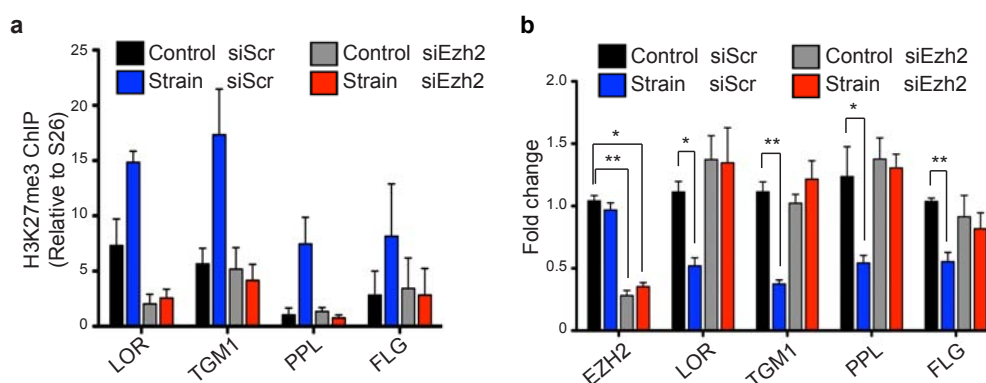


**Fig. 4.5.2. PRC2 activity is required for strain-repressed differentiation genes expression.** *a.* Depletion of Ezh2 prevents strain-induced accumulation of H3K27me3 at promoters of PRC2 targets (mean + SEM, n=3 independent experiments). *b.* qPCR analysis shows that Ezh2 is required to repress the expression of late differentiation gene upon strain (mean + SEM, n=4 independent experiments, \* $p < 0.05$ , \*\* $p < 0.01$ , Kruskal-Wallis/Dunn's).

### 4.5.3 Strain-induced repression of transcription in an Emd-dependent manner

We next asked whether Emd was also necessary to repress the expression of EPC lineage genes upon strain. Emd-depleted cells were exposed to strain followed by RT-

qPCR. The result showed that strain repressed the expression of lineage specific genes as well as non-lineage genes (Fig. 4.5.3). This was accompanied by accumulation of H3K27me3 at promoters of both lineage and non-lineage specific PRC2 target genes. Furthermore, depletion of Emd prohibited strain-induced transcription repression (Fig. 4.5.3), confirming that Emd is required to transmit force to the nucleus to regulate EPC lineage commitment.

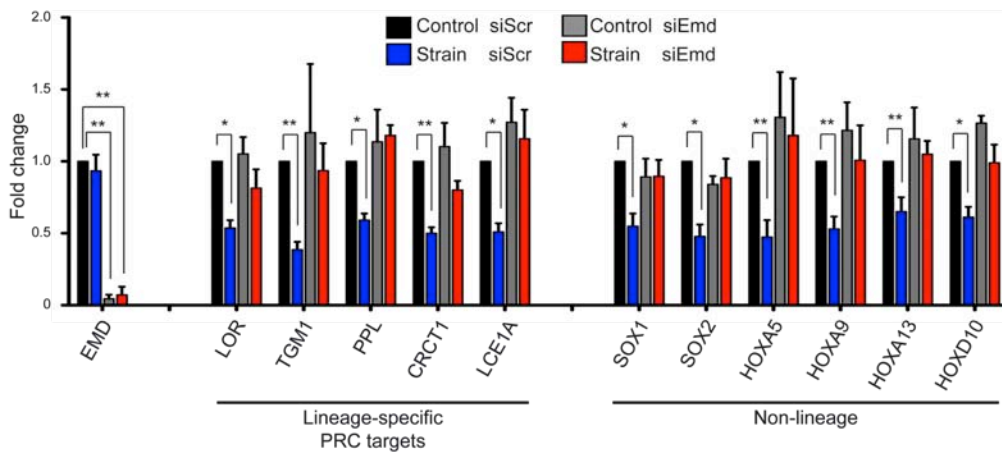


**Fig.4.5.3. Strain-induced repression of transcription in an Emd-dependent manner.** qPCR analysis of PRC2 target genes in Emd-depleted EPCs shows that Emd is required for repressing the expression of PRC2 target genes upon strain (mean + SEM, n=4 independent experiments, \* $p < 0.05$ , \*\* $p < 0.008$ , Kruskal-Wallis/Dunn's).

#### 4.5.4 Nuclear actin is required to mediate the adjustment of transcription

To confirm that nuclear actin mediated the effect of strain on EPC differentiation XPO6 knock-down cells were exposed to strain, followed by RT-qPCR analysis of differentiation gene expression. The result showed that restoring nuclear actin levels upon strain by XPO6 depletion rescued the expression of differentiation genes, such as LOR, TGM1, PPL, CRCT1, LCE1A, and SPRR2D, without affecting the expression of basal lineage identity K14 (Fig. 4.5.4A). Interestingly, decreasing nuclear actin levels by depleting of IPO9 mimicked the effect of strain on late differentiation gene

expression (Fig. 4.5.4B). These experiments confirmed that nuclear actin mediates transcription.

Together, these data indicate that strain attenuates EPC differentiation. This effect depends on actomyosin, Emd, and PRC2 activity as well as on nuclear actin levels.

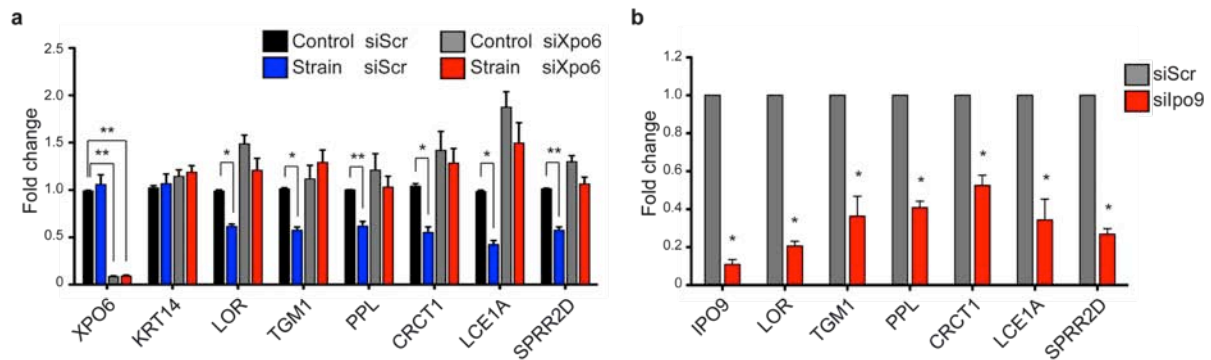


**Fig. 4.5.4. Nuclear actin mediates the effects of strain on gene expression. a.** Depletion of *Xpo6* blocks the attenuation of differentiation gene expression in strained cells (mean + SEM,  $n=4$ ,  $*p<0.04$ ,  $**p<0.01$ , Kruskal-Wallis/Dunn's). **b.** Depletion of *Importin 9* (*siIpo9*) decreases expression of EPC late differentiation genes (mean + SEM,  $n=3$ ,  $*p<0.03$ , Mann-Whitney).

#### 4.6 NMIIA activity regulates terminal differentiation *in vivo*

Our data had revealed an important role of the Emd-actin-NMIIA mechanosensory complex in relaying extrinsic forces on the nucleus, to regulate EPC lineage commitment. To investigate whether this mechanosensory rheostat regulates epidermal differentiation and thus morphogenesis *in vivo*, we first analyzed wild-type mouse EPCs for the effect of strain on transcription and PRC2 activity in order to validate the usefulness of the mouse as an *in vivo* model. Immunofluorescence analysis of mouse EPCs showed that strain at 10%-100 mHz decreased RNAPII-S2p and increased H3K27me3 intensity after 12 h (Fig. 4.6.1A). Furthermore, RT-qPCR analysis confirmed that strain repressed the expression of differentiation genes and non-lineage

specific genes after 12 h (Fig. 4.6.1B). These experiments indicate that the effect of strain is conserved in mouse EPCs.

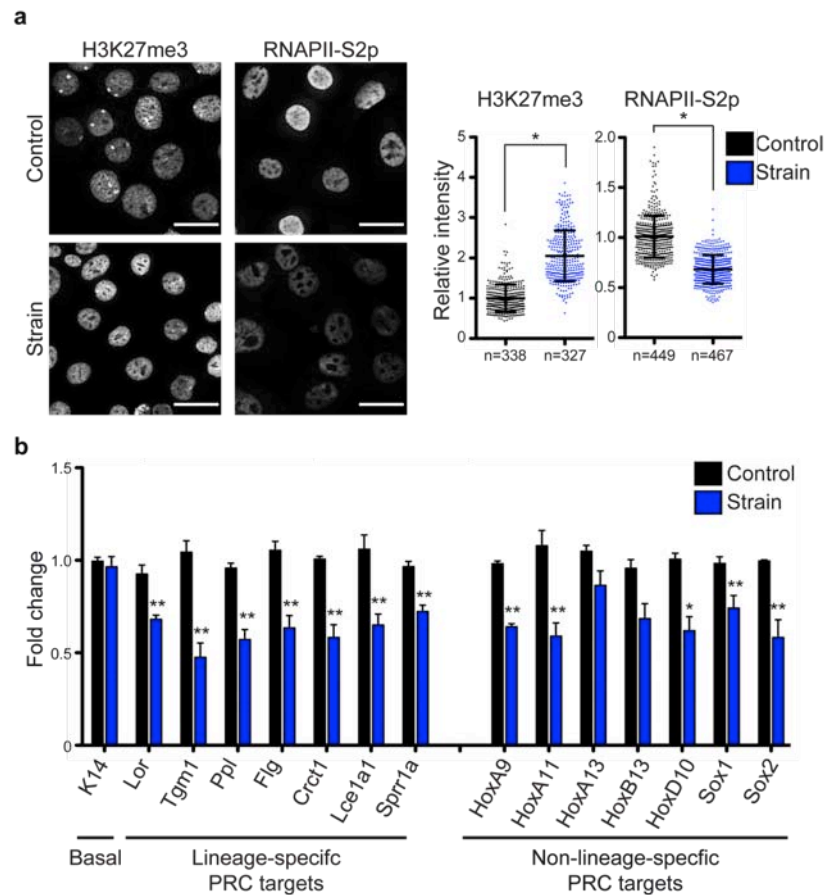


**Fig. 4.6.1. The effect of strain is conserved for mouse keratinocytes.** *a.* Immunofluorescence analysis of mouse keratinocytes shows increased H3K27me3 and decreased RNAPII-S2p after 12 h of strain (scale 30  $\mu$ m, mean  $\pm$  SD,  $n > 200$  cells from 4 independent experiments,  $*p < 0.05$ , Mann-Whitney). *b.* qPCR analysis shows that strain repress the expression of lineage-specific and non-lineage PRC2 target genes in mouse keratinocytes after 12 h (mean + SEM,  $n = 6$ ,  $*p = 0.027$ ,  $**p < 0.008$ , Mann-Whitney).

Our previous data showed that NMIIA displays an important role in regulating the response of EPCs upon strain. An epidermis-specific deletion of the myosin heavy polypeptide 9 (Myh9<sup>EKO</sup>) gene encoding for the heavy chain of NMIIA was generated by crossing Myh9 floxed/floxed mice (Conti et al., 2004) with mice expressing Keratin-14 Cre (Hafner et al., 2004). The mouse experiments described below were performed by other laboratory members.

Epidermis-specific deletion of NMIIA resulted in perinatal lethality. EPCs isolated from Myh9<sup>EKO</sup> showed abnormal cell shape, absence of stress fibers and aberrant membrane protrusions (Fig. 4.6.2A), indicating that NMIIA is required for generating tension and for organizing the actomyosin cytoskeleton. Hematoxylin/Eosin staining of skin revealed, a thinner epidermal layer and the arrest of hair follicle morphogenesis in Myh9<sup>EKO</sup> mice at P0 (Fig. 4.6.2B), indicating defects in epidermal morphogenesis. Immunofluorescence analysis using the terminal differentiation marker K10 and the progenitor marker K14 showed thinner K10-positive layers and importantly, presence of K10-positive cells in the progenitor cells layer of Myh9<sup>EKO</sup> epidermis (Fig. 4.6.2C). In addition, staining with loricrin as a marker for the cornified layer revealed the absence of a proper spinous layer in Myh9<sup>EKO</sup>. These data explain the thinner epidermis in Myh9-deficient mice, and suggest that NMIIA is required for proper timing of terminal differentiation.

To further analyze the role of NMIIA in regulating epidermal differentiation, the expression of lineage specific genes was analyzed. ChIP-qPCR of H3K27me3 analysis revealed decreased occupancy of this mark on promoters of differentiation genes (Fig. 4.6.2D). RT-qPCR showed that these genes were upregulated upon loss of NMIIA (Fig. 4.6.2E), confirming that NMIIA plays important role in epidermal differentiation. Collectively, these data provide evidences that NMIIA is required for regulating of transcription and PRC2 activity, hence playing a vital role for lineage progression through epidermal morphogenesis.

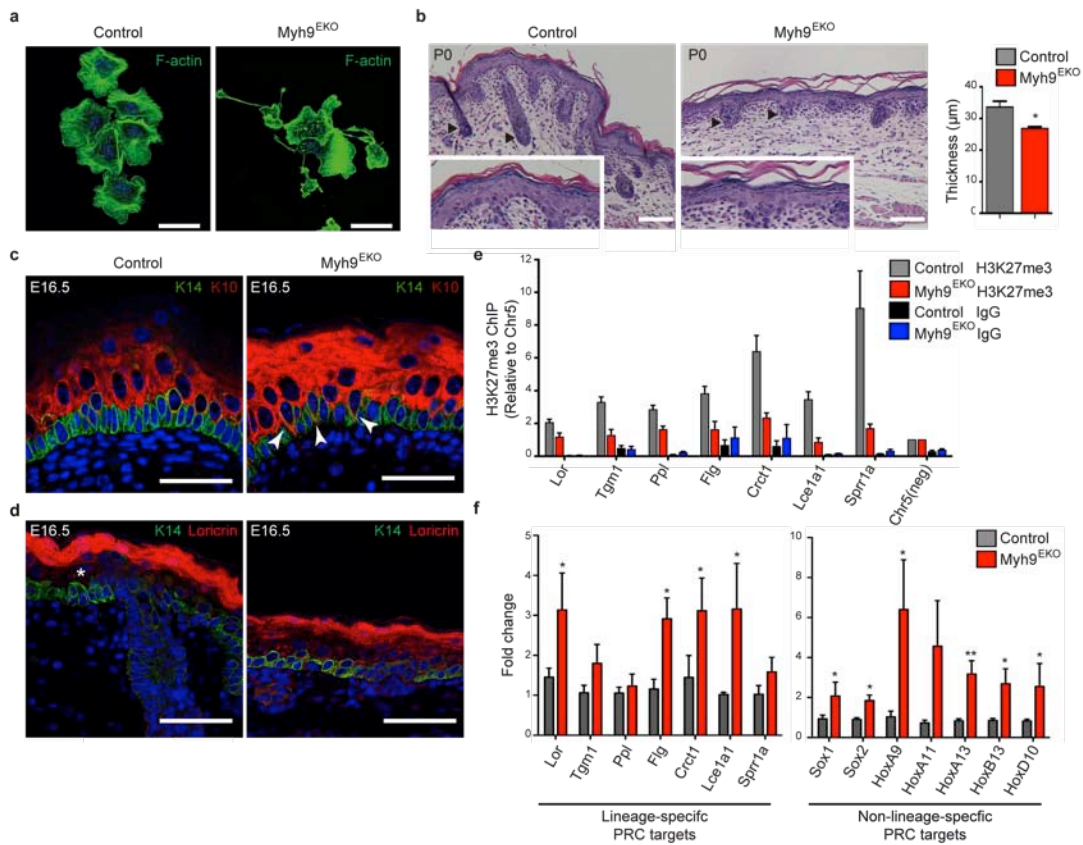


**Fig. 4.6.2. Myh9-deficient mice show defects in epidermal architecture and differentiation.** *a.* Immunofluorescence analysis of the actin cytoskeleton of keratinocytes isolated from control and Myh9<sup>EKO</sup> mice show absence of F-actin stress fibres and aberrant membrane protrusions in Myh9<sup>EKO</sup> keratinocytes. Scale bars 50 μm. *b.* Hematoxylin/Eosin staining shows a thinner epidermis and arrested hair follicle development in Myh9<sup>EKO</sup> mice (arrows; scale bars 50 μm). Quantification of epidermal thickness shows mean + SEM, n=4 mice/genotype, \*p=0.0286, Mann-Whitney. *c-d.* Immunofluorescence analysis of E16.5 skin using the EPC marker Keratin 14 (K14), K10 as marker of the differentiated spinous layer (*c*) and Loricrin as a marker for the cornified layer (*d*). The K10-positive layer of Myh9<sup>EKO</sup> epidermis is thinner and K10-positive cells can also be detected in the basal r layer (arrowheads). Loricrin expression is detected directly above the K14-positive basal layer, indicating absence of spinous layer (asterisk) in Myh9<sup>EKO</sup> epidermis. Scale bars 30 μm. *e.* qPCR analysis of H3K27me3-ChIP shows decreased occupancy of this mark on promoters of differentiation genes in Myh9<sup>EKO</sup> E16.5 epidermis (mean + SEM, n=8 mice/genotype). *f.* qPCR analysis of late differentiation genes in E16.5 epidermis of Myh9<sup>EKO</sup> and

*control mice shows upregulation of late differentiation gene expression in Myh9<sup>EKO</sup>  
(mean + SEM, n=4 mice/genotype, \*p<0.02, Mann-Whitney).*

## 5. Discussion

The actomyosin cytoskeleton plays a critical role in force generation and transmission. It provides a direct link to transduce mechanical forces through the cytoplasm to the nucleus and thus to the chromatin. As a consequence, it can direct cellular responses to forces. However, the molecular mechanisms underlying force-driven cellular responses have remained elusive. Here we show that extrinsic mechanical strain represses global transcription and induces chromatin rearrangements, as summarized in Fig. 5.

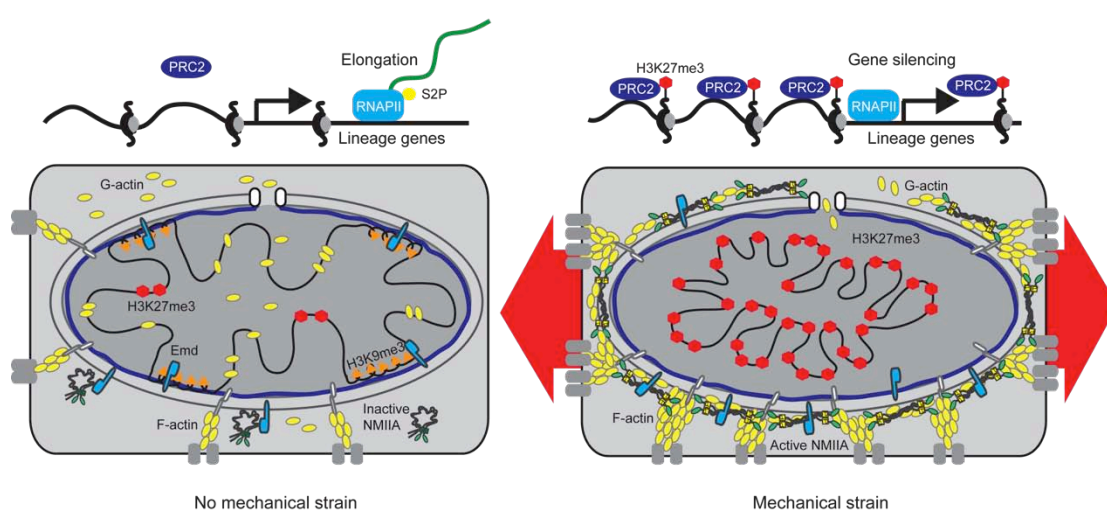


**Fig. 5. A proposed model describing force-induced transcriptional regulation, chromatin rearrangement and cell fate decisions.**

In summary, extrinsic cyclic biaxial mechanical strain at 10% elongation and 100 mHz mediates actin cytoskeleton remodeling and enhances myosin II activity. The actomyosin network in turn, transmits the force to the nucleus. At the NE, mechanical strain leads to enrichment of Emd, NMIIA and local actin polymerization. The enrichment of Emd at the ONM decreases Emd levels at the INM, resulting in loss of H3K9me<sub>2,3</sub> on LADs and major satellites. Importantly, cells maintain the silencing at these regions by acquiring H3K27me<sub>3</sub>, a repressive mark catalyzed by PRC2. This is accompanied by large-scale chromatin rearrangements. In parallel, Emd and NMIIA coordinate peri-nuclear F-actin polymerization, which decreases levels of nuclear G-actin. As nuclear actin regulates RNAPII activity, its reduction represses transcription

and subsequently induces recruitment of PRC2 to promoters of the downregulated genes. PRC2 then trimethylates H3K27 at these regions, thereby inducing gene silencing.

### **5.1 Strain induces global transcriptional repression and subsequent H3K27me3-mediated gene silencing**

Our data revealed that mechanical strain represses global transcription by attenuating RNAPII elongation. In line with a previous report (Riising et al., 2014), we observed subsequent enrichment of H3K27me3 at the promoter regions of these repressed genes, indicating that transcription regulates PRC2 activity. Interestingly, mechanical strain had the strongest effect on lineage-specific PRC2 target genes, thereby preventing terminal differentiation of strain-exposed EPCs. As the transcriptional repression was global, it is not completely clear why strain specifically impacts these differentiation genes. It was reported that epidermal terminal differentiation genes are under direct control of PRC2 (Ezhkova et al., 2009), indicating that altering PRC2 activity changes the expression of these genes. Importantly, PcG proteins have been shown to play crucial roles in maintaining stem cell pluripotency and lineage-specific identity (Morey et al., 2015; Yang et al., 2016). Depletion of *Suz12* or *Ezh2* in embryonic stem cells (ESCs) leads to global loss of H3K27me3. Interestingly, these ESCs have almost no defects in proliferation ability and viability, but fail to establish a proper differentiation program (Pasini et al., 2007; Shen et al., 2008). These reports indicate that PcG proteins are not required for SC self-renewal but critical for cell fate determination (Di Croce and Helin, 2013). Based on these observations, we hypothesize that the effect of strain on differentiation genes is due to EPC fate transition. We induced the differentiation process in EPCs by Ca<sup>2+</sup> switch prior to strain, as Ca<sup>2+</sup> acts as a trigger signal for the differentiation of EPCs (Bikle et al., 2012). Despite this strong differentiation signals, EPCs failed to switch on their differentiation gene expression program. This indicates that the PRC2 competes with RNAPII at promoter regions of lineage-specific genes to control their expression, and at promoters where transcription is initially low (such as the differentiation genes and non-lineage specific genes), the reduced RNAPII activity is sufficient to allow strong PRC2 occupancy and subsequent

complete silencing, whereas at constitutive genes the observed ~10% reduction in transcription is not substantial enough to allow recruitment of sufficient amounts of PRC2.

Non-lineage-specific genes are also under PRC2 control, they are expressed very low levels of mRNAs, known as “leaky” transcription (Alberts et al., 2007); (Consortium, 2012). It has been suggested that further compaction of chromatin at these regions could prevent the leaky transcription (Alberts et al., 2007). We detected a small but consistent enrichment of H3K27me3 occupancy at promoters of *Hox* and *Sox* genes. These enhanced H3K27me levels might prevent strained cells from the “leaky” expression of non-lineage genes. This effect was detectable at mRNA levels although it was not as strong as the effect on differentiation genes.

How could strain regulate transcriptional silencing on the molecular level? One potential model is that strain could induce the establishment of bivalent promoters, particularly at lineage-specific genes. Bivalent promoters have been suggested to maintain an open and accessible chromatin state as a checkpoint to ensure that only strong and sustained signals are capable of driving transcription (Brookes and Pombo, 2012; Laugesen and Helin, 2014). This is in line with our RNA-seq data showing a profile of strain repressed global transcription, suggesting a force-induced regulation of the chromatin state. We propose two potential bivalency models that could take place upon strain. 1) Several previous studies suggest that the establishment of bivalency allow the timely activation of lineage-specific genes while remaining inactive in the absence of differentiation signals. Thus one possibility could be that differentiation genes in EPCs exist in a bivalent state and strain-induced increased PRC2 activity could strengthen this state. This model could be tested by performing ChIP-seq analysis for bivalency in EPCs, Ca<sup>2+</sup>-treated EPCs and strained EPCs. 2) Alternatively, strain could establish bivalent domains *de novo* at PRC2 lineage-specific genes to maintain accessible promoters, allowing EPCs to stay in a plastic and inducible state. The bivalency could also explain the effect of strain on different gene categories; constitutively transcribed genes do not establish bivalent domains whereas PRC2 target genes do (Voigt et al., 2013). Regardless of which model is correct, genome-wide distribution of H3K27me3, H3K4me3 (an active histone mark) and RNAPII-S5p will help us to further test these hypotheses.

Consistent with previous reports on nuclear actin (Miyamoto and Gurdon, 2013), we showed that nuclear G-actin regulates RNAPII activity. However, it is unclear how nuclear actin affects gene expression, and whether there are some clusters of actin-driven genes that are more strongly influenced by actin and mechanical force. How nuclear actin and PRC2 coordinate their activity in regulating the expression of lineage-specific genes is an interesting open question. A genome-wide mapping for nuclear actin in addition can bring us more insight into how mechanical strain regulates lineage commitment.

Although no studies so far have been able to elucidate the mechanism of recruitment of PRC2, some studies suggest that non-coding (nc)RNAs might play a central role in regulating transcription, chromatin remodeling and PcG recruiting (Fang and Fullwood, 2016; Quinn and Chang, 2016). Our preliminary data on ncRNAs (data not shown) suggests that strain downregulates the expression of many ncRNAs. Therefore it is of great interest to study further the role of strain-mediated ncRNAs; for example, whether overexpression of some ncRNAs could rescue strain-induced transcription repression, or RNA pull-down assays to discover the interaction between ncRNAs, RNAPII and PcG proteins upon strain.

## **5.2 Strain regulates transcription through Emd**

Emd is a nuclear membrane protein, mainly localized at the INM. The N-terminal of Emd has a LEM domain, which interacts directly with numerous nuclear proteins, including BAF, lamins as well as chromatin-modifying complex, and is required to facilitate the formation of repressive heterochromatin at the NE (see 1.3.2.2). Furthermore, Emd has been shown to be associated with multiple protein complexes, which regulate gene expression and chromatin dynamics such as nuclear co-repressor (NCoR) complex (Demmerle et al., 2012), nuclear factor-Y (NF-Y) (Holaska and Wilson, 2007) and transcriptional regulation complex (with GCL, Btf and YT521-B) (Holaska and Wilson, 2006), suggesting that Emd could play important roles as a regulator of nuclear architecture, nuclear assembly and gene expression.

It has been suggested that the nucleus is an integral component of the mechanical response of the cell (Alam et al., 2014; Chang et al., 2015). Failure of cells to respond to mechanical forces due to impaired NE results in a broad range of diseases, for example dystrophy, cardiomyopathy, and premature aging (Isermann and Lammerding, 2013). We observed that mechanical strain leads to Emd retention at the ONM and in the ER. However, we do not fully understand the mechanism of Emd redistribution. We postulate that strain could promote changes in Emd at the molecular level. In line with previous report (Guilluy et al., 2014), our preliminary mass-spectrometry analysis on Emd (data not shown) suggests that strain could cause changes in PTMs of Emd. Further experiments are required to characterize the function of these PTMs to understand whether they contribute to the redistribution of Emd upon strain.

Emd together with Nesprin and SUN domain proteins establish the LINC complex, providing a physical link between the cytoskeleton and the nucleus. They have several functions in nuclear positioning, chromatin organization, cell fate decisions and migration (Chang et al., 2015; Horn, 2014). Importantly, recent studies also suggest the role of Nesprin and SUN domain proteins in force transmission to the chromatin (Isermann and Lammerding, 2013; Jahed et al., 2015). We discovered the role of Emd in response to force. However, it is still unknown if strain affects Emd alone or in complex with Nesprin and SUN domain proteins. It is quite likely that strain impacts the whole LINC complex rather than only Emd. How mechanical forces are sensed at this site remains an open question. An interesting possibility is that strain regulates members of the LINC complex through an allosteric mechanism, as has been shown for other mechanosensitive proteins such as  $\alpha$ -catenin (Yao et al., 2014; Yonemura et al., 2010). In response to force,  $\alpha$ -catenin is stretched, changes its conformation, and thereby recruits vinculin binding. Vinculin in turn stabilizes the “open” conformation of  $\alpha$ -catenin, allowing forces to be transmitted to the actin cytoskeleton. We hypothesize that LINC complex members could also undergo conformational changes in response to strain, increasing their affinity with actin, and thereby perhaps retaining Emd at the ONM. Therefore further researches are needed to study the effect of mechanical strain on the LINC complex, and the function of each component in response to strain.

The NPCs could also be a potential member of the nuclear force sensor complex, although little is known about its role in mechanotransduction. The NPCs provide gateways for exchanging macromolecule between the cytoplasm and the nucleus. Interestingly, they interact both with chromatin and the NE (Fedorchak et al., 2014) and also regulate many nuclear processes, including cell division, transcriptional mediation and histone PTMs (Sood and Brickner, 2014). In addition, as we observed changes in nuclear actin, this could also be a result of altered transport. Therefore it would be interesting to test whether strain has any impacts on the NPCs, such as increasing the pore size or disturbing the interaction between the NPCs and chromatin.

### **5.3 Strain induces large-scale rearrangement of chromatin through Emd**

We showed that strain-induced retention of Emd at the ONM led to decreased levels of H3K29me<sub>2,3</sub> at LADs and major satellites region. Importantly, H3K27me<sub>3</sub> was accumulated at these regions, indicating a compensation between H3K9me<sub>2,3</sub> and H3K27me<sub>3</sub>.

The strain-induced switch of histone PTMs resulted in large-scale chromatin rearrangements; the chromosome territories were more dispersed and diffused. It has been suggested that in certain circumstances, cells could switch their histone PTMs from H3K9me<sub>2,3</sub> to H3K27me<sub>3</sub> to ensure longstanding genome stability (Walter et al., 2016). We observed that strain had no effect on cell growth and viability. Importantly, no nuclear damage was detected. Therefore, we hypothesize that the compensation between H3K9me<sub>2,3</sub> and H3K27me<sub>3</sub> upon strain could be necessary to maintain genome stability during strain. It will be interesting to determine if the switch from H3K9me<sub>2,3</sub> to H3K27me<sub>3</sub> can also be achieved just by depletion of Emd or if it is a specific response to mechanical strain. ChIP analysis for H3K9me<sub>2,3</sub> and H3K27me<sub>3</sub> in Emd-depleted cells would be necessary to reveal this question.

LADs are well-known as repressive domains enriched in H3K9me<sub>2,3</sub>. H3K9me<sub>2,3</sub> has been implicated as a molecular signal for tethering heterochromatin to the NE (Towbin et al., 2012). Loss of H3K9 methyltransferase G9a leads to decreased interactions between LADs and the NE (Kind et al., 2013). Intriguingly, both repressive marks

H3K9me<sub>2,3</sub> and H3K27me<sub>3</sub> are found at the LAD borders, and are required for maintenance LADs at the nuclear periphery (Guelen et al., 2008; Harr et al., 2015). One remaining question in our model is whether strain-induced global chromatin remodeling and switching between two repressive marks are associated with detachment of LADs from the nuclear lamina. DNA adenine methyltransferase identification (DamID) profiles of lamins and Emd from cells exposed to strain would therefore be required to provide direct evidence of the association of chromatin with the nuclear lamina. DamID has been widely used and provides high-resolution studies of genome-nuclear lamina interactions (Guelen et al., 2008; Vogel et al., 2007). Both DamID and ChIP are methods to detect interactions between DNA and protein; however, DamID is not dependent on crosslinking reagents and antibody specificities but based on the low-level expression of a fusion protein composed of the target protein and the Dam from *E. coli*. Because endogenous methylation of adenine does not occur in humans, Dam will target and methylate its motif sequence (GATC) near the site of fused protein-DNA interaction. These sites can then be amplified and detected. With the advancement of next generation sequencing, DamID-seq profiling is now possible to be combined with other functional genomic data (Aughey and Southall, 2016; Kind et al., 2015). Harnessing the potential of this technique, it is of great interest to generate DamID-lamin and DamID-Emd profiles and integrate them with H3K27me<sub>3</sub> and H3K9me<sub>2,3</sub>-ChIP-seq data from strained EPCs. These results would allow us to gain more knowledge about the effect of mechanical force on nuclear architecture, in particular, interactions between chromatin and nuclear lamina as well as the roles of these two histone marks.

The switch from H3K9me<sub>2,3</sub> and H3K27me<sub>3</sub> upon strain was accompanied by the global rearrangement of chromatin. However, it is still unclear if loss of Emd at the INM would first mediate the switch from H3K9me<sub>2,3</sub> to H3K27me<sub>3</sub>, followed by chromatin rearrangement or vice versa. As mentioned, H3K9me<sub>2,3</sub> has been reported to be essential for the sequestration of heterochromatin at the NE (Harr et al., 2015; Towbin et al., 2012), suggesting that strain first reduces H3K9me<sub>2,3</sub> levels, and thereby results in chromatin rearrangement and the compensation of H3K27me<sub>3</sub>. Further studies on this epigenetic switch are required for better understanding the spatiotemporal sequence of events.

The data so far demonstrated the effects of strain on H3K27me3 and H3K9me2,3. In light of the global rearrangements of chromosome territories, it seems likely that other changes could also occur. Therefore, it would be interesting to determine if strain regulates global histone PTMs including H2AK119Ub (a marker for PRC1 activity) and H3K4me3. Histone PTMs have various functions, such as transcriptional regulation, gene repression, chromatin state, DNA repair, cell cycle progression, as well as many unknown functions. Interestingly, the coexistence of several marks can lead to crosstalk between histone PTMs (Bannister and Kouzarides, 2011; Du et al., 2015), and thus their global analyses may shed new light in understanding the mechanism of strain-mediated chromatin remodeling and other DNA-related processes. This could be achieved for example by performing quantitative mass spectrometry (Britton et al., 2011; Zhang et al., 2014).

#### **5.4 Perspective**

Emery-Dreifuss muscular dystrophy (EDMD) is a degenerative disease that mainly affects muscle cells. This disease is due to mutations or misregulation of lamin A/C or Emd (Koch and Holaska, 2014). Many models have been proposed to explain the tissue-specificity of EDMD, suggesting multiple roles of Emd and lamin A/C in tissue-specific gene expression, signal transduction and mechanical stability. Intriguingly, it is becoming evident that no single model can explain the EDMD mechanism entirely, but a combination of them, where mechanical signaling pathways that integrate nuclear architecture and gene expression could play a central role (Holaska and Wilson, 2006; Lammerding et al., 2004). Our results suggest a potential model that explains why EDMD mainly affects tissues that undergo high mechanical loading and why these tissues display severe phenotypes, including abnormal nuclear structure and apoptosis. These phenotypes may be the consequence of an inability to reorganize chromatin conformation as a response to mechanical stress as seen in Emd-deficient cells.

## **5.5 Strain-induced Emd-actin-NMIIA nuclear force sensor affects nuclear actin availability**

Interestingly, Emd has been shown to function as a nuclear force sensor in isolated-nuclei (Guilluy et al., 2014). However, it does not provide information on the interaction of nuclear-cytoskeleton and the trafficking of molecules between the cytoplasm and the nucleus, which only exist in intact cells. In our model, we observed that force induces enrichment of Emd, actin and NMIIA at the ONM. Besides, Emd has been demonstrated to interact directly with both monomeric and filamentous forms of actin (Holaska et al., 2004; Holaska and Wilson, 2007). In line with these observations, we showed that actin and NMIIA interacted with Emd. Moreover, strain further enhanced this interaction, in particular with the active form of myosin. Although it is unknown whether NMIIA binds directly to Emd or through actin, we hypothesize the formation of an Emd-actin-NMIIA complex at the ONM that serves as a nuclear force sensor.

We demonstrated that mechanical strain leads to accumulation of Emd at the ONM together with actin and NMIIA as a nuclear-force sensor; it is still unclear how this structure forms. We expect that the formation of this mechanosensor could be a step-wise process, in which strain induces the actomyosin remodeling process, especially the nuclear actin ring, to prevent the nucleus from deformation. The nuclear actin structure is suggested as an immediate cellular response to extrinsic force (Shao et al., 2015). This actin ring could function as a trap, preventing Emd from diffusion to the INM. Besides, actin could also compete against Lamin A/C to interact with Emd based on the fact that their binding sites on Emd are overlapped (Berk et al., 2013; Yuan and Xue, 2015). Since strain induced strong F-actin stress-fibers polymerization at the ONM, this actin structure may not only prevent Emd from diffusion to the INM, but also recruit Emd from the INM. Live-cell imaging assay and a competition assay between Emd, actin and lamin A/C are therefore required to provide answers to these important questions.

Furthermore, in contrast to the previous report (Shao et al., 2015), we observed that the strain-induced nuclear actin ring is stable. This could arise from Emd and NMIIA as stabilizing factors for local actin polymerization upon a long period of force

stimulation. Moreover, we also showed that a pool of nuclear actin is decreased upon mechanical strain, which is dependent on Emd, as a component of the nuclear force sensor. As mentioned, force also induced a robust local actin polymerization at the ONM, suggesting that the strain-induced reduction in nuclear actin is a consequence of this local polymerization. This robust polymerization might function as a barrier to block the flow of actin to the nucleus and induce monomeric actin recruitment to the ONM, thereby affecting the availability of nuclear actin.

## **5.6 Nuclear actin is required to mediate transcription activity**

Actin is involved in many essential processes in the cell. Recent studies have identified the roles of actin in the nucleus. Nuclear actin has been shown to associate with transcriptional machinery as well as with nascent transcripts (Dopie et al., 2012; Hofmann et al., 2004; Kapoor et al., 2013). However, the precise mechanisms remain unclear. It is suggested that nuclear actin modulates the elongation process of RNAPII to facilitate the modifications of chromatin structure at this site (Visa and Percipalle, 2010). In agreement with these observations, our data revealed that strain-induced reduction of nuclear actin levels result in the repression of transcriptional activity through reduced RNAPII-S2p occupancy at the gene bodies of PRC2-driven-lineage-specific genes. Lack of transcriptional activity recruited PRC2 to mediate the silencing at these genes, thereby regulating lineage progression. Additionally, our findings suggest a molecular mechanism for the direct correlation between nuclear actin levels and quiescent state (Spencer et al., 2011).

Although IPO9 and XPO6 were reported to be specific for actin flow between the cytoplasm and the nucleus, they also transport other proteins, including cofilin and profilin, respectively. These proteins are well known as regulators of actin dynamics. This raises a curious question as to how mechanical strain regulates cofilin, profilin, and nuclear actin dynamics and whether they are involved in regulating RNAPII activity. Thus, methods to precisely regulate nuclear actin levels are required to solve this central concern.

In summary, we have identified a novel nuclear-mechanosensor that regulates transcription, chromatin remodeling and lineage commitment. For the first time, this study reveals unknown functions of Emd, and provides a mechanism for the missing link as to how extrinsic mechanical forces couple the actomyosin contractile network to transduce signals to the nucleus in order to drive cellular responses. However, many unsolved questions remain. Further studies will help us to fully understand how forces induce transcription repression, chromatin remodeling and cell fate decisions.

## References

- Adelman, K., and Lis, J.T. (2012). Promoter-proximal pausing of RNA polymerase II: emerging roles in metazoans. *Nat Rev Genet* *13*, 720-731.
- Alam, H., Sehgal, L., Kundu, S.T., Dalal, S.N., and Vaidya, M.M. (2011). Novel function of keratins 5 and 14 in proliferation and differentiation of stratified epithelial cells. *Mol Biol Cell* *22*, 4068-4078.
- Alam, S., Lovett, D.B., Dickinson, R.B., Roux, K.J., and Lele, T.P. (2014). Nuclear forces and cell mechanosensing. *Prog Mol Biol Transl Sci* *126*, 205-215.
- Alberts, B., Johnson, A., Lewis, J., Raff, M., Roberts, K., and Walter, P. (2007). *Molecular biology of the cell*, 5th edition. Garland Science.
- Allis, C.D., and Jenuwein, T. (2016). The molecular hallmarks of epigenetic control. *Nat Rev Genet* *17*, 487-500.
- Aughey, G.N., and Southall, T.D. (2016). Dam it's good! DamID profiling of protein-DNA interactions. *Wiley Interdiscip Rev Dev Biol* *5*, 25-37.
- Avgustinova, A., and Benitah, S.A. (2016). Epigenetic control of adult stem cell function. *Nat Rev Mol Cell Biol*.
- Bai, L., and Morozov, A.V. (2010). Gene regulation by nucleosome positioning. *Trends Genet* *26*, 476-483.
- Bannister, A.J., and Kouzarides, T. (2011). Regulation of chromatin by histone modifications. *Cell Res* *21*, 381-395.
- Becker, J.S., Nicetto, D., and Zaret, K.S. (2016). H3K9me3-Dependent Heterochromatin: Barrier to Cell Fate Changes. *Trends Genet* *32*, 29-41.
- Berk, J.M., Tiffit, K.E., and Wilson, K.L. (2013). The nuclear envelope LEM-domain protein emerin. *Nucleus* *4*, 298-314.
- Betapudi, V. (2014). Life without double-headed non-muscle myosin II motor proteins. *Front Chem* *2*, 45.
- Bickmore, W.A., and van Steensel, B. (2013). Genome architecture: domain organization of interphase chromosomes. *Cell* *152*, 1270-1284.
- Bikle, D.D., Xie, Z., and Tu, C.L. (2012). Calcium regulation of keratinocyte differentiation. *Expert Rev Endocrinol Metab* *7*, 461-472.
- Blackledge, N.P., Rose, N.R., and Klose, R.J. (2015). Targeting Polycomb systems to regulate gene expression: modifications to a complex story. *Nat Rev Mol Cell Biol* *16*, 643-649.
- Blanchard, G.B., Kabla, A.J., Schultz, N.L., Butler, L.C., Sanson, B., Gorfinkiel, N., Mahadevan, L., and Adams, R.J. (2009). Tissue tectonics: morphogenetic strain rates, cell shape change and intercalation. *Nat Methods* *6*, 458-464.
- Blanpain, C., and Fuchs, E. (2009). Epidermal homeostasis: a balancing act of stem cells in the skin. *Nat Rev Mol Cell Biol* *10*, 207-217.
- Britton, L.M., Gonzales-Cope, M., Zee, B.M., and Garcia, B.A. (2011). Breaking the histone code with quantitative mass spectrometry. *Expert Rev Proteomics* *8*, 631-643.
- Brookes, E., de Santiago, I., Hebenstreit, D., Morris, K.J., Carroll, T., Xie, S.Q., Stock, J.K., Heidemann, M., Eick, D., Nozaki, N., *et al.* (2012). Polycomb associates genome-wide with a specific RNA polymerase II variant, and regulates metabolic genes in ESCs. *Cell Stem Cell* *10*, 157-170.
- Brookes, E., and Pombo, A. (2009). Modifications of RNA polymerase II are pivotal in regulating gene expression states. *EMBO Rep* *10*, 1213-1219.
- Brookes, E., and Pombo, A. (2012). Code breaking: the RNAPII modification code in pluripotency. *Cell Cycle* *11*, 1267-1268.
- Burke, B., and Stewart, C.L. (2013). The nuclear lamins: flexibility in function. *Nat Rev Mol Cell Biol* *14*, 13-24.
- Campbell, I.D., and Humphries, M.J. (2011). Integrin structure, activation, and interactions. *Cold Spring Harb Perspect Biol* *3*.
- Campos, E.I., and Reinberg, D. (2009). Histones: annotating chromatin. *Annu Rev Genet* *43*, 559-599.
- Casella, J.F., Flanagan, M.D., and Lin, S. (1981). Cytochalasin D inhibits actin polymerization and induces depolymerization of actin filaments formed during platelet shape change. *Nature* *293*, 302-305.
- Chang, W., Worman, H.J., and Gundersen, G.G. (2015). Accessorizing and anchoring the LINC complex for multifunctionality. *J Cell Biol* *208*, 11-22.
- Chaumet, A., Wright, G.D., Seet, S.H., Tham, K.M., Gounko, N.V., and Bard, F. (2015). Nuclear envelope-associated endosomes deliver surface proteins to the nucleus. *Nat Commun* *6*, 8218.

Ciabrelli, F., and Cavalli, G. (2015). Chromatin-driven behavior of topologically associating domains. *J Mol Biol* *427*, 608-625.

Clark, K., Langeslag, M., Figdor, C.G., and van Leeuwen, F.N. (2007). Myosin II and mechanotransduction: a balancing act. *Trends Cell Biol* *17*, 178-186.

Clayton, E., Doupe, D.P., Klein, A.M., Winton, D.J., Simons, B.D., and Jones, P.H. (2007). A single type of progenitor cell maintains normal epidermis. *Nature* *446*, 185-189.

Cohen, T.V., Hernandez, L., and Stewart, C.L. (2008). Functions of the nuclear envelope and lamina in development and disease. *Biochem Soc Trans* *36*, 1329-1334.

Connelly, J.T., Gautrot, J.E., Trappmann, B., Tan, D.W., Donati, G., Huck, W.T., and Watt, F.M. (2010). Actin and serum response factor transduce physical cues from the microenvironment to regulate epidermal stem cell fate decisions. *Nat Cell Biol* *12*, 711-718.

Consortium, E.P. (2012). An integrated encyclopedia of DNA elements in the human genome. *Nature* *489*, 57-74.

Conti, M.A., and Adelstein, R.S. (2008). Nonmuscle myosin II moves in new directions. *J Cell Sci* *121*, 11-18.

Conti, M.A., Even-Ram, S., Liu, C., Yamada, K.M., and Adelstein, R.S. (2004). Defects in cell adhesion and the visceral endoderm following ablation of nonmuscle myosin heavy chain II-A in mice. *J Biol Chem* *279*, 41263-41266.

Cooper, G.M., and Hausman, R.E. (2013). *The Cell: A Molecular Approach*. 6th edition. Sinauer Associates: Sunderland.

Crisp, M., and Burke, B. (2008). The nuclear envelope as an integrator of nuclear and cytoplasmic architecture. *FEBS Lett* *582*, 2023-2032.

Dahl, K.N., Ribeiro, A.J., and Lammerding, J. (2008). Nuclear shape, mechanics, and mechanotransduction. *Circ Res* *102*, 1307-1318.

Dechat, T., Pflieger, K., Sengupta, K., Shimi, T., Shumaker, D.K., Solimando, L., and Goldman, R.D. (2008). Nuclear lamins: major factors in the structural organization and function of the nucleus and chromatin. *Genes Dev* *22*, 832-853.

Dejardin, J. (2015). Switching between Epigenetic States at Pericentromeric Heterochromatin. *Trends Genet* *31*, 661-672.

Dekker, J., Marti-Renom, M.A., and Mirny, L.A. (2013). Exploring the three-dimensional organization of genomes: interpreting chromatin interaction data. *Nat Rev Genet* *14*, 390-403.

Demmerle, J., Koch, A.J., and Holaska, J.M. (2012). The nuclear envelope protein emerlin binds directly to histone deacetylase 3 (HDAC3) and activates HDAC3 activity. *J Biol Chem* *287*, 22080-22088.

Di Croce, L., and Helin, K. (2013). Transcriptional regulation by Polycomb group proteins. *Nat Struct Mol Biol* *20*, 1147-1155.

Dmitrieff, S., and Nedelec, F. (2016). Amplification of actin polymerization forces. *J Cell Biol* *212*, 763-766.

Dopie, J., Skarp, K.P., Rajakyla, E.K., Tanhuanpaa, K., and Vartiainen, M.K. (2012). Active maintenance of nuclear actin by importin 9 supports transcription. *Proc Natl Acad Sci U S A* *109*, E544-552.

Du, J., Johnson, L.M., Jacobsen, S.E., and Patel, D.J. (2015). DNA methylation pathways and their crosstalk with histone methylation. *Nat Rev Mol Cell Biol* *16*, 519-532.

DuFort, C.C., Paszek, M.J., and Weaver, V.M. (2011). Balancing forces: architectural control of mechanotransduction. *Nat Rev Mol Cell Biol* *12*, 308-319.

Dupont, S., Morsut, L., Aragona, M., Enzo, E., Giulitti, S., Cordenonsi, M., Zanconato, F., Le Digabel, J., Forcato, M., Bicciato, S., *et al.* (2011). Role of YAP/TAZ in mechanotransduction. *Nature* *474*, 179-183.

Ea, V., Baudement, M.O., Lesne, A., and Forne, T. (2015). Contribution of Topological Domains and Loop Formation to 3D Chromatin Organization. *Genes (Basel)* *6*, 734-750.

Entrevan, M., Schuettengruber, B., and Cavalli, G. (2016). Regulation of Genome Architecture and Function by Polycomb Proteins. *Trends Cell Biol* *26*, 511-525.

Evans, N.D., Oreffo, R.O., Healy, E., Thurner, P.J., and Man, Y.H. (2013). Epithelial mechanobiology, skin wound healing, and the stem cell niche. *J Mech Behav Biomed Mater* *28*, 397-409.

Ezhkova, E., Pasolli, H.A., Parker, J.S., Stokes, N., Su, I.H., Hannon, G., Tarakhovskiy, A., and Fuchs, E. (2009). Ezh2 orchestrates gene expression for the stepwise differentiation of tissue-specific stem cells. *Cell* *136*, 1122-1135.

Fang, Y., and Fullwood, M.J. (2016). Roles, Functions, and Mechanisms of Long Non-coding RNAs in Cancer. *Genomics Proteomics Bioinformatics* *14*, 42-54.

Fedorchak, G.R., Kaminski, A., and Lammerding, J. (2014). Cellular mechanosensing: getting to the nucleus of it all. *Prog Biophys Mol Biol* *115*, 76-92.

Fortin, J.P., and Hansen, K.D. (2015). Reconstructing A/B compartments as revealed by Hi-C using long-range correlations in epigenetic data. *Genome Biol* 16, 180.

Fridkin, A., Penkner, A., Jantsch, V., and Gruenbaum, Y. (2009). SUN-domain and KASH-domain proteins during development, meiosis and disease. *Cell Mol Life Sci* 66, 1518-1533.

Fuchs, E. (2008). Skin stem cells: rising to the surface. *J Cell Biol* 180, 273-284.

Ganz, A., Lambert, M., Saez, A., Silberzan, P., Buguin, A., Mege, R.M., and Ladoux, B. (2006). Traction forces exerted through N-cadherin contacts. *Biol Cell* 98, 721-730.

Giresi, P.G., Kim, J., McDaniell, R.M., Iyer, V.R., and Lieb, J.D. (2007). FAIRE (Formaldehyde-Assisted Isolation of Regulatory Elements) isolates active regulatory elements from human chromatin. *Genome Res* 17, 877-885.

Goldman, R.D., Gruenbaum, Y., Moir, R.D., Shumaker, D.K., and Spann, T.P. (2002). Nuclear lamins: building blocks of nuclear architecture. *GENES & DEVELOPMENT* 16, 533-547.

Golomb, E., Ma, X., Jana, S.S., Preston, Y.A., Kawamoto, S., Shoham, N.G., Goldin, E., Conti, M.A., Sellers, J.R., and Adelstein, R.S. (2004). Identification and characterization of nonmuscle myosin II-C, a new member of the myosin II family. *J Biol Chem* 279, 2800-2808.

Gonzalez-Sandoval, A., and Gasser, S.M. (2016). On TADs and LADs: Spatial Control Over Gene Expression. *Trends Genet* 32, 485-495.

Griffis, E.R., Xu, S., and Powers, M.A. (2003). Nup98 Localizes to Both Nuclear and Cytoplasmic Sides of the Nuclear Pore and Binds to Two Distinct Nucleoporin Subcomplexes. *Molecular Biology of the Cell Vol. 14*, 600-610.

Grosse, R., and Vartiainen, M.K. (2013). To be or not to be assembled: progressing into nuclear actin filaments. *Nat Rev Mol Cell Biol* 14, 693-697.

Guelen, L., Pagie, L., Brasset, E., Meuleman, W., Faza, M.B., Talhout, W., Eussen, B.H., de Klein, A., Wessels, L., de Laat, W., *et al.* (2008). Domain organization of human chromosomes revealed by mapping of nuclear lamina interactions. *Nature* 453, 948-951.

Guilluy, C., and Burridge, K. (2015). Nuclear mechanotransduction: forcing the nucleus to respond. *Nucleus* 6, 19-22.

Guilluy, C., Osborne, L.D., Van Landeghem, L., Sharek, L., Superfine, R., Garcia-Mata, R., and Burridge, K. (2014). Isolated nuclei adapt to force and reveal a mechanotransduction pathway in the nucleus. *Nat Cell Biol* 16, 376-381.

Guolla, L., Bertrand, M., Haase, K., and Pelling, A.E. (2012). Force transduction and strain dynamics in actin stress fibres in response to nanonewton forces. *J Cell Sci* 125, 603-613.

Haase, K., Macadangang, J.K., Edrington, C.H., Cuerrier, C.M., Hadjiantoniou, S., Harden, J.L., Skerjanc, I.S., and Pelling, A.E. (2016). Extracellular Forces Cause the Nucleus to Deform in a Highly Controlled Anisotropic Manner. *Sci Rep* 6, 21300.

Hafner, M., Wenk, J., Nenci, A., Pasparakis, M., Scharffetter-Kochanek, K., Smyth, N., Peters, T., Kess, D., Holtkotter, O., Shephard, P., *et al.* (2004). Keratin 14 Cre transgenic mice authenticate keratin 14 as an oocyte-expressed protein. *Genesis* 38, 176-181.

Hahn, S. (2004). Structure and mechanism of the RNA Polymerase II transcription machinery. *Nature structural & molecular biology* 11, 394-403.

Harr, J.C., Luperchio, T.R., Wong, X., Cohen, E., Wheelan, S.J., and Reddy, K.L. (2015). Directed targeting of chromatin to the nuclear lamina is mediated by chromatin state and A-type lamins. *J Cell Biol* 208, 33-52.

Hartman, M.A., and Spudich, J.A. (2012). The myosin superfamily at a glance. *J Cell Sci* 125, 1627-1632.

Hartsock, A., and Nelson, W.J. (2008). Adherens and tight junctions: structure, function and connections to the actin cytoskeleton. *Biochim Biophys Acta* 1778, 660-669.

Hawkins, R.D., Hon, G.C., Lee, L.K., Ngo, Q., Lister, R., Pelizzola, M., Edsall, L.E., Kuan, S., Luu, Y., Klugman, S., *et al.* (2010). Distinct epigenomic landscapes of pluripotent and lineage-committed human cells. *Cell Stem Cell* 6, 479-491.

Hetzer, M.W. (2010). The nuclear envelope. *Cold Spring Harb Perspect Biol* 2, a000539.

Hoffman, B.D., Grashoff, C., and Schwartz, M.A. (2011). Dynamic molecular processes mediate cellular mechanotransduction. *Nature* 475, 316-323.

Hofmann, W.A., Stojiljkovic, L., Fuchsova, B., Vargas, G.M., Mavrommatis, E., Philimonenko, V., Kysela, K., Goodrich, J.A., Lessard, J.L., Hope, T.J., *et al.* (2004). Actin is part of pre-initiation complexes and is necessary for transcription by RNA polymerase II. *Nat Cell Biol* 6, 1094-1101.

Holaska, J.M., Kowalski, A.K., and Wilson, K.L. (2004). Emerin caps the pointed end of actin filaments: evidence for an actin cortical network at the nuclear inner membrane. *PLoS Biol* 2, E231.

Holaska, J.M., and Wilson, K.L. (2006). Multiple roles for emerin: implications for Emery-Dreifuss muscular dystrophy. *Anat Rec A Discov Mol Cell Evol Biol* 288, 676-680.

Holaska, J.M., and Wilson, K.L. (2007). An emerin "proteome": purification of distinct emerin-containing complexes from HeLa cells suggests molecular basis for diverse roles including gene regulation, mRNA splicing, signaling, mechanosensing, and nuclear architecture. *Biochemistry* *46*, 8897-8908.

Hood, J.D., and Cheresch, D.A. (2002). Role of integrins in cell invasion and migration. *Nat Rev Cancer* *2*, 91-100.

Horn, H.F. (2014). LINC complex proteins in development and disease. *Curr Top Dev Biol* *109*, 287-321.

Horn, H.F., Kim, D.I., Wright, G.D., Wong, E.S., Stewart, C.L., Burke, B., and Roux, K.J. (2013). A mammalian KASH domain protein coupling meiotic chromosomes to the cytoskeleton. *J Cell Biol* *202*, 1023-1039.

Houben, F., Ramaekers, F.C., Snoeckx, L.H., and Broers, J.L. (2007). Role of nuclear lamina-cytoskeleton interactions in the maintenance of cellular strength. *Biochim Biophys Acta* *1773*, 675-686.

Huveneers, S., and de Rooij, J. (2013). Mechanosensitive systems at the cadherin-F-actin interface. *J Cell Sci* *126*, 403-413.

Ingber, D.E. (2006). Cellular mechanotransduction: putting all the pieces together again. *FASEB J* *20*, 811-827.

Isermann, P., and Lammerding, J. (2013). Nuclear mechanics and mechanotransduction in health and disease. *Curr Biol* *23*, R1113-1121.

Jaalouk, D.E., and Lammerding, J. (2009). Mechanotransduction gone awry. *Nat Rev Mol Cell Biol* *10*, 63-73.

Jadhav, U., Nalapareddy, K., Saxena, M., O'Neill, N.K., Pinello, L., Yuan, G.C., Orkin, S.H., and Shivdasani, R.A. (2016). Acquired Tissue-Specific Promoter Bivalency Is a Basis for PRC2 Necessity in Adult Cells. *Cell* *165*, 1389-1400.

Jahed, Z., Shams, H., and Mofrad, M.R. (2015). A Disulfide Bond Is Required for the Transmission of Forces through SUN-KASH Complexes. *Biophys J* *109*, 501-509.

Jao, C.Y., and Salic, A. (2008). Exploring RNA transcription and turnover in vivo by using click chemistry. *PNAS* *105*, 15779-15784.

Jenuwein, T., and Allis, C.D. (2001). Translating the Histone Code. *Science* *293*, 1074-1080.

Jiang, L., Schlesinger, F., Davis, C.A., Zhang, Y., Li, R., Salit, M., Gingeras, T.R., and Oliver, B. (2011). Synthetic spike-in standards for RNA-seq experiments. *Genome Res* *21*, 1543-1551.

Kabachinski, G., and Schwartz, T.U. (2015). The nuclear pore complex - structure and function at a glance. *Journal of Cell Science* *128*, 423-429.

Kapoor, P., Chen, M., Winkler, D.D., Luger, K., and Shen, X. (2013). Evidence for monomeric actin function in INO80 chromatin remodeling. *Nat Struct Mol Biol* *20*, 426-432.

Kapoor, P., and Shen, X. (2014). Mechanisms of nuclear actin in chromatin-remodeling complexes. *Trends Cell Biol* *24*, 238-246.

Katta, S.S., Smoyer, C.J., and Jaspersen, S.L. (2014). Destination: inner nuclear membrane. *Trends Cell Biol* *24*, 221-229.

Kim, D.I., Birendra, K.C., and Roux, K.J. (2015). Making the LINC: SUN and KASH protein interactions. *Biol Chem* *396*, 295-310.

Kim, J., and Kim, H. (2012). Recruitment and Biological Consequences of Histone Modification of H3K27me3 and H3K9me3. *ILAR J* *53*, 232-239.

Kind, J., Pagie, L., de Vries, S.S., Nahidiazar, L., Dey, S.S., Bienko, M., Zhan, Y., Lajoie, B., de Graaf, C.A., Amendola, M., *et al.* (2015). Genome-wide maps of nuclear lamina interactions in single human cells. *Cell* *163*, 134-147.

Kind, J., Pagie, L., Ortabozkoyun, H., Boyle, S., de Vries, S.S., Janssen, H., Amendola, M., Nolen, L.D., Bickmore, W.A., and van Steensel, B. (2013). Single-cell dynamics of genome-nuclear lamina interactions. *Cell* *153*, 178-192.

Koch, A.J., and Holaska, J.M. (2014). Emerin in health and disease. *Semin Cell Dev Biol* *29*, 95-106.

Korn, E.D. (2000). Coevolution of head, neck, and tail domains of myosin heavy chains. *PNAS* *97*, 12559-12564.

Kovacs, M., Toth, J., Hetenyi, C., Malnasi-Csizmadia, A., and Sellers, J.R. (2004). Mechanism of blebbistatin inhibition of myosin II. *J Biol Chem* *279*, 35557-35563.

Kukalev, A., Nord, Y., Palmberg, C., Bergman, T., and Percipalle, P. (2005). Actin and hnRNP U cooperate for productive transcription by RNA polymerase II. *Nat Struct Mol Biol* *12*, 238-244.

Ladoux, B., Nelson, W.J., Yan, J., and Mege, R.M. (2015). The mechanotransduction machinery at work at adherens junctions. *Integr Biol (Camb)* *7*, 1109-1119.

Lammerding, J., Hsiao, J., Schulze, P.C., Kozlov, S., Stewart, C.L., and Lee, R.T. (2005). Abnormal nuclear shape and impaired mechanotransduction in emerin-deficient cells. *J Cell Biol* *170*, 781-791.

Lammerding, J., Schulze, P.C., Takahashi, T., Kozlov, S., Sullivan, T., Kamm, R.D., Stewart, C.L., and Lee, R.T. (2004). Lamin A/C deficiency causes defective nuclear mechanics and mechanotransduction. *Journal of Clinical Investigation* *113*, 370-378.

Lanzuolo, C., and Orlando, V. (2012). Memories from the polycomb group proteins. *Annu Rev Genet* *46*, 561-589.

Laugesen, A., and Helin, K. (2014). Chromatin repressive complexes in stem cells, development, and cancer. *Cell Stem Cell* *14*, 735-751.

Lawrence, M., Daujat, S., and Schneider, R. (2016). Lateral Thinking: How Histone Modifications Regulate Gene Expression. *Trends Genet* *32*, 42-56.

Lecuit, T., Lenne, P.F., and Munro, E. (2011). Force generation, transmission, and integration during cell and tissue morphogenesis. *Annu Rev Cell Dev Biol* *27*, 157-184.

Lei, K., Zhanga, X., Dinga, X., Muyun Chena, X.G., Zhua, B., Xua, T., Zhuanga, Y., Xua, R., and Han, M. (2009). SUN1 and SUN2 play critical but partially redundant roles in anchoring nuclei in skeletal muscle cells in mice. *PNAS* *106*, 10207-10212.

Lombardi, M.L., Jaalouk, D.E., Shanahan, C.M., Burke, B., Roux, K.J., and Lammerding, J. (2011). The interaction between nesprins and sun proteins at the nuclear envelope is critical for force transmission between the nucleus and cytoskeleton. *J Biol Chem* *286*, 26743-26753.

Loven, J., Orlando, D.A., Sigova, A.A., Lin, C.Y., Rahl, P.B., Burge, C.B., Levens, D.L., Lee, T.I., and Young, R.A. (2012). Revisiting global gene expression analysis. *Cell* *151*, 476-482.

Marenholz, I., Zirra, M., Fischer, D.F., Backendorf, C., Ziegler, A., and Mischke, D. (2001). Identification of Human Epidermal Differentiation Complex (EDC)-Encoded Genes by Subtractive Hybridization of Entire YACs to a Gridded Keratinocyte cDNA Library. *Genome Res* *11*, 341-355.

Markiewicz, E., Tilgner, K., Barker, N., van de Wetering, M., Clevers, H., Dorobek, M., Hausmanowa-Petrusewicz, I., Ramaekers, F.C.S., Broers, J.L.V., Blankesteyn, M.W., *et al.* (2006). The inner nuclear membrane protein Emerin regulates  $\beta$ -catenin activity by restricting its accumulation in the nucleus. *The EMBO Journal* *25*, 3275-3285.

Mekhail, K., and Moazed, D. (2010). The nuclear envelope in genome organization, expression and stability. *Nat Rev Mol Cell Biol* *11*, 317-328.

Melcon, G., Kozlov, S., Cutler, D.A., Sullivan, T., Hernandez, L., Zhao, P., Mitchell, S., Nader, G., Bakay, M., Rottman, J.N., *et al.* (2006). Loss of emerin at the nuclear envelope disrupts the Rb1/E2F and MyoD pathways during muscle regeneration. *Hum Mol Genet* *15*, 637-651.

Miyamoto, K., and Gurdon, J.B. (2013). Transcriptional regulation and nuclear reprogramming: roles of nuclear actin and actin-binding proteins. *Cell Mol Life Sci* *70*, 3289-3302.

Moll, R., Franke, W.W., Schiller, D.L., Geiger, B., and Krepler, R. (1982). The catalog of human cytokeratins: Patterns of expression in normal epithelia, tumors and cultured cells. *Cell* *31*, 11-24.

Morey, L., Santanach, A., and Di Croce, L. (2015). Pluripotency and Epigenetic Factors in Mouse Embryonic Stem Cell Fate Regulation. *Mol Cell Biol* *35*, 2716-2728.

Murrell, M., Oakes, P.W., Lenz, M., and Gardel, M.L. (2015). Forcing cells into shape: the mechanics of actomyosin contractility. *Nat Rev Mol Cell Biol* *16*, 486-498.

Niessen, C.M., Leckband, D., and Yap, A.S. (2011). Tissue organization by cadherin adhesion molecules: dynamic molecular and cellular mechanisms of morphogenetic regulation. *Physiol Rev* *91*, 691-731.

Nurnberg, A., Kitzing, T., and Grosse, R. (2011). Nucleating actin for invasion. *Nat Rev Cancer* *11*, 177-187.

Nusbaum, C., Zody, M.C., Borowsky, M.L., Kamal, M., Kodira, C.D., Taylor, T.D., Whittaker, C.A., Chang, J.L., Cuomo, C.A., Dewar, K., *et al.* (2005). DNA sequence and analysis of human chromosome 18. *Nature* *437*, 551-555.

Oberdoerffer, P., and Sinclair, D.A. (2007). The role of nuclear architecture in genomic instability and ageing. *Nat Rev Mol Cell Biol* *8*, 692-702.

Orr, A.W., Helmke, B.P., Blackman, B.R., and Schwartz, M.A. (2006). Mechanisms of mechanotransduction. *Dev Cell* *10*, 11-20.

Ostlund, C., Folker, E.S., Choi, J.C., Gomes, E.R., Gundersen, G.G., and Worman, H.J. (2009). Dynamics and molecular interactions of linker of nucleoskeleton and cytoskeleton (LINC) complex proteins. *J Cell Sci* *122*, 4099-4108.

Paluch, E.K., Nelson, C.M., Biais, N., Fabry, B., Moeller, J., Pruitt, B.L., Wollnik, C., Kudryasheva, G., Rehfeldt, F., and Federle, W. (2015). Mechanotransduction: use the force(s). *BMC Biol* *13*, 47.

Parsons, J.T., Horwitz, A.R., and Schwartz, M.A. (2010). Cell adhesion: integrating cytoskeletal dynamics and cellular tension. *Nat Rev Mol Cell Biol* *11*, 633-643.

Pasini, D., Bracken, A.P., Hansen, J.B., Capillo, M., and Helin, K. (2007). The polycomb group protein Suz12 is required for embryonic stem cell differentiation. *Mol Cell Biol* *27*, 3769-3779.

Pederson, T., King, M.C., and Marko, J.F. (2015). Forces, fluctuations, and self-organization in the nucleus. *Mol Biol Cell* 26, 3915-3919.

Percipalle, P. (2013). Co-transcriptional nuclear actin dynamics. *Nucleus* 4, 43-52.

Percipalle, P., and Visa, N. (2006). Molecular functions of nuclear actin in transcription. *J Cell Biol* 172, 967-971.

Peters, A.H.F.M., Kubicek, S., Mechtler, K., O'Sullivan, R.J., Derijck, A.A.H.A., Perez-Burgos, L., Kohlmaier, A., Opravil, S., Tachibana, M., Shinkai, Y., *et al.* (2003). Partitioning and Plasticity of Repressive Histone Methylation States in Mammalian Chromatin. *Molecular Cell* 12, 1577-1589.

Phatnani, H.P., and Greenleaf, A.L. (2006). Phosphorylation and functions of the RNA polymerase II CTD. *Genes Dev* 20, 2922-2936.

Pollard, T.D., and Earnshaw, W.C. (2007). *Cell Biology*, 2nd Edition. Saunders-Elsevier, 928.

Pope, B.D., Ryba, T., Dileep, V., Yue, F., Wu, W., Denas, O., Vera, D.L., Wang, Y., Hansen, R.S., Canfield, T.K., *et al.* (2014). Topologically associating domains are stable units of replication-timing regulation. *Nature* 515, 402-405.

Poulson, N.D., and Lechler, T. (2012). Asymmetric cell divisions in the epidermis. *Int Rev Cell Mol Biol* 295, 199-232.

Probst, A.V., Dunleavy, E., and Almouzni, G. (2009). Epigenetic inheritance during the cell cycle. *Nat Rev Mol Cell Biol* 10, 192-206.

Provenzano, P.P., and Keely, P.J. (2011). Mechanical signaling through the cytoskeleton regulates cell proliferation by coordinated focal adhesion and Rho GTPase signaling. *J Cell Sci* 124, 1195-1205.

Quan, T., Wang, F., Shao, Y., Rittie, L., Xia, W., Orringer, J.S., Voorhees, J.J., and Fisher, G.J. (2013). Enhancing structural support of the dermal microenvironment activates fibroblasts, endothelial cells, and keratinocytes in aged human skin in vivo. *J Invest Dermatol* 133, 658-667.

Quinn, J.J., and Chang, H.Y. (2016). Unique features of long non-coding RNA biogenesis and function. *Nat Rev Genet* 17, 47-62.

Radovanac, K., Morgner, J., Schulz, J.N., Blumbach, K., Patterson, C., Geiger, T., Mann, M., Krieg, T., Eckes, B., Fassler, R., *et al.* (2013). Stabilization of integrin-linked kinase by the Hsp90-CHIP axis impacts cellular force generation, migration and the fibrotic response. *EMBO J* 32, 1409-1424.

Razafsky, D., and Hodzic, D. (2009). Bringing KASH under the SUN: the many faces of nucleocytoplasmic connections. *J Cell Biol* 186, 461-472.

Reichelt, J. (2007). Mechanotransduction of keratinocytes in culture and in the epidermis. *Eur J Cell Biol* 86, 807-816.

Richly, H., Aloia, L., and Di Croce, L. (2011). Roles of the Polycomb group proteins in stem cells and cancer. *Cell Death Dis* 2, e204.

Riising, E.M., Comet, I., Leblanc, B., Wu, X., Johansen, J.V., and Helin, K. (2014). Gene silencing triggers polycomb repressive complex 2 recruitment to CpG islands genome wide. *Mol Cell* 55, 347-360.

Rompolas, P., Mesa, K.R., Kawaguchi, K., Park, S., Gonzalez, D., Brown, S., Boucher, J., Klein, A.M., and Greco, V. (2016). Spatiotemporal coordination of stem cell commitment during epidermal homeostasis. *Science* 352, 1471-1474.

Rosa, S., and Shaw, P. (2013). Insights into chromatin structure and dynamics in plants. *Biology (Basel)* 2, 1378-1410.

Saksouk, N., Simboeck, E., and Déjardin, J. (2015a). Constitutive heterochromatin formation and transcription in mammals. *Epigenetics Chromatin* 8.

Saksouk, N., Simboeck, E., and Déjardin, J. (2015b). Constitutive heterochromatin formation and transcription in mammals. *Epigenetics & Chromatin* 8.

Salpingidou, G., Smertenko, A., Hausmanowa-Petrucewicz, I., Hussey, P.J., and Hutchison, C.J. (2007). A novel role for the nuclear membrane protein emerlin in association of the centrosome to the outer nuclear membrane. *J Cell Biol* 178, 897-904.

Sarkar, S., Egelhoff, T., and Baskaran, H. (2009). Insights into the Roles of Non-Muscle Myosin Iia in Human Keratinocyte Migration. *Cell Mol Bioeng* 2, 486-494.

Sasai, Y. (2013). Cytosystems dynamics in self-organization of tissue architecture. *Nature* 493, 318-326.

Schooley, A., Vollmer, B., and Antonin, W. (2012). Building a nuclear envelope at the end of mitosis: coordinating membrane reorganization, nuclear pore complex assembly, and chromatin de-condensation. *Chromosoma* 121, 539-554.

Schreiner, S.M., Koo, P.K., Zhao, Y., Mochrie, S.G., and King, M.C. (2015). The tethering of chromatin to the nuclear envelope supports nuclear mechanics. *Nat Commun* 6, 7159.

Schwartz, Y.B., and Pirrotta, V. (2014). Ruled by ubiquitylation: a new order for polycomb recruitment. *Cell Rep* 8, 321-325.

Shao, X., Li, Q., Mogilner, A., Bershadsky, A.D., and Shivashankar, G.V. (2015). Mechanical stimulation induces formin-dependent assembly of a perinuclear actin rim. *Proc Natl Acad Sci U S A* *112*, E2595-2601.

Shen, X., Liu, Y., Hsu, Y.J., Fujiwara, Y., Kim, J., Mao, X., Yuan, G.C., and Orkin, S.H. (2008). EZH1 mediates methylation on histone H3 lysine 27 and complements EZH2 in maintaining stem cell identity and executing pluripotency. *Mol Cell* *32*, 491-502.

Simon, D.N., and Wilson, K.L. (2011). The nucleoskeleton as a genome-associated dynamic 'network of networks'. *Nat Rev Mol Cell Biol* *12*, 695-708.

Simon, J.A., and Kingston, R.E. (2013). Occupying chromatin: Polycomb mechanisms for getting to genomic targets, stopping transcriptional traffic, and staying put. *Mol Cell* *49*, 808-824.

Simpson, C.L., Patel, D.M., and Green, K.J. (2011). Deconstructing the skin: cytoarchitectural determinants of epidermal morphogenesis. *Nat Rev Mol Cell Biol* *12*, 565-580.

Solovei, I., Thanisch, K., and Feodorova, Y. (2016). How to rule the nucleus: divide et impera. *Curr Opin Cell Biol* *40*, 47-59.

Sood, V., and Brickner, J.H. (2014). Nuclear pore interactions with the genome. *Curr Opin Genet Dev* *25*, 43-49.

Sotiropoulou, P.A., and Blanpain, C. (2012). Development and homeostasis of the skin epidermis. *Cold Spring Harb Perspect Biol* *4*, a008383.

Spencer, V.A., Costes, S., Inman, J.L., Xu, R., Chen, J., Hendzel, M.J., and Bissell, M.J. (2011). Depletion of nuclear actin is a key mediator of quiescence in epithelial cells. *J Cell Sci* *124*, 123-132.

Starr, D.A., and Fridolfsson, H.N. (2010). Interactions between nuclei and the cytoskeleton are mediated by SUN-KASH nuclear-envelope bridges. *Annu Rev Cell Dev Biol* *26*, 421-444.

Stewart, C.L., Roux, K.J., and Burke, B. (2007). Blurring the Boundary: The Nuclear Envelope Extends Its Reach. *Science* *318*, 1408-1412.

Strambio-De-Castillia, C., Niepel, M., and Rout, M.P. (2010). The nuclear pore complex: bridging nuclear transport and gene regulation. *Nat Rev Mol Cell Biol* *11*, 490-501.

Struhl, K., and Segal, E. (2013). Determinants of nucleosome positioning. *Nat Struct Mol Biol* *20*, 267-273.

Stüven, T., Hartmann, E., and Görlich, D. (2003). Exportin 6: a novel nuclear export receptor that is specific for profilin.actin complexes. *EMBO J* *22*, 5928-5940.

Subramanian, A., Tamayo, P., Mootha, V.K., Mukherjee, S., Benjamin L. Ebert, Gillette, M.A., Paulovich, A., Pomeroy, S.L., Golub, T.R., Lander, E.S., *et al.* (2005). Gene set enrichment analysis: A knowledge-based approach for interpreting genome-wide expression profiles. *PNAS* *102*, 15547.

Suh, H., Hazelbaker, D.Z., Soares, L.M., and Buratowski, S. (2013). The C-terminal domain of Rpb1 functions on other RNA polymerase II subunits. *Mol Cell* *51*, 850-858.

Swift, J., and Discher, D.E. (2014). The nuclear lamina is mechano-responsive to ECM elasticity in mature tissue. *J Cell Sci* *127*, 3005-3015.

Tajbakhsh, S., Rocheteau, P., and Le Roux, I. (2009). Asymmetric cell divisions and asymmetric cell fates. *Annu Rev Cell Dev Biol* *25*, 671-699.

Thompson, D.W. (1917). *On growth and form*. Cambridge : University Press.

Tietjen, J.R., Zhang, D.W., Rodriguez-Molina, J.B., White, B.E., Akhtar, M.S., Heidemann, M., Li, X., Chapman, R.D., Shokat, K., Keles, S., *et al.* (2010). Chemical-genomic dissection of the CTD code. *Nat Struct Mol Biol* *17*, 1154-1161.

Towbin, B.D., Gonzalez-Aguilera, C., Sack, R., Gaidatzis, D., Kalck, V., Meister, P., Askjaer, P., and Gasser, S.M. (2012). Step-wise methylation of histone H3K9 positions heterochromatin at the nuclear periphery. *Cell* *150*, 934-947.

Towbin, B.D., Gonzalez-Sandoval, A., and Gasser, S.M. (2013). Mechanisms of heterochromatin subnuclear localization. *Trends Biochem Sci* *38*, 356-363.

Tsukada, Y., Fang, J., Erdjument-Bromage, H., Warren, M.E., Borchers, C.H., Tempst, P., and Zhang, Y. (2006). Histone demethylation by a family of JmjC domain-containing proteins. *Nature* *439*, 811-816.

Tzur, Y.B., Wilson, K.L., and Gruenbaum, Y. (2006). SUN-domain proteins: 'Velcro' that links the nucleoskeleton to the cytoskeleton. *Nature Reviews Molecular Cell Biology* *7*, 782-788

Uren, D., Hwang, H.K., Hara, Y., Takeda, K., Kawamoto, S., Tullio, A.N., Yu, Z.X., Ferrans, V.J., Tresser, N., Grinberg, A., *et al.* (2000). Gene dosage affects the cardiac and brain phenotype in nonmuscle myosin II-B-depleted mice. *J Clin Invest* *105*, 663-671.

Uyeda, T.Q., Abramson, P.D., and Spudich, J.A. (1996). The neck region of the myosin motor domain acts as a lever arm to generate movement. *PNAS* *93*, 4459-4464.

van den Boom, V., Maat, H., Geugien, M., Rodriguez Lopez, A., Sotoca, A.M., Jaques, J., Brouwers-Vos, A.Z., Fusetti, F., Groen, R.W., Yuan, H., *et al.* (2016). Non-canonical PRC1.1 Targets Active Genes Independent of H3K27me3 and Is Essential for Leukemogenesis. *Cell Rep* *14*, 332-346.

Venkatesh, S., and Workman, J.L. (2015). Histone exchange, chromatin structure and the regulation of transcription. *Nat Rev Mol Cell Biol* *16*, 178-189.

Vicente-Manzanares, M., Ma, X., Adelstein, R.S., and Horwitz, A.R. (2009). Non-muscle myosin II takes centre stage in cell adhesion and migration. *Nat Rev Mol Cell Biol* *10*, 778-790.

Visa, N., and Percipalle, P. (2010). Nuclear functions of actin. *Cold Spring Harb Perspect Biol* *2*, a000620.

Vogel, M.J., Peric-Hupkes, D., and van Steensel, B. (2007). Detection of in vivo protein-DNA interactions using DamID in mammalian cells. *Nat Protoc* *2*, 1467-1478.

Voigt, P., Tee, W.W., and Reinberg, D. (2013). A double take on bivalent promoters. *Genes Dev* *27*, 1318-1338.

Wagers, A.J., and Weissman, I.L. (2004). Plasticity of Adult Stem Cells. *Cell* *116*, 639-648.

Walter, M., Teissandier, A., Perez-Palacios, R., and Bour'his, D. (2016). An epigenetic switch ensures transposon repression upon dynamic loss of DNA methylation in embryonic stem cells. *Elife* *5*.

Wang, N., Tytell, J.D., and Ingber, D.E. (2009). Mechanotransduction at a distance: mechanically coupling the extracellular matrix with the nucleus. *Nature Reviews Molecular Cell Biology* *10*, 75-82.

Watt, F.M. (2002). The stem cell compartment in human interfollicular epidermis. *J Dermatol Sci* *28*, 173-180.

Watt, F.M., and Fujiwara, H. (2011). Cell-extracellular matrix interactions in normal and diseased skin. *Cold Spring Harb Perspect Biol* *3*.

Watt, F.M., and Huck, W.T. (2013). Role of the extracellular matrix in regulating stem cell fate. *Nat Rev Mol Cell Biol* *14*, 467-473.

Whetstine, J.R., Nottke, A., Lan, F., Huarte, M., Smolikov, S., Chen, Z., Spooner, E., Li, E., Zhang, G., Colaiacovo, M., *et al.* (2006). Reversal of histone lysine trimethylation by the JMJD2 family of histone demethylases. *Cell* *125*, 467-481.

Wolff, N., Gilquin, B., Courchay, K., Callebaut, I., Worman, H.J., and Zinn-Justin, S. (2001). Structural analysis of emerin, an inner nuclear membrane protein mutated in X-linked Emery-Dreifuss muscular dystrophy. *FEBS Letters* *501*, 171-176.

Wozniak, M.A., and Chen, C.S. (2009). Mechanotransduction in development: a growing role for contractility. *Nat Rev Mol Cell Biol* *10*, 34-43.

Yang, C.S., Chang, K.Y., Dang, J., and Rana, T.M. (2016). Polycomb Group Protein Pcgf6 Acts as a Master Regulator to Maintain Embryonic Stem Cell Identity. *Sci Rep* *6*, 26899.

Yao, M., Qiu, W., Liu, R., Efremov, A.K., Cong, P., Seddiki, R., Payre, M., Lim, C.T., Ladoux, B., Mege, R.M., *et al.* (2014). Force-dependent conformational switch of alpha-catenin controls vinculin binding. *Nat Commun* *5*, 4525.

Yonemura, S., Wada, Y., Watanabe, T., Nagafuchi, A., and Shibata, M. (2010). alpha-Catenin as a tension transducer that induces adherens junction development. *Nat Cell Biol* *12*, 533-542.

Yuan, J., and Xue, B. (2015). Role of structural flexibility in the evolution of emerin. *J Theor Biol* *385*, 102-111.

Zaidel-Bar, R., Zhenhuan, G., and Luxenburg, C. (2015). The contractome--a systems view of actomyosin contractility in non-muscle cells. *J Cell Sci* *128*, 2209-2217.

Zhang, C., Gao, S., Molascon, A.J., Liu, Y., and Andrews, P.C. (2014). Quantitative proteomics reveals histone modifications in crosstalk with H3 lysine 27 methylation. *Mol Cell Proteomics* *13*, 749-759.

Zhang, J., Felder, A., Liu, Y., Guo, L.T., Lange, S., Dalton, N.D., Gu, Y., Peterson, K.L., Mizisin, A.P., Shelton, G.D., *et al.* (2010). Nesprin 1 is critical for nuclear positioning and anchorage. *Hum Mol Genet* *19*, 329-341.

Zhao, K., Wang, W., Rando, O.J., Xue, Y., Swiderek, K., Kuo, A., and Crabtree, G.R. (1998). Rapid and Phosphoinositol-Dependent Binding of the SWI/SNF-like BAF Complex to Chromatin after T Lymphocyte Receptor Signaling. *Cell* *95*, 625 - 636.

Zhu, C., Bao, G., and Wang, N. (2000). Cell Mechanics: Mechanical Response, Cell Adhesion, and Molecular Deformation. *Annual Review of Biomedical Engineering* *2*, 189-226.

## Appendix

	<b>Gene Set</b>	<b>ES</b>	<b>NES</b>	<b>NOM p-val</b>	<b>FDR q-val</b>
1	Mikkelsen MCV6 HCP with H3K27me3	0.14	3.00	0.000	0.000
2	Benporath PRC2 targets	0.12	2.98	0.000	0.000
3	Mikkelsen MEF HCP with H3K27me3	0.11	2.67	0.000	0.001
4	Kondo prostate cancer with H3K27me3	0.22	2.66	0.004	0.001
5	Meissner NPC HCP with H3K4me2 and H3K27me3	0.13	2.54	0.000	0.002
6	Benporath Suz12 targets	0.07	2.34	0.002	0.008
7	Benporath ES with H3K27me3	0.07	2.17	0.000	0.022

ES = Enrichment score      NES = Normalized enrichment score

NOM p-val = nominal p-value      FDR q-val= false discovery rate q-value

**Appendix Table 1. GSEA analysis** revealed 7 significantly enriched gene sets (FDR q-value < 0.025).

## ABBREVIATIONS

ACTB	beta actin
B2M	Beta-2-Microglobulin
Bleb	Blebbistatin
BM	basement membrane
ChIP	chromatin immunoprecipitation
Chr	chromosome
CRCT1	Cysteine Rich C-Terminal 1
Cyto D	Cytochalasin D
DMSO	dimethyl sulfoxide
DNA	Deoxyribonucleic acid
DRB	5,6-dichloro-1- $\beta$ -D-ribofuranosylbenzimidazole
EDMD	Emery-Dreifuss muscular dystrophy
Emd	emerin
EPCs	epidermal stem/progenitor cells
ER	endoplasmic reticulum
ERCC	External RNA Controls Consortium
Ezh2	Enhancer Of Zeste 2
FAIRE	Formaldehyde-assisted isolation of regulatory elements
GAPDH	Glyceraldehyde 3-phosphate dehydrogenase
H3K27me3	trimethylation of lysine 27 on histone 3
H3K9me2,3	di-/tri-methylation of lysine 9 on histone 3
HOX	Homeobox
INM	inner nuclear membrane
IP	immunoprecipitation
IPO9	importin-9
K10 / K14	Keratin 10 / 14
KLK8	Kallikrein Related Peptidase 8
LADs	Lamin-associated domains
LCE	late cornified envelope
LOR	Loricrin

mRNA	messenger Ribonucleic acid
Myh9 <sup>EKO</sup>	epidermis-specific deletion of Myosin 9
ncRNA	non-coding RNA
NE	nuclear envelop
neg	negative
NMIIA	Non-muscle myosin IIA
NPC	nuclear pore complex
ONM	outer nuclear membrane
P-MLC	Phospho-myosin light chain
PcG	Polycomb Group
PPL	Periplakin
PRC	Polycomb repressive complex
PTM	post translational modification
RNAPII-S2p	RNA polymerase II – serine 2 phosphorylation
RT	room temperature
Scr	scrambled RNA
seq	sequencing
siRNA	Small interfering RNA
SOX	(Sex-determining Region Y)-box
SPRR	Small Proline Rich Proteins
TGM1	Transglutaminase 1
V	volume
XPO6	exportin-6

## ACKNOWLEDGMENTS

I would like to thank all those who gave me the possibility to complete this thesis.

First of all, I would like to thank Dr. Sara Wickström for giving me an opportunity to work on this interesting project and for her great supervision and support throughout my PhD life. Thank you for all the fruitful and inspiring discussions and for being so patient with me. It is a pleasure for me being a member of her lab.

I would like to thank Prof. Matthias Hammerschmidt, Prof. Angelika Noegel and Dr. Sandra Iden for being my PhD committee.

I want to express my grateful to all Wickström lab members. Chloe Yeung, Jessica Morgner and Sushmita Ghatak, thank you very much for sharing good and bad moments during such a long and challenging journey. Thank you for accompanying me to so many food adventures in Cologne, and for your great support inside and outside the lab, especially during writing this thesis. Juliana Du for giving me a very warm welcome to the lab. Many thanks to Nadine Bremicker, for helping me with lots of experiments, without her I cannot complete this project. Kristina Behrendt for setting up this project at the beginning. Carlos Chacon, David Schneider, Torsten Buecher, Janis Koester and Saman Honarnejad for being great colleagues and for such an excellent atmosphere in the lab.

I would like to thank Tessarz lab, Niessen lab, Iden lab, Larsson Department, Dermatology Department, MPI-AGE core facilities for sharing techniques, reagents, equipment as well as for their great support during my PhD.

Last but not least, I would like to express my deepest gratitude to my parents, my brother and my best friends, Stephan Hansen, Trung Vu and Trinh Nguyen for always being there whenever I need them.

## **Publication**

**Le, H.Q.**, Ghatak, S., Yeung, C.C., Tellkamp, F., Gunschmann, C., Dieterich, C., Yeroslaviz, A., Habermann, B., Pombo, A., Niessen, C.M., and *Wickstroem, S. A.* (2016). Mechanical regulation of transcription controls Polycomb-mediated gene silencing during lineage commitment. *Nat Cell Biol* 18, 864–875.

## **Erklärung**

Ich versichere, dass ich die von mir vorgelegte Dissertation selbständig angefertigt, die benutzten Quellen und Hilfsmittel vollständig angegeben und die Stellen der Arbeit – einschließlich Tabellen, Karten und Abbildungen –, die anderen Werken im Wortlaut oder dem Sinn nach entnommen sind, in jedem Einzelfall als Entlehnung kenntlich gemacht habe; dass diese Dissertation noch keiner anderen Fakultät oder Universität zur Prüfung vorgelegen hat; dass sie – abgesehen von unten angegebenen Teilpublikationen – noch nicht veröffentlicht worden ist sowie, dass ich eine solche Veröffentlichung vor Abschluss des Promotionsverfahrens nicht vornehmen werde. Die Bestimmungen der Promotionsordnung sind mir bekannt. Die von mir vorgelegte Dissertation ist von Frau Dr. Sara A. Wickström betreut worden.

Köln, den

## Lebenslauf

---

---

### Persönliche Angaben

Name: Quang-Huy Le  
Geburtsort/ Geburtstag: Hochiminh Stadt, den 12. März 1986  
Nationalität: vietnamesisch

---

---

### Schulbildung

1992 – 1997 Hanh Thong Grundschule, Hochiminh Stadt, Vietnam  
1997 – 2001 Nguyen Van Troi Mittelschule, Hochiminh Stadt, Vietnam  
2001 – 2004 Nguyen Cong Tru Gymnasium, Hochiminh Stadt, Vietnam

### Studium

**9/2004 – 09/2008 Bachelor of Science in Biologie**  
University for Natural Sciences – Vietnam National University, Hochiminh Stadt, Vietnam. Bachelorarbeit in der Abteilung für Biochemie.

**10/2010 – 10/2012 Master of Science in Molecular Bioengineering**  
Technische Universität Dresden. Masterarbeit am DFG-Forschungszentrum für regenerative Therapien Dresden (CRTD), Arbeitsgruppe “Animal models of Regeneration”, Prof. Elly M. Tanaka, TU Dresden.

**Seit 01/2013 Doktorarbeit**  
Max Planck Institut für Biologie des Alterns unter der Anleitung von Dr. Sara A. Wickström  
Thema: „Mechanisms of force-mediated regulation of transcription, chromatin remodeling and cell fate decisions”

### Publikationen

Le, H.Q., Ghatak, S., Yeung, C.Y.C., Tellkamp, F., Günschmann, C., Dieterich, C., Yeroslaviz, A., Habermann, B., Pombo, A., Niessen, C.M., Wickström, S.A.

Mechanical regulation of transcription controls Polycomb-mediated gene silencing during lineage commitment. *Nature Cell Biology* (2016), doi:10.1038/ncb3387 .

Nacu, E., Glausch, M., **Le, H.Q.**, Damanik, F.F.R., Schuez, M., Knapp, D., Khattak, S.R., T., Tanaka, E.M. Connective tissue cells, but not muscle cells, are involved in establishing the proximodistal outcome of limb regeneration in the axolotl. *Development* 140, 513-518 (2013), doi: 10.1242/dev.081752.